A STUDY OF WINTER WHEAT GROWTH AND DEVELOPMENT IN OKLAHOMA USING A HIERARCHICAL BAYESIAN APPROACH

By

PRATISHTHA POUDEL

Bachelor of Science in Agriculture
Tribhuvan University
Kathmandu, Nepal
2013

Master of Science in Plant and Soil Science
Oklahoma State University
Stillwater, OK
2016

Submitted to the Faculty of the
Graduate College of the
Oklahoma State University
in partial fulfillment of
the requirements for
the Degree of
DOCTOR OF PHILOSOPHY
July, 2021

A STUDY OF WINTER WHEAT GROWTH AND DEVELOPMENT IN OKLAHOMA USING A HIERARCHICAL BAYESIAN APPROACH

Dissertation Approved:

Dr. Phillip D. Alderman

Dissertation Advisor

Dr. Brett F. Carver

Dr. Tyson E. Ochsner

Dr. Ye Liang

ACKNOWLEDGMENTS

I express deep gratitude to my advisor Dr. Phillip Alderman for his unwavering support and guidance throughout the Ph.D. program. The knowledge and skills I learned from him are invaluable assets for my professional career. I acknowledge Dr. Brett Carver, Dr. Tyson Ochsner, Dr. David Marburger, and Dr. Ye Liang for serving in my advisory committee and for their inputs in shaping this study. I am thankful to Dr. Romulo Lollato for providing the datasets. I sincerely thank Dr. Nora Bello for her thoughtful comments on my manuscripts and for helping me with data analysis. I am grateful to my colleagues Andrew Baird, Brandon Vaverka, Blake MacNelly, and Dr. Uvirkaa Akumaga for a cordial workplace, in addition to their immense help during the data collection process. I thank Tina Johnson, Nathan Stepp, and Robert Calhoun for their coordination during data collection. A special thank you to my friends and family for their love and support while I went through this journey. Finally, I dedicate this dissertation to my parents, who are the foundation behind my achievements.

Acknowledgments reflect the views of the author and are not endorsed by committee members or Oklahoma State University.

Name: PRATISHTHA POUDEL

Date of Degree: JULY, 2021

Title of Study: A STUDY OF WINTER WHEAT GROWTH AND DEVELOPMENT IN OKLAHOMA USING A HIERARCHICAL BAYESIAN APPROACH

Major Field: CROP SCIENCE

Abstract: In this dissertation, we discussed the underlying mechanisms behind growth and yield patterns in Oklahoma wheat and simultaneously introduced a unique approach to data analysis in crop science. First, the relationships between wheat yield, yield components, and weather variables were explored to understand source-sink balance. The analysis was performed using a Bayesian hierarchical model. Bayesian analysis quantifies uncertainties around the parameter values which helps to realize confidence in the results. Environmental factors were found to explain more yield variability than genotypic factors and wheat yield was found to be limited by both source and sink in Oklahoma. Second, wheat growth patterns in Oklahoma were investigated using a repeated measures dataset on leaf area index and biomass using a dynamic ordinary differential equation (ODE) modeling approach within a Bayesian hierarchical framework. Dynamic crop models are often complex with many parameters which limit their scope. In this dissertation, we have proposed a simple dynamic ODE model with few parameters. The proposed dynamic ODE model was also compared to a traditional data analysis method (linear mixed model) for repeated measures data. Results showed that neither model outperformed the other in terms of prediction. However, the dynamic ODE model offered an advantage of biologically meaningful parameters that was not apparent with the linear models. Third, the dynamic ODE model was extended to include a water balance component in order to investigate how changes in soil moisture throughout the growing season impacts wheat yield production. It was established that the water balance component is most important to make yield predictions under water limiting conditions. Further research is required to overcome the limitations of the water balance model.

TABLE OF CONTENTS

Chapter Page

Chapter Page

LIST OF TABLES

LIST OF FIGURES

Figure Page

CHAPTER I

GENERAL INTRODUCTION

Wheat (*Triticum aestivum* L.) is grown in almost all regions of the world with a total of 220 million planted hectares making it the most widely grown crop worldwide (Braun, Atlin, & Payne, 2010). This diversity is sustained by different wheat genotypes tailored to fit a specific growing environment through continuous breeding and selection procedures. These genotypes, however, differ in growth patterns and productivity both across and between environments since the environments are a dynamic entity characterized with space, time, or both.

Understanding the physiological mechanisms behind wheat growth and yield dynamics will allow the breeding programs to refine their goals and strategies. Breeding strategies are mainly associated with modification of certain plant traits, which in turn are a function of the physiological mechanisms. The goal of this project was to explain underlying mechanisms behind wheat growth and yield production while simultaneously introducing new statistical methodologies for data analysis with an intent to better understand the system.

This study was conducted in the United States in the state of Oklahoma, which has variable climatic conditions resulting in diverse environments. Temperature and precipitation are important meteorological factors contributing to yield variability in this region because most of the wheat is rainfed. Precipitation patterns vary from year to year and location to location in Oklahoma. For instance, in 2020, the cumulative annual precipitation across Oklahoma ranged from 258 mm in Boise city, OK (Northwest region of the state) to 1977 mm in Mt. Herman, OK (Northeast

region of the state) and in the past 20 years, the average annual rainfall throughout the state has ranged from 3976 mm in 2012 to 8603 mm in 2015. It has been reported that wheat yields are water limited if growing season rainfall is less than 250 mm (Patrignani, Lollato, Ochsner, Godsey, & Edwards, 2014). Wheat is the predominant crop in Oklahoma with more than 1.7 million hectares planted every year (USDA, 2019); 97.1% of which is occupied by hard red winter wheat (HRWW) (Vitale, Adam, & Vitale, 2020).

Wheat yields have been stagnant in Oklahoma since 1980 (Patrignani et al., 2014), but the inter-annual yield variability has increased (Vitale et al., 2020). Munaro et al. (2020) show that for Colorado, Kansas, and Oklahoma the environmental difference across years and locations accounted for 46% of wheat yield variability. Munaro et al. (2020) also found that the minimal effect of genotype on yield variability is a result of the good adaptation of the performance trial genotypes to the region. Furthermore, wheat yields are reported not to be limited by genetic potential because achievable yields have been reported up to 6.59 $Mg\ ha^{-1}$, whereas average state yield is only about 2 $Mg\ ha^{-1}$ (Patrignani et al., 2014).

This dissertation explored the yield and growth dynamics of wheat in Oklahoma under different environmental conditions with three studies, one of which addressed the yield variability across genotypes and environments and the two that explored the growth patterns in a single geotype (Iba) across different environments. In addition, this dissertation also utilized an unconventional approach to analyze the datasets to capture the non-linearity and randomness in the system.

Different methodological approaches have been used to analyze the multi-environment trial data in order to investigate G $\times$ E interaction. The most frequently used statistical modeling approaches are different types of regression analyses (Mohammadi & Amri, 2008; Williams, O'Brien, Eagles, Solah, & Jayasena, 2008; Yan & Hunt, 2001). Some common approaches are linear mixed model (Munaro et al., 2020), partial

least squares regression (M. Reynolds, Trethowan, Crossa, Vargas, & Sayre, 2002), principal component analysis (Yan & Hunt, 2001), analysis of variance (Williams et al., 2008), and non-parametric methods (Mohammadi, Abdulahi, Haghparast, & Armion, 2007). Most of these analyses are traditionally performed within a frequentist framework, whereas few research have used Bayesian framework to study G $\times$ E interaction (Montesinos-López et al., 2019; Cuevas et al., 2017; Cotes, Crossa, Sanches, & Cornelius, 2006). In addition to these, dynamic crop models such as DSSAT (Jones et al., 2003b) and APSIM (Keating et al., 2003) are frequently used to simulate crop growth and to understand G $\times$ E interaction in crops (Anar et al., 2019; Attia et al., 2016; Scott C Chapman, 2008; S. Chapman, Cooper, Hammer, & Butler, 2000). In between the ends of this spectrum from purely statistical to complex dynamic models, we have proposed a simple dynamic model within a statistical framework in this dissertation.

We introduced an ordinary differential equations (ODE) modeling approach in conjunction with the Bayesian framework in the second study. The system of ODE models is commonly utilized in many crop models such as DSSAT and APSIM. Ordinary differential equations (ODEs) are a system of equations that characterize the changes of a response variable (e.g. yield, biomass, etc.) with respect to time (Hoops et al., 2016). However, the ODE models are often deterministic i.e. the output is determined based on initial conditions and the parameter values, while any random components that may be present in a system are left unaddressed. On the contrary, the statistical models such as linear regression are statistically robust but lack other important features of ODE models. Thus, in this project, we combined the two types of models in order to leverage the strengths of both and introduce stochasticity into ODE modeling.

Furthermore, a Bayesian hierarchical framework was used for data analysis. Bayesian analysis is gaining popularity in recent days due to its ability to quan-

tify uncertainties around the parameter values rather than obtaining a single value estimate for a parameter (Alderman & Stanfill, 2017). This is especially true in cases of dynamic models where selecting a reliable parameter value is of paramount importance since the estimated parameter acts as a connection between observations and simulations. A measure of uncertainty or a distribution around these values help researchers to realize the confidence in their results. In addition, Bayesian framework also allows us to utilize prior information on a system in the forms of prior distribution. For highly researched areas, informative priors can be used, whereas for novel research areas, a vague prior can be constructed. A vague prior refers to a distribution which is wide enough to encompass all possible values of a parameter while avoiding theoretically impossible ranges. Lastly, advanced computational tools have made sampling from the posterior distribution, and quantifying and visualizing the distributions easier.

This dissertation is comprised of three studies. The first study is addressed in Chapter 2 in which we explored eco-physiological mechanisms behind yield variability in Oklahoma with a Bayesian hierarchical framework. This chapter provides insight into G $\times$ E interaction in Oklahoma wheat with data on fifteen genotypes and eight environments. This was a field based study where data were collected from the Oklahoma State University wheat variety performance trials at three locations and three years from a total of fifteen genotypes. The objectives of this study were to explain wheat yield as a function of yield components and to assess their association with weather conditions.

Chapter 3 addresses the second study which involved two separate analyses on the same dataset, one using a linear model and one with a dynamic ODE model thereby comparing and contrasting these two methods. A repeated measures growth dataset on LAI and biomass on a single wheat genotype across multiple environments was utilized from a previous study by Lollato and Edwards (2015). The objective of this

chapter was to propose a new methodology to analyze repeated measures data while simultaneously delivering physiological inferences.

Chapter 4 addresses the third study in which we extend the dynamic ODE model in Chapter 3 to include a simple water balance model. The objectives of this study were to understand the impact of water availability throughout the growing season on wheat growth and yield, to quantify the level of improvement in model prediction after adding water balance, and to investigate the impact of data availability and diversity on model performance.

The final chapter summarizes findings from the preceeding chapters and draws some general conclusions. Hence, the unique contributions of this dissertation project are to add to the understanding of winter wheat growth and yield dynamics in Oklahoma by identifying the underlying processes, and to introduce a new analytical framework for data analysis to potentially facilitate biological interpretations from statistical analyses.

CHAPTER II

ECOPHYSIOLOGICAL MODELING OF YIELD AND YIELD COMPONENTS IN WINTER WHEAT USING HIERARCHICAL BAYESIAN ANALYSIS

2.1 Abstract

Yield components are widely recognized as drivers of wheat (*Triticum aestivum* L.) yield across environments and genotypes. In this study, we used a hierarchical Bayesian approach to model wheat grain yield in Oklahoma on an eco-physiological basis using yield component traits thousand kernel weight (TKW) and non-yield biomass (NYB). The main objectives of this study were to 1) explain wheat yield as a function of component traits TKW and NYB, thus examine source-sink balance, and 2) assess their association with weather conditions during key stages of wheat development. Fifteen wheat genotypes planted in three locations in Oklahoma (Altus, Chickasha, and Lahoma) were evaluated across three harvest years (2017 to 2019), whereby the combination of location and year defined an environment. Results indicate that the environment explained the greatest proportion of the variability in yield than genotypes or than genotype-by-environment (G $\times$ E) interaction; however, evidence for G $\times$ E was substantial. Yield was expected to increase with increasing TKW and NYB, which would suggest a source limitation to achieve potential yield. Yet, the contribution of reproductive stage weather variables to the relationship between yield and NYB pointed in the direction of sink strength being compromised. In summary, our approach provides evidence for source-sink co-limitation in grain yield of this

sample of hard red winter wheat genotypes.

2.2 Introduction

Wheat (*Triticum aestivum L.*) is a staple food crop in many countries that supplies the most calories and protein to the population worldwide (Peña-Bautista, Hernandez-Espinosa, Jones, Guzmán, & Braun, 2017). However, wheat genotypes, wheat-growing environments, and wheat yields differ worldwide across regions, years, and growing seasons. Climate variation was found to explain 32-39% of inter-annual yield variability in maize, rice, wheat, and soybean globally (Ray, Gerber, MacDonald, & West, 2015). Yield variability exists not only between different regions in the world but also within the specific regions across locales and growing seasons. Understanding the mechanisms behind yield variability within a wheat-growing region would allow breeding programs to develop wheat genotypes tailored to reduce the gap between the maximum attainable yield and observed yield.

This study was conducted in the United States in the state of Oklahoma. The wide range of environments across the state makes it an ideal region to study yield variability as a result of variable weather conditions. A wide range of environmental conditions are present in Oklahoma driven mostly by a temperature gradient from south to north and a precipitation gradient from east to west, along with yearly fluctuations in temperature and precipitation patterns (Tian & Quiring, 2019). As a result, wheat yields are variable across the state (Calhoun et al., 2019; USDA, 2019). For instance, in 2019, wheat yield ranged from 1.8 ton/ha in Southwest Oklahoma to 4.2 ton/ha in East Central Oklahoma (USDA, 2019).

Environmental effects (E), different genotypes (G), and genotype-by-environment (G $\times$ E) interactions play an important role in explaining yield variability (Mohammadi et al., 2010; Roozeboom, Schapaugh, Tuinstra, Vanderlip, & Milliken, 2008). Specifically, G $\times$ E effects on wheat yield are ultimately driven by different physiological

mechanisms. For instance, the crop environment at the early reproductive stages of plant growth impacts wheat yield primarily through changes in grain number (Ugarte, Calderini, & Slafer, 2007; R.A. Fischer, 1985) whereas the environmental conditions during anthesis and the grain filling stage can affect wheat yield mainly via changes in grain size (Serrago & Miralles, 2014; Wardlaw & Moncur, 1995). These traits are simultaneously driven by the combined effects of genetics and environmental impact, thus leading to G $\times$ E interaction.

Multi-environment trials are a well-established component of crop breeding programs to study G $\times$ E interactions. These trials are important to characterize the performance of wheat genotypes over a wide range of environments. In this study, we utilize data from wheat variety performance trials, a multi-environment trial, conducted yearly by Oklahoma State University (OSU). Most multi-environment trials focus mainly on yield (Sukumaran, Crossa, Jarquin, & Reynolds, 2017; Mohammadi et al., 2010; Roozeboom et al., 2008; Kaya, Akcura, Ayranci, & Taner, 2006) as this is one of the more important outcomes of a variety, for which producers base their choice. Yet, yield data provides limited insight into the mechanisms for differential responses of genetic varieties to changing environments. Grain yield is a function of multiple component traits including kernel weight and size, kernels per spike, spikes per tillers, and the number of tillers amongst others, each at different levels of trait plasticity (Gustavo A Slafer, Savin, & Sadras, 2014). Stable components of yield such as grain size are placed at the lowest level of trait plasticity denoting that they are mostly governed by genetic factors. In turn, components such as the number of tillers show high plasticity as they are highly influenced by the environment (Victor O Sadras & Slafer, 2012). We postulate that further partitioning of yield into its component traits could help explain the observed variability in yield and thus increase the quality of predictions.

Wheat yield can be effectively partitioned into two main yield component traits,

namely grain number and average grain weight; these are modulated by a source-sink balance (RA Fischer, 2008; Ugarte et al., 2007). In most conditions, wheat is a sink limited crop (Borrás, Slafer, & Otegui, 2004). Sink limitations are due to stress during early reproductive stages, which leads to the setting of fewer grains than what can be filled later during grain filling. In contrast, post-anthesis abiotic and biotic stresses can reduce grain size or weight; this is an example of a source limited condition. The balance between source and sink is crucial to realizing yield potential.

Ultimately, our goal is to explain wheat yield variability on an eco-physiological basis. The main objectives of this study were to 1) explain wheat yield as a function of component traits thousand kernel weight (TKW) and non-yield biomass (NYB), thus examine source-sink balance, and 2) assess their association with weather conditions during key stages of wheat development. We leverage a hierarchical Bayesian modeling framework to naturally reflect the hierarchical features of the biological question. Thus, as a secondary objective, we introduce Bayesian estimation for eco-physiological modeling.

2.3 Materials and Methods

The samples for this study were collected from the wheat variety performance trials conducted by OSU on a yearly basis. The OSU wheat variety testing program features replicated trials at more than 20 different test sites and nonreplicated trials at more than 40 demonstration sites, representing major wheat-growing areas in the state.

2.3.1 Wheat genotypes included in this study

For this study, we selected wheat genotypes based on acreage planted in Oklahoma (Table 2.1). Some of the genotypes included in this study changed across years as newer varieties replaced older ones. The genotypes selected for this study showed a range of plant heights, maturity, yield potential, disease resistance, test weight, kernel

Table 2.1: Wheat genotypes included in this study by season.

Genotypes	2016-17	2017-18	2018-19
Bentley		X	X
Billings	X		
Doublestop CL+	X	X	X
Duster	X	X	X
Endurance	X		
Gallagher	X	X	X
Iba	X	X	X
LCS Chrome		X	X
Lonerider		X	X
Ruby Lee	X	X	X
Smith's Gold		X	X
SY Achieve CL2		X	X
SY Flint	X	X	X
SY Llano	X		
WB4458	X	X	

size, drought tolerance, Hessian fly resistance, and dual-purpose suitability, but all were intended to represent the diversity of wheat grown in Oklahoma (Marburger, Hunger, Carver, & Royer, 2018; OSU Small Grains Extension, 2020). For example, the wheat genotypes Doublestop CL+, Endurance, and Iba were chosen for their late maturity, whereas Gallagher, Lonerider, SY Achieve CL2, and SY Llano are chosen for their early maturity; meanwhile, Billings, SY Flint, and WB4458 were chosen for their medium-early maturity. Likewise, Billings has a high grain-only yield potential but is not suitable for dual-purpose systems (Hunger et al., 2014) whereas Smith's Gold has excellent yield potential and is suitable for both grain-only and dual-purpose production systems. Bentley has yield stability under drought conditions but lower test weight, and Doublestop CL+ has yield stability across a wide range of environments along with high test weight (OSU Small Grains Extension, 2020). The genotypes also differ in disease resistance; Billings, Duster, Gallagher, Iba, and LCS Chrome exhibit good stripe and leaf rust (caused by *Puccinia striiformis* and *Puccinia triticina*) resistance, whereas Bentley, Doublestop CL+, Endurance, Smith's Gold, and SY Flint are moderately resistant. Meanwhile, Ruby Lee is moderately susceptible to stripe rust only. Furthermore, Duster has above-average tillering capacity with intermediate straw strength whereas LCS Chrome has both high tillering ability and good straw strength (Marburger, Hunger, et al., 2018).

2.3.2 Sites and management description

For this study, a total of three sites were selected for sample collection from the set of locations within the OSU wheat variety performance trials, namely Altus, Chickasha and, Lahoma. The selected sites represent diversity in latitude, longitude, elevation, climatic conditions, and soil types across the state (Table 2.2). The seasonal rainfall and temperature estimates for the months of October through June were calculated from the preceding fifteen years of data (2003-4 to 2018-19) obtained from nearby

Table 2.2: Description of experimental sites included in the study. Average seasonal cumulative rainfall (Rainfall) and average seasonal temperature (Temperature) from October through June calculated from the preceding fifteen years of data (2003/4 to 2018/19) obtained from nearby Oklahoma Mesonet stations.

Site	Latitude	Longitude	Elevation (m)	Rainfall (mm)	Temperature (°C)	Soil type
Altus	34.63 N	99.33 W	426	388	12 ± 7.94	Hollister silty clay loam
Chickasha	35.05 N	97.94 W	339	534	11.1 ± 7.9	Dale silt loam
Lahoma	36.39 N	98.09 W	380	437	9.87 ± 8.16	Pond creek silt loam

stations of the Oklahoma Mesonet (McPherson et al., 2007; Brock et al., 1995). All trials were conducted as a randomized complete block design (RCBD) with four replicates using a conventional tillage system. Trials at each site followed standard management practices for the area, with a 67 $kg\ ha^{-1}$ seeding rate and 56 $kg\ ha^{-1}$ of 18-46-0 ($N - P_2O_5 - K_2O$) applied in-furrow at the time of planting, using a Hege 500 small-plot cone seeder (Wintersteiger). Each plot consisted of eight rows spaced 15 cm apart.

2.3.3 Experimental design and data collection

Data were collected at the three sites over the course of three growing seasons (2016-17, 2017-18, and 2018-19), excluding Altus in 2016-17. Thus, we used the combination of site and year to define eight environments. A total of ten genotypes were sampled in the first year, twelve in the second year, and eleven in the third year from each site. Thus, not all genotypes were observed in all environments.

From each plot in each of the four field replicates, a meter row of the selected genotypes (0.5m on two 'second from outer' rows) was hand-harvested at physiological maturity with a sickle at ground level to produce one sample per plot. Samples were dried for 72 hours at 60 °C. An ALMACO Plant and Head Thresher (Allan Machine Company, Ames, IA) was used to thresh the samples, and dry biomass and grain weights were recorded for each plot. Yield ($g\ m^{-2}$) was calculated from sample grain weight. Non-yield biomass (NYB; g) was calculated by subtracting the sample grain weight (g) from total sample biomass (g).

Average kernel weight (mg) was obtained for each sample using the Single Kernel Characterization System 4100 (SKCS, Perten Instruments North America Inc., Springfield, IL) following standard operating procedures as outlined in the instruction manual (Instruments, 1995). From a sample of approximately 20 g per field plot, the SKCS 4100 provided a mean, standard deviation, and distribution for single kernel weight (mg) of 300 machine-singulated sound kernels(Osborne & Anderssen, 2003; Martin, Rousser, & Brabec, 1993). Thousand kernel weight (TKW; g) was calculated from the mean obtained for SKCS kernel weight.

Data on weather variables, daily values of minimum and maximum temperatures (°C), precipitation (mm), and solar radiation (MJm^{-2}), were obtained from the Oklahoma Mesonet for each location and year (McPherson et al., 2007; Brock et al., 1995). The air temperature was calculated as the average of minimum and maximum temperatures. Cumulative precipitation, average solar radiation, and average air temperature were calculated to summarize the weather variables over two growth periods per season to represent the reproductive stage (from six weeks prior to the heading date until two weeks after it) and grain filling stage two weeks after the heading date until two weeks prior to the harvest date for each trial. Heading dates and harvest dates were obtained from the variety performance trial reports (Calhoun et al., 2019; Marburger, Calhoun, Carver, et al., 2018; Marburger et al., 2017).

2.3.4 Model specification and data analysis

Although the individual field trials followed a RCBD design, the combination of multiple trials for data analysis reflected a split-plot like structure where the field trials served as main plots. Each field trial correspond to a unique site-year combination or environment as described above. A basic statistical model was specified to reflect the structure of the whole dataset. Specifically, random effects included in the linear predictor were environment, block nested within an environment (the blocking structure for genotypes), genotype, and G× E. The residual represented the remaining noise at the individual plot level. Three alternative models were specified according to the objective of explaining yield as a function of its component traits, namely:

Alternative 1) Model including Genotype × Environment effects (Model GE):

Model GE:

$$Y_{ijk} = \beta_0 + Env_k + Geno_j + [Geno * Env]_{jk} + Block[Env]_{i[k]} + e_{ijk} \qquad (2.3.1)$$

where,

Y_{ijk} = Observed yield ($g\ m^{-2}$) from the plot corresponding to the i^{th} block (i = 1, ..., 4) in the k^{th} environment (k = 1, ..., 8) planted with the j^{th} genotype (j = 1, ..., 15).

β_0 = Overall intercept, interpretable as expected yield for a "typical" genotype in a "typical" environment, whereby typical is defined as the population expectation for genotypic effects, environmental effects and their combination i.e. $E(Geno_j) = E(Env_k) = E(Geno * Env)_{jk} = 0$.

$Geno_j$ = Differential effect of the j^{th} genotype, assumed $Geno_j \sim NIID(0, \sigma^2_{geno})$

Env_k = Differential effect of the k^{th} environment, assumed $Env_k \sim NIID(0, \sigma^2_{env})$

$[Geno * Env]_{jk}$ = Differential effect of the j^{th} genotype planted in the k^{th} environment, assumed $[Geno * Env]_{jk} \sim NIID(0, \sigma^2_{ge})$.

$Block[Env]_{i[k]}$ = Differential effect of the i^{th} block nested within the k^{th} environment and assumed $Block[Env]_{i[k]} \sim NIID(0, \sigma_b^2)$.

e_{ijk} = Residual unique to the observation collected on ijk^{th} plot and assumed $e_{ijk} \sim NIID(0, \sigma_r^2)$

Alternative 2) Model including effects of Genotype $\times$ Environment and yield components (Model GE-YC):

Model GE-YC:

$$Y_{ijk} = \beta_0 + Env_k + Geno_j + \beta_1 * nyb_{ijk} + \beta_2 * tkw_{ijk} + [Geno * Env]_{jk} + Block[Env]_{i[k]} + e_{ijk} \quad (2.3.2)$$

where,

$Y_{ijk}, \beta_0, Env_k, Geno_j, [Geno * Env]_{jk}, Block[Env]_{i[k]}$, *and* e_{ijk} are as previously defined for model GE.

nyb_{ijk} = Observed NYB corresponding to the plot in the i^{th} block of the k^{th} environment planted with the j^{th} genotype, and expressed as the deviation from its mean.

tkw_{ijk} = Observed TKW corresponding to the plot in the i^{th} block of the k^{th} environment planted with the j^{th} genotype, and expressed as the deviation from its mean.

β_1 = Slope coefficient, indicating the rate of change of yield per unit increase in NYB, for a typical genotype and environment as previously defined.

β_2 = Slope coefficient, indicating the rate of change of yield per unit increase in TKW for a typical genotype and environment as previously defined.

Alternative 3) Model including Genotype $\times$ Environment and a hierarchical specification of yield components (Model GE-YC-hierarchy):

Model GE-YC-hierarchy:

$$Y_{ijk} = \beta_0 + Env_k + Geno_j + \beta_{nyb,k} * nyb_{ijk} + \beta_{tkw,k} * tkw_{ijk} + [Geno * Env]_{jk} + Block[Env]_{i[k]} + e_{ijk} \quad (2.3.3)$$

with a hierarchical specification of yield components such that:

$$\beta_{nyb,k} = \beta_{10} + \beta_{11} * temp1_k + \beta_{12} * srad1_k + \beta_{13} * rain1_k \quad (2.3.4)$$

$$\beta_{tkw,k} = \beta_{20} + \beta_{21} * temp2_k + \beta_{22} * srad2_k + \beta_{23} * rain2_k \quad (2.3.5)$$

where,

$Y_{ijk}, \beta_0, Env_k, Geno_j, [Geno * Env]_{jk}, Block[Env]_{i[k]}, \ and \ e_{ijk}$ are as previously defined for model GE; and nyb_{ijk} and tkw_{ijk} are as previously defined for model GE-YC.

$temp1_k, \ srad1_k, \ rain1_k$ = Temperature, solar radiation, and precipitation, respectively, for the k^{th} environment during the reproductive growth stage, expressed as the deviations from their respective means.

$temp2_k, \ srad2_k, \ rain2_k$ = Temperature, solar radiation, and precipitation, respectively, for the k^{th} environment, during the grain filling stage, expressed as the deviations from their respective means.

β_{10} = Intercept for the hierarchical specification of NYB, indicating the expected rate of change of yield per unit increase in NYB for a typical genotype at average temperature, precipitation, and solar radiation for the reproductive growth stage.

$\beta_{11}, \beta_{12}, \beta_{13}$ = Expected change in the slope of NYB on yield per unit increase of temperature, solar radiation, and precipitation, respectively, during the reproductive growth stage.

β_{20} = Intercept for the hierarchical specification of TKW, indicating the expected rate of change of yield per unit increase in TKW for a typical genotype at average

temperature, precipitation, and solar radiation during the grain filling stage.

$\beta_{21}, \beta_{22}, \beta_{23}$ = Expected change in the slope of TKW on yield per unit increase of temperature, solar radiation, and precipitation, respectively, during the grain filling stage.

For data analysis, the statistical models were fitted using a hierarchical Bayesian framework.

2.3.5 Prior specification

Specification of priors for all hyperparameters was performed using the prior predictive checks approach proposed by (Schad, Betancourt, & Vasishth, 2019). Briefly, hyperparameters were included in the prior predictive model in a stepwise fashion of increasing model complexity, following model hierarchy from alternative models 1 to 3. At each step, prior predictive checks were performed to ensure that predictions from the priors were within a biologically plausible, though vague, boundary. The boundary was set based on the average wheat yields throughout the world and was allowed to vary up to around 1800 $g\ m^{-2}$, which could be considered weakly informative given that it is in excess of maximum observed wheat yields globally. A prior predictive check was conducted by sampling from the defined priors and simulating model predictions for the variable of interest based on those samples. If the predictions are biophysically plausible, the priors passed the check, but if the priors produce nonsensible predictions, priors were revised to produce predictions aligned with our beliefs and prior knowledge about the system under study. Prior specifications for vague predictions were intended to put the weight of posterior inference on the data. Prior specifications for parameters in modeling alternatives 1-3 are presented next in the form of $N(\mu, \sigma^2)$, such that:

$\beta_0 \sim N(300, 80^2)$

$\beta_1 \sim N(0, 1^2)$

$\beta_2 \sim N(0, 15^2)$

$\beta_{10} \sim N(0, 0.5^2)$

$\beta_{20} \sim N(0, 15^2)$

$\beta_{11} \sim N(0, 1^2)$

$\beta_{12} \sim N(0, 1^2)$

$\beta_{13} \sim N(0, 0.1^2)$

$\beta_{21} \sim N(0, 1^2)$

$\beta_{22} \sim N(0, 0.5^2)$

$\beta_{23} \sim N(0, 1^2)$

$\sqrt{\sigma^2_{env}} \sim N(0, 150^2)$ truncated at zero.

$\sqrt{\sigma^2_{geno}} \sim N(0, 80^2)$ truncated at zero.

$\sqrt{\sigma^2_{ge}} \sim N(0, 10^2)$ truncated at zero.

$\sqrt{\sigma^2_{b}} \sim N(0, 50^2)$ truncated at zero.

$\sqrt{\sigma^2_{r}} \sim N(0, 250^2)$ truncated at zero.

2.3.6 Software implementation

Statistical models were fitted using a hierarchical Bayesian framework based on Hamiltonian Monte Carlo as implemented by the software Stan (Stan Development Team, 2018) through the R statistical software environment (R Core Team, 2020; Stan Development Team, 2019). For each model, four Markov chain Monte Carlo (MCMC) chains with 10,000 iterations and 50% burn-in were run, resulting in a total of 20,000 saved iterations for posterior inference. Traceplots and R-hat values were used to monitor chain convergence (Gelman et al., 2013). Auto-correlations and effective sample size (ESS) for key lower-level parameters were computed. Specifically, the MCMC chains were tuned to ensure that ESS for the hyperparameters σ_{geno}, σ_{env}, σ_{ge}, and σ_b was greater than 3,000 in all models.

Figures were generated using the ggplot2 package in R (Wickham, 2016). The highest posterior density intervals (HDIs) were computed using the HDInterval package

(Meredith & Kruschke, 2018). Figures and tables were generated or rendered using the R packages knitr (Xie, 2020) and kableExtra (Zhu, 2019). The R package tidyverse was used for data cleaning and organization (Wickham et al., 2019; Wickham, Hadley, 2017).

The computing for this project was performed on the TIGER research cloud at the Oklahoma State University High Performance Computing Center using a KVM virtual machine backed by a hypervisor node with dual Intel "Skylake" 6130 CPUs and 768 GB RAM.

2.3.7 Bayesian approach to data analysis

In Bayesian data analyses, estimation of parameters of interest and subsequent inference, as well as predictions, come in the form of posterior densities that are obtained numerically from the MCMC. In contrast, the reader may recall that deterministic methods produce parameter-specific point estimates only. The availability of posterior densities is highly desirable as it provides considerably more information about the parameters of interest (or functions thereof), thus enabling not only point estimation but also assessments of uncertainty. Specifically, from a posterior density, one may select amongst a number of possible location descriptors for the most appropriate point estimate, say mean, median, or mode, depending on the symmetry (or lack thereof) of the posterior density for the parameter of interest. Even more compelling is the fact that posterior densities also enable an assessment of uncertainty around the selected point estimator (Gelman et al., 2013). In a statistical sense, uncertainty is an indicator of precision of the estimate based on the amount of information available in the data, and thus, an indicator of how likely we are to reproduce those estimates under similar conditions. For example, posterior intervals such as Highest Density Interval (HDI), or alternatively, Posterior Probability Interval (PPI) indicate the range of values within which one can expect to find the parameter of interest with 95%

probability (Gelman et al., 2013). These intervals may be considered analogous to the concept of confidence intervals in frequentist statistics, though their Bayesian interpretation is straightforward, thus more intuitive and directly aligned with research objectives. That is, we are 95% confident that the parameter takes values contained within the boundaries of the interval. Specifically, a 95% PPI is the interval in the distribution that contains the middle 95% of the posterior samples and thus has equal tails (Gelman et al., 2013). In turn, the HDI of a posterior distribution is the shortest possible interval which captures 95% of the posterior samples with the highest probability densities (Grieve, 1991). It is worth noting that this statistical definition of uncertainty on individual parameters or individual predictions is different from variability across model-derived point predictions.

In this article, we report posterior summaries for each parameter of interest (and functions thereof) using posterior medians and 95% HDI.

2.3.8 Model comparison

Model 3:GE-YC-hierarchy was our model of preference, because its hierarchical nature offers insights into relevant physiological mechanisms. The model comparison was performed to determine if the added complexity in Model3:GE-YC-hierarchy compromised the predictive ability of the model. Alternative models were compared using statistical metrics for goodness-of fit and predictive ability. Specifically, Bayesian R-squared, and root mean square error (RMSE) were calculated to assess goodness-of-fit, and expected log predictive density (elpd) was calculated in a q-fold cross-validation with Q=10 for each alternative model. Approximately 315 data points were used as training vs 35 holdout data points for each fold of cross-validation.

First, a Bayesian R-squared statistic was calculated for each MCMC iteration (s) as described in Gelman, Goodrich, Gabry, and Vehtari (2019), such that:

$$Bayesian\ R_s^2 = \frac{var(\hat{y})^s}{var(\hat{y})^s + {\sigma_r^2}^s} \tag{2.3.6}$$

where, $\boldsymbol{var(\hat{y})}$ = Variance between predicted values at iteration s, whereby s = 1, 2, ..., S is the length of post-burnin MCMC , ${\sigma_r^2}^s$ = Posterior sample of residual variance (σ_r^2) for each MCMC iteration s.

Then, RMSE was also calculated for each MCMC iteration (s) as:

$$RMSE_s = \sqrt{\frac{1}{N}\sum_{n=1}^{N}(y_n - \hat{y_n}^s)^2} \tag{2.3.7}$$

where, N = Total number of data points, $y_n = n^{th}$ observation, and $\hat{y_n}$ = Predicted value for the n^{th} observation sampled in MCMC iteration s.

Finally, elpd was calculated following equations 20 and 21 in Aki Vehtari, Gelman, and Gabry (2017) such that:

$$elpd = \sum_{q=1}^{Q}\sum_{m=1}^{M_q} log(\frac{1}{S}\sum_{s=1}^{S} p(y_m|\theta^{-q,s})) \tag{2.3.8}$$

where,

Q = The number of folds, M_q = number of observations within the q^{th} fold, S = Number of saved post burn-in MCMC iterations, y_m = data point m within the q^{th} fold, and $\theta^{-q,s}$ = parameters corresponding to the q^{th} holdout subset and iteration s, and $p(y_m|\theta^{-q,s})$ = probability of y_m given $\theta^{-q,s}$.

Models with smaller values of RMSE, and with larger values of Bayesian R-squared, and elpd were considered preferable.

2.4 Results

2.4.1 Model comparison

Table 2.3 shows selected criteria used for model comparison, specifically, Bayesian R-squared and RMSE to assess goodness-of-fit, and elpd to assess the predictive ability

of each alternative model considered. Smaller Bayesian R-squared and larger RMSE both indicate impaired fit of Model 1:GE relative to Models 2:GE-YC and Model 3: GE-YC-hierarchy, thus clearly suggesting a preference for the latter two. Meanwhile, Model 3:GE-YC-hierarchy showed the the largest value of Bayesian R-square and the smallest RMSE. Yet, numerical differences in both fit criteria were minor relative to Model 2:GE-YC, thus indicating little evidence for preference of either model over the other in terms of relative fit to data.

In terms of predictive ability, Model 3:GE-YC-hierarchy performed best, as supported by the smallest elpd value, followed closely by Model 2:GE-YC and lastly by Model1:GE. Model 3:GE-YC-hierarchy and Model 2:GE-YC showed a minor difference in predictive ability, as indicated by an elpd difference close to zero and of smaller magnitude than the standard error of such difference, indicating inadequate evidence in favor of any one model in terms of predictive ability. For further inference, we made the decision to proceed with Model 3:GE-YC-hierarchy based on a combination of 1) best or comparable fit relative to other model alternatives considered in this study, and 2) its hierarchical nature, which enables insight into specific physiological mechanisms contributing to yield differences without compromising predictive ability.

Figure 2.1 illustrates the posterior density of the Bayesian R-squared for Model 3:GE-YC-hierarchy selected for further inference. Notably, the 95% HDI for Bayesian R-squared for this model had a lower bound of 0.88 and an upper bound of 0.91, indicating a 95% probability that Model 3 captures somewhere between 88 to 91% of the variability observed in the data.

2.4.2 Genotypic, Environmental, and G × E effects on wheat yield

Table 2.4 shows posterior inference of variance components for genotypic (σ^2_{geno}), environmental (σ^2_{env}) and G × E effects (σ^2_{ge}), as well as residual-level (σ^2_r), for the alternative models considered in this study. As expected, the addition of NYB and

Table 2.3: Model comparison based on Bayesian R-squared, root mean square error (RMSE; expressed as posterior median [HDI]), and difference in expected log predictive density (elpd_diff ± s.e.; expressed relative to Model 3: GE-YC-hierarchy as Model x - Model 3)

	Bayesian R-squared		RMSE		
Models	Median	HDI	Median	HDI	elpd_diff ± s.e.
1) GE	0.759	(0.718, 0.799)	103.48	(98.29, 109.05)	-142.6 ± 28.0
2) GE-YC	0.896	(0.877, 0.914)	67.86	(64.42, 71.88)	-3.6 ± 28.3
3) GE-YC-hierarchy	0.899	(0.880, 0.917)	66.77	(63.06, 70.71)	0

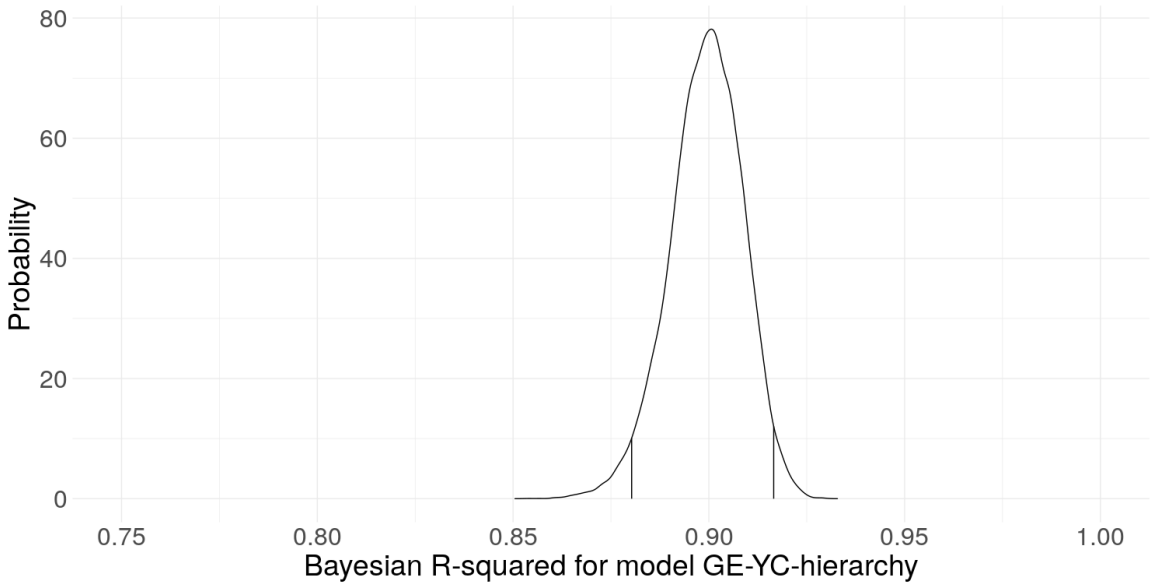

Figure 2.1: Posterior distribution of R-squared and 95 % HDI as indicated by the vertical lines in the density plot.

TKW as explanatory variable to Model 2:GE-YC and Model 3:GE-YC-hierarchy caused a substantial decrease of approximately one order of magnitude in the residual variance (σ_r^2) and the environmental variance (σ_{env}^2) compared to Model 1:GE. Based on the posterior medians for Model 3:GE-YC-hierarchy, environmental variance (σ_{env}^2) showed the greatest magnitude with six times the amount of variance attributed to genotypic effects (σ_{geno}^2) or G $\times$ E interaction (σ_{ge}^2) (Table 2.4). When comparing the point estimates (medians) for genotype-specific and G $\times$ E effects, their magnitudes appear similar, however, upon further analysis, it was found that there is a 61.6% probability that the genotype-specific effects were higher than the G $\times$ E effects.

Figure 2.2 illustrates the posterior median of environment-specific yield predictions for each of the wheat genotypes present in all environments in this study. All predictions were obtained using results from Model 3:GE-YC-hierarchy. Specifically, panel (a) depicts predictions based on effects of G, E, and G $\times$ E at average values of NYB and TKW, whereas panel (b) depicts predictions based on effects of G, E, and G $\times$ E at values of NYB and TKW specific to that environment. Both panels depict presence of G $\times$ E interaction on wheat yield, as indicated by the change in rank of the genotypes across environments. The difference in G $\times$ E patterns depicted by the two panels may be explained by the fact that the contributions of NYB and TKW represent a portion of the G $\times$ E interaction that is attributable to the eco-physiological processes for which they are proxies. Whereas, the term G $\times$ E stated explicitly in Model 3 may be interpreted as the remaining unattributable portion of the environment-specific genotype effect on wheat yield.

2.4.3 Association between yield component traits and wheat yield

Table 2.5 shows posterior summaries for location parameters (β) of Model 3:GE-YC-hierarchy across hierarchical levels. As a benchmark reference, we articulate posterior inference for β_0 indicates that yield for a "typical" genotype member of the population

Table 2.4: Posterior summary (posterior median and 95% highest posterior density interval (HDI)) on variance components (genotype (geno), environment (env), genotype by environment interaction (ge), and residuals (r) for alternative models

	σ^2_{geno}		σ^2_{env}		σ^2_{ge}		σ^2_r	
Models	Median	HDI	Median	HDI	Median	HDI	Median	HDI
1) GE	1102.54	(0.01, 3158.75)	39574.91	(11592.48, 93647.42)	1087.51	(0.0006, 2746.35)	10760.34	(8937.15, 12875)
2) GE-YC	1181.33	(170.21, 3098.04)	4686.17	(428.28, 17098.25)	1218.47	(337.99, 2031.73)	4637.45	(3849.4, 5566.9)
3) GE-YC-hierarchy	1280	(184.33, 3192.07)	7918.37	(1123.51, 27753.57)	1068.13	(282.38, 1974.75)	4490	(3686.04, 5370.17)

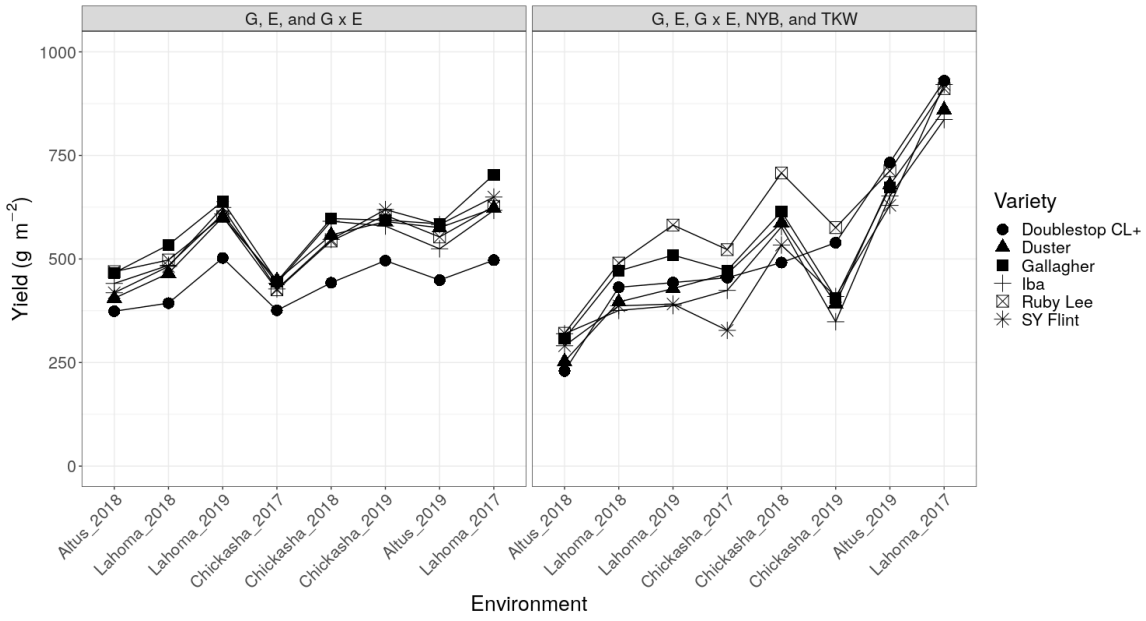

Figure 2.2: Predicted wheat yield for selected genotypes across environments based on Model 3, considering (a) genotype (G), environment (E), and G × E effects at average NYB and TKW, and (b) G, E, G × E effects, as well as non-yield biomass (NYB), and thousand kernel weight (TKW) at the corresponding environments.

in a "typical" environment (i.e. $E(Geno_j) = E(Env_k) = E(Geno * Env)_{jk})) = 0$) at average values of NYB and TKW can be expected to be approximately 490 $g\ m^{-2}$, ranging from 404 to 557 $g\ m^{-2}$, with 95% probability.

Furthermore, posterior inference on β_{10} and β_{20} indicates that one may expect the behavior of wheat yield to change as a function of the sink-source balance represented here by NYB and TKW (Table 2.5). Specifically, posterior inference on β_{10} indicates an expected increase in yield per unit increase in NYB of approximately 0.43 $g\ m^{-2}$, and ranging from 0.38 to 0.47 $g\ m^{-2}$ with 95% probability with typical weather conditions during the reproductive growth stage. The values for NYB in this dataset ranged from 325 to 2326 $g\ m^{-2}$. Taking this range into account, one can expect the yield to change by 140 to 1000 $g\ m^{-2}$ as a result of change in NYB. Likewise, posterior inference on β_{20} supports an expected increase in yield per unit increase in TKW of approximately 13 $g\ m^{-2}$, ranging from 9 to 16 $g\ m^{-2}$, with 95% probability at typical weather conditions during the grain-filling stage. Taking into account the range for TKW in this dataset (14 to 39 g), the yield can be expected to change by 182 to 507 $g\ m^{-2}$ as a result of change in TKW.

2.4.4 Contribution of weather variables to the relationships between yield and yield component traits

Table 2.5 presents posterior summaries on parameters $\beta_{11},\ \beta_{12},\ \beta_{13}$, which characterize the contribution of temperature, solar radiation, and precipitation, respectively, to wheat yield through NYB during the reproductive stage, allowing us to look into source-sink balance in the population. Specifically, at the reproductive stage, solar radiation showed a positive effect on β_{nyb}, that is the expected rate of change of wheat yield as a function of NYB, as indicated by the positive sign of both boundaries of 95% HDI of β_{12}. Specifically, for every one unit ($MJm^{-2}d^{-1}$) increase in solar radiation, one might expect an increase of 0.05 $g\ m^{-2}/g\ m^{-2}$ in the coefficient β_{nyb}

Table 2.5: Posterior median and highest density interval (HDI) for the intercept and the regression coefficients in the Model GE-YC-hierarchy

Parameter	Description	Median	HDI
β_0	Yield at typical conditions	490	(404, 557)
β_{10}	Expected change in yield per unit increase in NYB under average weather conditions during reproductive stage	0.43	(0.38, 0.47)
β_{20}	Expected change in yield per unit increase in TKW under average weather conditions during grain filling stage	13	(9, 16)
β_{11}	Change in β_{10} per unit increase in reproductive stage temperature	0.01	(-0.029, 0.054)
β_{12}	Change in β_{10} per unit increase in reproductive stage solar radiation	0.05	(0.006, 0.098)
β_{13}	Change in β_{10} per unit increase in reproductive stage precipitation	0.01	(-0.001, 0.020)
β_{21}	Change in β_{20} per unit increase in grain filling stage temperature	-0.14	(-1.425, 1.123)
β_{22}	Change in β_{20} per unit increase in grain filling stage solar radiation	-0.002	(-0.961, 0.960)
β_{23}	Change in β_{20} per unit increase in grain filling stage precipitation	0.32	(-0.140, 0.789)

that quantifies the association between wheat yield and NYB, with a 95% probability that this increase ranges between 0.006 and 0.098. Taking into account the range in solar radiation values for this dataset, the change in β_{nyb} can be expected to range from -0.13 to 0.09, on average, as a result of the effects of solar radiation. These values were obtained by multiplying the range for solar radiation values in the data with the median for β_{13}. Furthermore, posterior inference on β_{13} indicates a 96% probability for a positive contribution of precipitation to the expected rate of change of wheat yield as a function of NYB (i.e. β_{nyb}) during the reproductive stage. The contribution of every unit of increased precipitation (cm) to β_{nyb} has a posterior median at 0.01 with a posterior standard deviation of 0.005. In context of this dataset, this effect on β_{nyb} can be expected to range from -0.12 to 0.09. In turn, evidence for a contribution of temperature (β_{11}) to the association between yield and NYB (i.e. β_{nyb}) was weaker, as the HDI for β_{11} shows substantial overlap with the null value zero and the posterior probability of a non-zero positive effect is approximately 70%.

Furthermore, the joint posterior densities for β_{12} and β_{13} indicate a strong correlation between the contributions of precipitation and that of solar radiation to β_{nyb}, that is, the rate of change of yield as a function of NYB during the reproductive stage (Figure 2.3, panel 3). Specifically, this correlation was estimated at 0.83, suggesting the possibility of multicollinearity between these weather contributors. In contrast, the estimated posterior correlations between the contributions of temperature (β_{11}) and any of the remaining weather variables (β_{12} and β_{13}) to β_{nyb} was small, at –0.06 and –0.01 respectively (Figure 2.3, panels 1 and 2 respectively).

Table 2.5 also shows posterior inference on parameters $\beta_{21},\ \beta_{22},\ \beta_{23}$, which characterize the TKW-mediated contribution of temperature, solar radiation, and precipitation, respectively, to wheat yield during the grain filling stage thus providing further insight into source-sink balance. Specifically, posterior inference on β_{23} further indicates a 91% probability for a non-zero positive contribution of precipitation to the

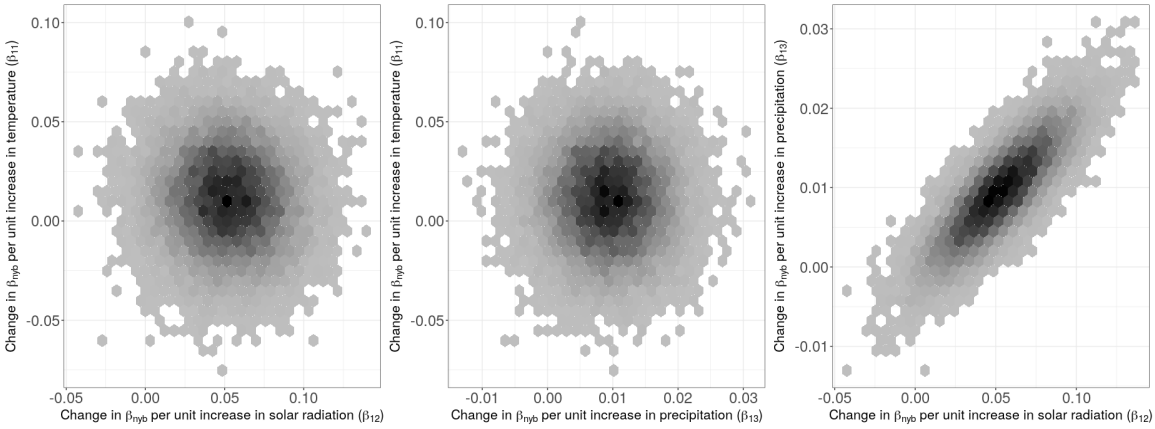

Figure 2.3: Pairwise joint posterior densities for parameters β_{11}, β_{12}, β_{13} characterizing the contribution of weather variables to the relationship between yield and NYB during the reproductive stage.

expected rate of change of wheat yield as a function of TKW (i.e. β_{tkw}) during the grain filling stage. The contribution of every unit of increased precipitation to β_{tkw} had a posterior median at 0.32 with a posterior standard deviation of 0.24. For this dataset, this effect on β_{tkw} can be expected to range from -2.36 to 4.73. By contrast, posterior inference for the remaining coefficients β_{21} and β_{22} showed 95% HDIs that overlapped with zero, thus suggesting little, if any contributions of temperature and solar radiation to wheat yield through TKW, given the range of temperature in this dataset. In addition, posterior correlations between β_{21}, β_{22}, β_{23} during the grain filling stage were small in magnitude (below 0.25) (Figure 2.4) suggesting negligible dependence between weather contributions to source mechanisms for wheat yield.

2.5 Discussion

In this study, we implemented a hierarchical Bayesian approach to model wheat yield in Oklahoma on an eco-physiological basis, that is, as a function of two yield component traits related to sink-source relations, namely non-yield biomass (NYB) and thousand kernel weight (TKW). We further leveraged hierarchical models to

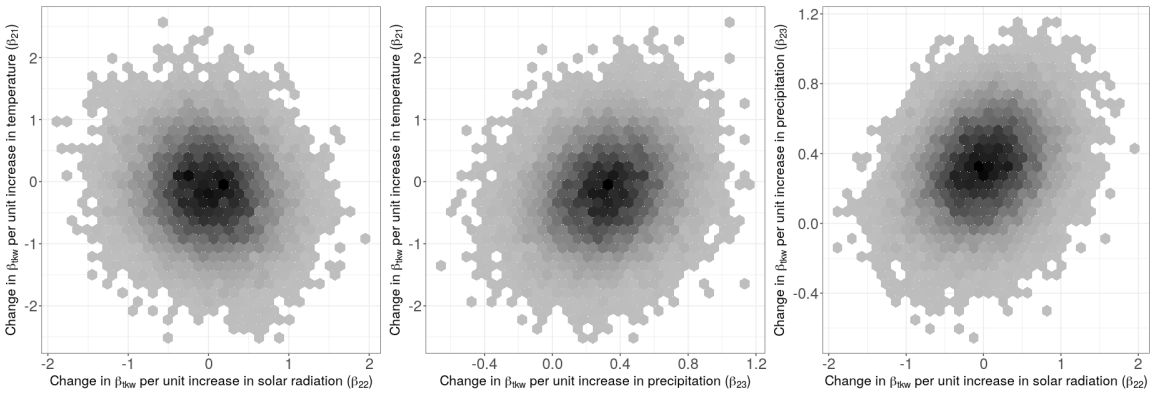

Figure 2.4: Pairwise joint posterior densities for parameters β_{21}, β_{22}, β_{23} characterizing the contribution of weather variables to the relationship between yield and TKW during the grain filling stage.

assess the contribution of weather variables to the relationships between yield and yield component traits at different growth stages.

2.5.1 Model comparison

Based on a combination of model fit criteria and hierarchical structure of the biological question of interest, we proceeded with inference using Model 3:GE-YC-hierarchy. In particular, Bayesian R-square indicated that the selected model was well suited to fit the data, as its posterior density was centered at 0.89 with a lower HDI bound of 0.85. In addition, the estimated RMSE for this model was 67 $g\ m^{-2}$, which is within range of other reports in the literature ranging from as low as 10 $g\ m^{-2}$ up to 150 $g\ m^{-2}$ (Huang et al., 2016; Z. Li et al., 2015; Kogan et al., 2013; Nain, Dadhwal, & Singh, 2004).

2.5.2 Genotypic, Environmental, and G $\times$ E interaction effects on yield

In this section, we interpret the changes in variance components for environment (σ^2_{env}), genotype (σ^2_{geno}) and G $\times$ E (σ^2_{ge}) interaction across alternative models, GE, GE-YC, and GE-YC-hierarchy. Recall that Model 1:GE did not account for yield component

traits NYB and TKW. As a result, a large portion of the total variability likely fell to the environment. The posterior estimates for environmental variance decreased by an order of magnitude when yield component traits were added in Model 2:GE-YC and Model 3:GE-YC-hierarchy, indicating that a large proportion of the variance originally explained by the environment and left-over noise in Model 1:GE was explained by the yield component traits in Models 2:GE-YC and 3:GE-YC-hierarchy. The inclusion of yield components NYB and TKW in models 2:GE-YC and 3:GE-YC-hierarchy were intended to help explain yield variation in terms of eco-physiological mechanisms. In turn, the similarity in magnitudes of variance estimates for genotypic and G $\times$ E components across all three models suggest that NYB and TKW do not explain the variance associated with genotype and G $\times$ E interaction effects.

For Model 3:GE-YC-hierarchy, based on the point estimates (medians) of the posterior distributions for the variance components for genotypic, environmental, and G $\times$ E interaction effects ($\sigma^2_{geno}, \sigma^2_{env}$, and σ^2_{ge}, respectively), σ^2_{env} was found to be the largest by at least 6-fold (Table 2.4). In addition to this point estimate, the HDI for σ^2_{env} also indicates much larger lower and upper bounds compared to the HDIs for σ^2_{geno} and σ^2_{ge} (Table 2.4). This suggests that the environment (i.e. site-year) accounted for a considerable part of the total variability in wheat yield. In turn, posterior medians for σ^2_{geno} and σ^2_{ge} were on a comparable order of magnitude indicating that genotypic effects as well as G $\times$ E interaction effects explain yield variability comparably. However, upon subsequent analysis, it was revealed that the probability of effect of genotype-specific effects on wheat yield is higher than the effect of G $\times$ E interaction. Although small, the G $\times$ E effects were manifested as re-ranking of genotypes across environments. For instance, SYFlint was ranked in the lowest half for yield in Altus_2018, but ranked highly the following year, particularly in the Altus_2019 environment (Figure 2.2).

In terms of overall growing conditions of the environments, the growing season of

2016-17, i.e. harvest year 2017, reportedly showed optimal growing conditions (Marburger et al., 2017). However, during that season, the Chickasha site suffered a severe and early infection of leaf rust (Marburger et al., 2017); this is probably the reason behind Chickasha_2017 being the lowest yielding environment. On the other hand, the growing conditions during the season of 2017-18 in Oklahoma were characterized by overall cooler temperatures at early growth stages and record cold temperatures in April with a spring-freeze, thus resulting in slow growth and development of the crop (Marburger, Calhoun, Carver, et al., 2018). Weather conditions in Oklahoma were further compounded with hotter temperatures and lack of rainfall during the grain filling stage, including record hot temperatures in May (Marburger, Calhoun, Carver, et al., 2018). Finally, the 2018-2019 growing season had mostly favorable growing conditions for both growth and development and grain filling stages, with some exceptions of wet conditions and waterlogged soil at the time of harvest in some locations (Calhoun et al., 2019).

2.5.3 Association between wheat yield and yield component traits

One of the objectives of this study was to model wheat yield as a function of yield component traits to be able to identify physiological mechanisms contributing to source-sink balance. Specifically, we used non-yield biomass (NYB) as a source indicator because it is an independent measure of the source which doesn't contain the variable we are trying to predict (yield). Hence, it can be argued that NYB represents the source more clearly and uniquely than total crop biomass. Specifically, the ratio of yield to NYB can be expressed in terms of Harvest Index (HI) as $Yield/NYB = HI/(1 - HI)$. For clarity and detail, recall that $HI = Yield/Biomass$ and also, $NYB = Biomass - Yield$. One may then express $NYB/Yield = (Biomass - Yield)/Yield$, such that $NYB/yield = 1/(HI - 1)$, leading to re-expressing β_{nyb} as $Yield/NYB = HI/(1 - HI)$. This identity enabled us to draw connections between

our study and the published literature. So defined, HI is commonly used to assess source-sink balance in wheat (Matthew P. Reynolds et al., 2017; H. Zhang, Turner, & Poole, 2010).

The slope parameter connecting wheat yield and NYB, β_{nyb}, is equal to β_{10} at average weather conditions in Model 3:GE-YC-hierarchy. The HDI for β_{10} was (0.38, 0.47 $g\ m^{-2}/g\ m^{-2}$). The positive value of β_{nyb} indicates that source is one of the drivers for yield in these environments. Other studies have reported theoretical maximums for HI in wheat to be 0.62, 0.64, and 0.66 (Foulkes et al., 2011; Shearman, Sylvester-Bradley, Scott, & Foulkes, 2005; Austin et al., 1980). However, the HI for maximum attainable yields in the Southern Great Plains has been estimated at not more than 0.41 (Lollato & Edwards, 2015). In addition, a survey on five different classes of wheat across the United States reported the HI of hard red winter wheat (the most commonly grown wheat in Oklahoma) to be 0.33, the lowest among all wheat classes (Dai et al., 2016). An HI far lower than the attainable HI suggests that yield increase could be achieved through better utilization of available source through improved dry matter partitioning.

Further, our results indicate a positive slope coefficient between wheat yield and TKW (i.e. β_{tkw} in Model3:GE-YC-hierarchy), suggesting that the genotypes in this population did not consistently achieve their genetic potential for TKW across environments. This finding could be interpreted as an insufficient source to match the sink strength, thus a source-sink imbalance in the population within many of the target environments. TKW is generally a stable trait with high heritability. Moreover, we had expected that some portion of the genotypic variance would be explained by the yield component TKW, as this trait is generally considered to vary more between genotypes than between environments (Victor O Sadras, 2007). This expectation is based on the understanding that wheat is generally considered to be a sink-limited crop under many conditions (Alonso et al., 2018; Serrago, Alzueta, Savin, & Slafer, 2013; H. Zhang

et al., 2010; Gustavo A Slafer & Savin, 1994). When the yield is sink-limited, genetic potential TKW is consistently achieved, the yield is limited by grain number, and the relationship between yield and TKW is at or near zero (Gustavo A Slafer et al., 2014; M. Reynolds, Pellegrineschi, & Skovmand, 2005). However, when source-limitation is at play, differences in TKW across environments would be greater than differences between genotypes, resulting in a non-zero slope for the relationship between yield and TKW. Thus, our findings of a positive slope for TKW, and a positive slope between yield and NYB (i.e., an increase in yield with an increase in the source) both point towards source limitation for yield.

2.5.4 Contribution of weather variables in the relationships between yield and yield component traits

We incorporated the weather variables as hierarchical regressors that qualify the nature of the relationship between yield and each of NYB and TKW, thus extending Model 2:GE-YC to Model 3:GE-YC-hierarchy. If the inclusion of hierarchical levels to account for weather variables made any contribution to explaining noise in the data, this contribution seemed to be mild at best, as the posterior density for the residual variance was only slightly decreased in magnitude from Model 2:GE-YC to Model 3:GE-YC-hierarchy (Table 2.4). This is not necessarily surprising as the explanatory role of weather was not at the first hierarchical level of the model; rather, weather variables were fitted at a second level of the model hierarchy, thus intended for a decomposition of the slopes connecting wheat yield to TKW and NYB. The hierarchical structure of the model allowed us to evaluate the contributions of weather conditions to the rate of change of wheat yield as a function of yield component traits. For the reproductive stage, the effects of solar radiation (β_{12}) and precipitation (β_{13}) on the slope of yield vs. NYB (β_{nyb}) were positive. It is noted that these two effects were also tightly correlated with each other a posteriori. This is consistent with

the previously reported relationship between radiation use efficiency and water use efficiency (Caviglia & Sadras, 2001; V. Sadras, Whitfield, & Connor, 1991). Specifically, a positive correlation of substantial magnitude was reported between cumulative water consumed and photosynthetically active radiation intercepted in durum wheat (Rezig, M'hamed, & Naceur, 2015).

Conditions of both higher solar radiation and adequate rainfall are considered favorable for plant growth. Higher solar radiation corresponds to increased photosynthesis and higher assimilate supply, and higher rainfall ensures no drought stress. Therefore, the observed positive effects of solar radiation and precipitation during the reproductive stage (β_{12} and β_{13}) on the rate of change of yield per NYB (β_{nyb}) indicate that the amount of yield produced per unit NYB is higher under favorable conditions. These findings can be interpreted as the source (NYB) being utilized more efficiently for yield formation as a result of better sink strength, given that this is a period when florets are developing and thus, grain number is determined (Ugarte et al., 2007; Savin & Slafer, 1991; R.A. Fischer, 1985).

For the grain filling stage, only precipitation was found to contribute to the rate of yield change per TKW (β_{20}), although the evidence was weaker (i.e. posterior probability $P(\beta_{23} > 0|y) = 70\%$). The positive slope between yield and TKW indicating potential source limitation during grain filling and the weak evidence of weather variables contributing to that points towards other factors that might affect source strength during grain filling such as disease or residual soil moisture. In turn, the evidence of the precipitation effect, although weak, is consistent with a report that the effect of precipitation during the grain filling stage on wheat yield was mainly mediated by TKW (He et al., 2013).

2.6 Conclusion

A major portion of the total variability in wheat yield was explained by the environmental component. The inclusion of yield component traits, namely NYB and TKW, as explanatory variables in the model helped explained a substantial amount of environmental variance but did not seem to help explain genotypic or G $\times$ E variance. A positive relationship was observed between both yield component traits and wheat yield supporting the idea that yield is driven by source mechanisms. However, the fact that the slope of yield as a function of NYB was responsive to weather conditions during the reproductive stage indicates that sink mechanisms may also be at play. These results suggest the presence of source-sink co-limitation in wheat yield.

CHAPTER III

A HIERARCHICAL BAYESIAN APPROACH TO DYNAMIC ODE MODELS FOR REPEATED MEASURES DATA ON WHEAT GROWTH

3.1 Abstract

Experimental data collected on growth and development of plants over a growing season are typically analyzed using a linear mixed model, analogous to a hierarchical linear model in a Bayesian setting. Alternative modeling approaches for repeated measures data involve ecophysiological dynamic models based on a system of ordinary differential equations (ODE). Yet, current implementations of ODE models are mostly deterministic in nature, which negates recognition of uncertainty in the data generation process and thus impairs inference and prediction. In this study, our objectives were to 1) to implement dynamic ODE models using a stochastic Bayesian framework to accommodate uncertainty into the modeling exercise, and 2) to compare performance to traditional linear mixed models for repeated measures. Using a hierarchical Bayesian implementation, we fit both an ODE model and a linear mixed model to data on leaf area index (LAI) and biomass from a winter wheat dataset. In the context of this application, neither modeling approach seemed to outperform the other in terms of goodness of fit or prediction accuracy as indicated by similar values for root mean squared error (RMSE), Willmott's agreement index (d), and Nash-Sutcliffe efficiency (NSE). The prediction statistics for the ODE model and hierarchical linear model, respectively, were: $RMSE_p$ of 1.38 and 1.21, d_p of 0.91 and 0.93, and NSE_p of 0.69

and 0.76 for LAI and $RMSE_p$ of 274.27 and 253.50, d_p of 0.95 and 0.95, and NSE_p of 0.82 and 0.84 for biomass. However, the parameterization of the dynamic ODE model enabled biologically meaningful interpretations relevant to the research question that were not apparent from the linear modeling approach.

3.2 Introduction

In crop production, data are often collected throughout a growing season in order to study the dynamic interplay between plant genetic varieties, management practices, and environmental conditions over time on the growth and development of crops. Crop modeling approaches often use ecophysiological dynamic models based on a system of ordinary differential equations (ODE) that express the growth and development of a cropping system as derivatives with respect to time (Paine et al., 2012). For instance, crop models such as DSSAT (Jones et al., 2003b) and APSIM (Keating et al., 2003) are widely used by crop scientists to describe how the biological system as a whole changes over time based on an ODE core. When integrated numerically, dynamic ODE systems can naturally capture the non-linear evolution of crop growth and development over a season. In addition, in ODE models, dynamic relationships between response variables are embedded in the model, thus allowing for seamless integration of multiple responses in the system.

However, implementation of ODE models is often based on numerical optimizations and thus they are mostly deterministic in nature; that is, a set of inputs and parameter values always gives the same output. As a consequence, ODE models fitted through numerical optimizations are not capable of recognizing the inherent uncertainty of working with sampled data nor of accommodating any non-systematic sources of variability in the data, thus impairing inference and prediction. Stochastic models that incorporate random components are likely to handle uncertainties in a system, and thus may be better suited for studying crop systems. In this study, we implement

ODE models in a Bayesian framework that explicitly accommodates the stochastic components needed to accommodate sources of uncertainty in the data.

Alternatively, repeated measures data from designed experiments are often analyzed using linear mixed models that naturally accommodate uncertainty through random effects. In addition, linear mixed models can incorporate tailored covariance structures to recognize repeated observations collected over time on a given plant or plot (Piepho, Büchse, & Richter, 2004). However, linear constraints inherent to this approach often require that many parameters be specified to enable the modeling flexibility needed to accommodate dynamic processes.

In addition, it is often the case with linear mixed models that different response variables from the same experiment are analyzed separately (i.e. single-response models). This approach limits understanding of the inherent interrelationships between outcomes (Chitakasempornkul et al., 2019), thus impairing cohesive insight into the cropping system as a whole. Multivariate extensions to mixed models can be used to infer correlations between multiple response variables, but cannot assess any directional relationships among them (Valente & de Magalhães Rosa, 2013).

From a data collection standpoint, designed experiments with repeated measures often require that measurements be taken at predefined timepoints and that such timepoints are shared across the conditions that the scientist wants to compare. By contrast, in large experimental crop settings, the logistical scale of data collection forces a more fluid schedule that is often mismatched with pre-defined timepoints. ODE models allow units to be followed over time, without the limitation of data collection at pre-specified intervals. Furthermore, ODE model parameters are specified in ways biologically meaningful to the dynamic processes of interest, thus enabling a more straightforward interpretation.

In this study, our objectives were 1) to implement dynamic ODE models using a stochastic Bayesian framework to accommodate uncertainty into the modeling

exercise, and 2) to compare performance to traditional linear mixed models (analogous to hierarchical linear models in the Bayesian setting) for repeated measures. We use a winter wheat dataset consisting of measurements on leaf area index (LAI) and biomass collected repeatedly over growing seasons.

3.3 Methodology

3.3.1 Experimental design and data description

Data was obtained from a previous study by Lollato and Edwards (2015) conducted over a period of two years (2012-13 and 2013-14) in three locations in Oklahoma, namely Chickasha, Stillwater, and Perkins. For the purpose of this study, each unique combination of location and year was defined as a block; this is analogous to the concept of contemporary groups. Within each block, each treatment was assigned to four plots. Within the blocks pertaining to Stillwater and Perkins, two treatments, namely irrigated and rainfed, were assigned to four plots each. Only the rainfed treatment was implemented in blocks pertaining to Chickasha. All plots were planted with the wheat variety Iba. In all cases, field preparation consisted of conventional tillage and non-limiting nitrogen fertilization. The fields were intensively managed for weeds, insects, and diseases throughout the experiment. Irrigation on irrigated treatments was based on soil water depletion in the effective rooting zone. Further details on the experimental protocol can be found in Lollato and Edwards (2015).

Data on LAI ($m^2\ m^{-2}$) and biomass ($g\ m^{-2}$) were collected from each plot at multiple time points at intervals of 2-3 weeks throughout the growing season lasting approximately eight months. For data collection, one-meter length of row of above-ground biomass was destructively sampled from a plot at each time point. Green leaves were scanned with an optical leaf area meter to record leaf area and samples were oven-dried to obtain biomass. In each plot, observations on LAI and biomass

were collected repeatedly at timepoints recorded as days after planting (DAP). A new variable called categorical DAP (i.e. DAP_c) was defined to categorize DAP into time intervals, as needed for modeling purposes (see later). Specifically, DAP_c consisted of rounding the observed DAP to the nearest ten day mark, thus categorizing DAPs into ten-days intervals. The choice of 10-day intervals for DAP_c was made in anticipation of the leave-one-group-out cross-validation approach later in the analysis, to ensure at least two observations per interval for each treatment.

Weather variables were collected for inclusion in the dynamic ODE model. Specifically, daily average temperature ($^\circ C$) and daily solar radiation ($MJm^{-2}d^{-1}$) were obtained for each block (i.e. location-year combination) from the Oklahoma Mesonet (McPherson et al., 2007; Brock et al., 1995). Missing values in the weather data were filled in using linear interpolation across days.

3.3.2 The dynamic model

The ODE component of the dynamic model consists of three state variables, namely Thermal Time (TT), Leaf Area Index (LAI), and biomass (BM), whereby TT denotes the thermal time age of the crop (expressed in $^\circ C$ days), LAI is the area of leaves per unit ground area (adimensional), and BM denotes dry biomass of crop per square meter of ground area (expressed in $g\ m^{-2}$). At time zero, LAI and BM were initialized at nominal non-zero values of 0.01 and 0.1, respectively, whereas TT was initialized at zero. For weather variables, daily averages of temperature and solar radiation throughout the growing season were used.

Although many crop models make use of piecewise functions to capture biophysical processes, piecewise functions are not continuously differentiable due to breaks created by conditioning statements. In this project, we use a type of Markov Chain Monte Carlo (MCMC) algorithm called Hamiltonian Monte Carlo (HMC) which requires continuously differentiable functions. More details on HMC are provided in section

3.3.5. In this study, the nominal forms of the functions used to capture biophysical processes were made continuously differentiable using sigmoidal switch functions (Kudryashov, 2015; Jordan, 1995). In the following descriptions of the ODE model equations, nominal piecewise forms for each state variable were given first, followed by the exact sigmoidal switch used for implementation with HMC.

The change in thermal time was calculated as a function of base temperature and daily average temperature. This method is commonly used to calculate thermal time also known as growing degree days (White, Kimball, Wall, and Ottman (2012); McMaster and Wilhelm (1997); Baker, Pinter Jr, Reginato, and Kanemasu (1986)).

$$\frac{dTT_t}{dt} \approx \begin{cases} Tavg_t - Tbase, & Tavg_t > Tbase \\ 0, & otherwise \end{cases} \tag{3.3.1}$$

$$\frac{dTT_t}{dt} = (Tavg_t - Tbase)\,\frac{1}{1 + e^{-100\left(\frac{Tavg_t}{Tbase} - 1\right)}} \tag{3.3.2}$$

where,

$\frac{dTT_t}{dt}$ = Rate of change of thermal time at time t.

$Tavg_t$ = Observed daily average air temperature time t, $^{\circ}C$.

$Tbase$ = Unknown parameter representing base temperature below which plant growth ceases, °C.

The change in LAI was calculated as a function of change in thermal time, leaf expansion rate, canopy light extinction coefficient, and rate of senescence. The growth stage end of leaf expansion was used as a threshold for leaf growth to switch to senescence.

$$\frac{dLAI_t}{dt} \approx \begin{cases} \frac{dTT_t}{dt} \cdot \alpha \cdot LAI_t \cdot e^{-K\ LAI_t}, & TT_t \leq TTL \\ -LAI_t \cdot senrate \cdot \frac{dTT_t}{dt}, & TT_t > TTL \end{cases} \tag{3.3.3}$$

$$\frac{dLAI_t}{dt} = \frac{dTT_t}{dt} \cdot \alpha \cdot LAI_t \cdot e^{-K\ LAI_t} \cdot \left(1 - \frac{1}{1 + e^{-100\ \left(\frac{TT_t}{TTL} - 1\right)}}\right) - LAI_t \cdot senrate \cdot \frac{dTT_t}{dt} \cdot \left(\frac{1}{1 + e^{-100\ \left(\frac{TT_t}{TTL} - 1\right)}}\right) \tag{3.3.4}$$

where,

$\frac{dLAI_t}{dt}$ = Rate of change of LAI at time t.

α = Unknown parameter representing relative rate of LAI increase when $TT_t \leq TTL$.

K = Unknown parameter representing light extinction coefficient, adimensional.

LAI_t = Observed LAI at time t.

TT_t = Observed thermal time at time t.

TTL = Unknown parameter representing thermal time threshold at the end of the vegetative phase of growth, °C d.

$senrate$ = Unknown parameter representing the rate of senescence per unit thermal time.

Biomass was calculated as a function of radiation use efficiency (RUE), solar radiation, and light interception. Light interception was calculated according to the relationship defined in Monsi and Saeki (2005).

$$\frac{dBM_t}{dt} \approx \begin{cases} RUE \cdot SRAD_t \left(1 - e^{-K\ LAI_t}\right), & TT_t \leq TTM \\ 0, & TT_t > TTM \end{cases} \tag{3.3.5}$$

$$\frac{dBM_t}{dt} = RUE \cdot SRAD_t \cdot \left(1 - e^{-K\ LAI_t}\right) \cdot \frac{dTT_t}{dt} \cdot \left(1 - \frac{1}{1 + e^{-100\ \left(\frac{TT_t}{TTM} - 1\right)}}\right) \tag{3.3.6}$$

where,

$\frac{dBM_t}{dt}$ = Rate of change of biomass at time t.

RUE = Unknown parameter representing radiation use efficiency, $g\ MJ^{-1}\ {}^{\circ}C^{-1}\ d^{-1}$.

$SRAD_t$ = Observed solar radiation at time t.

TTM = Unknown parameter representing thermal time threshold at crop maturity, °C d.

At each timestep, the value of the state variables were updated for each k^{th} block using Euler integration according to:

$$\mathbf{S}_{k\ t+1} = \mathbf{S}_{k\ t} + \frac{d\mathbf{S}_{k\ t}}{dt}\Delta t \tag{3.3.7}$$

where, $\mathbf{S}_{k\ t} = [TT_{k\ t},\ LAI_{k\ t},\ BM_{k\ t}]$ are the observed state variables for block k at time t, $\mathbf{S}_{k\ t+1} = [TT_{k\ t},\ LAI_{k\ t},\ BM_{k\ t}]$ at time $t+1$, and Δt is the fixed time step of one day. Alternative methods for integration including up to fourth order Runge-Kutta were evaluated. However, the differences in ODE model outputs were negligible compared to the magnitude of the variables. Therefore, Euler integration was selected to minimize computational costs.

For each i^{th} state variable in $\mathbf{S}$, the output of the ODE model is represented by $\beta^{ode}_{0ikt} = S_{i\ kt} = f(\mathbf{F}_k, \boldsymbol{\theta}, \mathbf{S}_0)$ where, f is the Euler integration of the ODEs from initial time point to time t, $\mathbf{F}_k$ is a matrix of forcings or input variables [$Tavg$ and $SRAD$] for the k^{th} block, $\boldsymbol{\theta}$ is a vector of unknown ODE model parameters, namely $\boldsymbol{\theta}$ = [$Tbase$, α, K, TTL, $senrate$, RUE, and TTM] as described above, and $\mathbf{S}_0$ is a vector of the initial values of state variables.

Thereby,

$$\beta^{ode}_{02kt} = f(\mathbf{F}, \boldsymbol{\theta}, \mathbf{S}_0) = S_{LAI\ kt} \tag{3.3.8}$$

$$\beta^{ode}_{03kt} = f(\mathbf{F}, \boldsymbol{\theta}, \mathbf{S}_0) = S_{BM\ kt} \tag{3.3.9}$$

where,

$S_{LAI\ kt}$ = State variable for biomass at time t for block k as defined by equations 3.3.7 and 3.3.3.

$S_{BM\ kt}$ = State variable for biomass at time t for block k as defined by equations 3.3.7 and 3.3.5.

Next, for response variables LAI and BM, we specify

$$Y_{ijklt} = \beta^{ode}_{0ikt} + \beta^{ode}_{0ikt} * Trt_{il} + Plot(Block * Trt)_{ij(kl)} + \epsilon_{ijklt} \tag{3.3.10}$$

where,

Y_{ijklt} = Observed value of the i^{th} response variable (i = 2 for LAI, i = 3 for Biomass) corresponding to j^{th} plot (j = 1, 2, 3, 4) on k^{th} block (k = 1, ..., 6) assigned to l^{th} treatment (l = 1, 2) at time t.

β^{ode}_{0ikt} = Predicted value of the i^{th} response variable for block k and time t, as obtained as output from the ODE model, i.e. numerical solution to integrals in ODE model equations that is specific to the k^{th} block at time t, and accommodates a block-specific non-linear process for the i^{th} response over time.

Trt_{il} = Differential effect of l^{th} treatment on the i^{th} response variable.

$Plot(Block*Trt)_{ij(kl)}$ = Differential random effect of j^{th} plot nested within a block and treatment combination on the i^{th} response variable, assumed $NIID(0, \sigma^2_{Plot\ i})$.

ϵ_{ijklt} = leftover residual random noise for the i^{th} variable specific to the jkl^{th} plot at time t, assumed $NIID(0, \sigma^2_{e\ i})$.

3.3.3 The hierarchical linear (mixed) model

The hierarchical linear (mixed) model was specified as follows:

$$\begin{aligned} Y_{ijklm} =& \beta^{lm}_{0i} + Block_{ik} + Trt_{il} + (Block * Trt)_{i(kl)} + Plot(Block * Trt)_{ij(kl)} + \\ & Time_{im} + (Trt * Time)_{i(lm)} + \epsilon_{ijklm} \end{aligned} \tag{3.3.11}$$

where,

i = 2 (LAI), 3 (Biomass) j = 1, ..., 4 k = 1, ..., 6 l = 1, 2 m = 1 , ..., 13

Y_{ijklm} = Observed value of the i^{th} response variable from j^{th} plot of block k and Treatment l at time interval m.

β_{0i}^{lm} = Intercept for the i^{th} response variable.

$Block_{ik}$ = Differential effect of k^{th} block on the i^{th} response variable, assumed $NIID(0, \sigma^2_{Block\ i})$.

Trt_{il} = Differential fixed effect of the l^{th} treatment on the i^{th} response variable.

$(Block * Trt)_{i(kl)}$ = Differential effect of l^{th} treatment on the k^{th} block for the i^{th} response variable, assumed $NIID(0, \sigma^2_{Block*Trt_{i[kl]}})$.

$Plot(Block * Trt)_{ij(kl)}$ = Differential effect of j^{th} plot nested within a block and treatment combination on the i^{th} response variable, assumed $NIID(0, \sigma^2_{Plot\ i})$.

$Time_{im}$ = Differential fixed effect of m^{th} time interval (i.e. as defined by DAP_c) on the i^{th} response variable.

$(Trt * Time)_{i(lm)}$ = Differential effect of l^{th} treatment at time interval m for the i^{th} response variable.

ϵ_{ijklm} = Left-over residual noise unique to the observation from $jklm^{th}$ plot for the i^{th} response variable and assumed $NIID(0, \sigma^2_{e\ i})$.

3.3.4 Bayesian specifications

Both dynamic and mixed models were implemented within a Bayesian hierarchical framework. The concept of Bayesian modeling is based on Bayes rule, such that $P(\boldsymbol{\phi}|\mathbf{y}) \propto P(\mathbf{y}|\boldsymbol{\phi})P(\boldsymbol{\phi})$, where $P(\boldsymbol{\phi}|\mathbf{y})$ is the target posterior distribution of the unknown parameters $\boldsymbol{\phi}$, and can be expressed as proportional to the product of the data likelihood $P(\mathbf{y}|\boldsymbol{\phi})$ (also referred to as sampling distribution of the data) and the prior distribution of the unknown parameters $\boldsymbol{\phi}$, namely $P(\boldsymbol{\phi})$ (Gelman et al., 2013). Prior distributions on each unknown parameter reflect prior knowledge or belief about the system and can usually be informed, at least partially, from the existing literature. For systems that have been extensively studied, priors can be set to convey very

precise information. Meanwhile, diffuse priors can be used to convey vague knowledge of a system that is not yet well studied; doing so facilitates the observed data to dominate posterior inference.

Prior specifications for all unknown parameters corresponding to the dynamic ODE and the hierarchical linear (mixed) models are presented below.

3.3.4.1 Dynamic ODE model:

Table 3.1 shows the prior distributions specified for ODE parameters and the reference source used to inform these priors. For each ODE parameter, priors were specified to follow a normal distribution truncated at zero as a lower bound, except for $Tbase$ which was specified as normal and unbounded, and for TTM for which the lower bound was set to TTL.

The prior for *senrate* was specified using a heuristic approach by testing different values of *senrate* such that the time it takes for a canopy to reach full senescence from maximum leaf area is on average 35 days assuming a maximum LAI of five and 30 °C days. The prior specification for *senrate* as a normal distribution truncated at 0 with a μ of 0.005 and σ of 0.001 allowed 99% of the prior density for this parameter within the range of 0.002 to 0.008, which would correspond to a duration for full canopy senescence of 60 to 20 days, respectively.

The prior for RUE was specified in $g\ MJ^{-1}C^{-1}$ for model implementation with a mean of 0.07 and $\sqrt{\sigma^2}$ of 0.0125; this is equivalent to values of 1.4 and 0.25 for the respective hyperparameters expressed in $g\ MJ^{-1}$ at 20 $°C$ (as specified in Table 3.1). For RUE, prior information and results from the posterior density are presented in $g\ MJ^{-1}$ for the ease of reference.

Table 3.1: Specification of prior hyperparameters for the ODE model parameters.

Parameter	Description	μ	σ^2	References
$Tbase$	Base temperature	0	2^2	Porter and Gawith, 1999
α	Relative rate of LAI increase before the end of leaf expansion	0.016	0.007^2	Rodriguez, Keltjens, and Goudriaan, 1998
K	Light extinction coefficient	0.6	0.1^2	Pradhan et al., 2018; Bechini, Bocchi, Maggiore, and Confalonieri, 2006; Muurinen and Peltonen-Sainio, 2006; O'Connell, O'leary, Whitfield, and Connor, 2004; Calderini, Dreccer, and Slafer, 1997
TTL	Thermal time threshold at the end of leaf expansion	950	100^2	McMaster et al., 2019; Bechini et al., 2006
$senrate$	Rate of senescence	0.005	0.001^2	
RUE	Radiation Use Efficiency	1.4	0.25^2	Bechini et al., 2006; Muurinen and Peltonen-Sainio, 2006; O'Connell et al., 2004; Calderini et al., 1997

Table 3.1: Specification of prior hyperparameters for the ODE model parameters. *(continued)*

Parameter	Description	μ	σ^2	References
TTM	Thermal time threshold at crop maturity	1950	150^2	McMaster et al., 2019; Bechini et al., 2006

To assess the influence of the prior specifications listed above on posterior inference, we conducted a sensitivity analysis allowing for more diffuse priors. In particular, for each of the ODE parameters listed in Table 3.1, we increased the square root of prior variance $\sqrt{\sigma^2}$ by ten-fold and evaluated changes in the posterior densities of interest.

For the remaining parameters in equation 3.3.10, prior information was specified following the prior predictive checking procedure described by Schad et al. (2019). Specifically, hyperparameters were specified such that predictions from prior distributions were biologically plausible with vague boundaries within the scale of each response variable, as follows:

$Trt_{il} \sim N(0, 0.5^2)$ for i = LAI.

$Trt_{il} \sim N(0, 0.25^2)$ for i = B.

$\sqrt{\sigma^2_{Plot\ i}} \sim N(0, 0.3^2)$ truncated at zero for i=LAI.

$\sqrt{\sigma^2_{Plot\ i}} \sim N(0, 45^2)$ truncated at zero for i = B.

$\sqrt{\sigma^2_{e\ i}} \sim N(0, 1^2)$ truncated at zero for i = LAI.

$\sqrt{\sigma^2_{e\ i}} \sim N(0, 100^2)$ truncated at zero for i = B.

3.3.4.2 Hierarchical linear model:

Table 3.2 shows prior specifications for parameters of the hierarchical linear model fitted to LAI (i = 2) and biomass (i = 3). Specifically, vague subjective priors were

Table 3.2: Priors for the hierarchical linear model parameters, where i = 1 is LAI and i = 2 is Biomass.

Parameter	Distribution	(μ, σ^2) for i = 1	(μ, σ^2) for i = 2
β_{0i}	Normal	$(4, 1^2)$	$(500, 100^2)$
Trt_{il}	Normal	$(0, 1^2)$	$(0, 300^2)$
$Time_{im}$	Normal	$(0, 1^2)$	$(0, 300^2)$
$(Trt * Time)_{i[lm]}$	Normal	$(0, 0.5^2)$	$(0, 150^2)$
$\sqrt{\sigma^2_{Block\ i}}$	Truncated normal	$(0, 1^2)$	$(0, 300^2)$
$\sqrt{\sigma^2_{Block*Trt\ i}}$	Truncated normal	$(0, 0.25^2)$	$(0, 100^2)$
$\sqrt{\sigma^2_{Plot\ i}}$	Truncated normal	$(0, 0.25^2)$	$(0, 100^2)$
$\sqrt{\sigma^2_{e\ i}}$	Truncated normal	$(0, 1.5^2)$	$(0, 200^2)$

specified for parameters β^{lm}_{0i}, Trt_{il}, $Time_{im}$, and $(Trt * Time)_{i(lm)}$ following the prior predictive checks approach described in Schad et al. (2019) to ensure that selected priors are consistent with domain expertise. In this case, priors were purposely specified to be diffuse, though avoiding practically-impossible ranges. For example, the prior on the intercept β^{lm}_{0i} was specified as $Normal(800, 100^2)$ for biomass; this implies biomass for the dryland treatment and at end of season to be on average 800 $g\ m^{-2}$ with a three-standard-deviation range from 500 to 1100 $g\ m^{-2}$.

Prior predictive models used for prior specification were formulated in three steps. For each response variable, we started with a model that included only intercept (i.e. β^{lm}_{0i}), then added parameters with subjective priors (i.e. Trt_{il}, $Time_{im}$, and $(Trt * Time)_{i[lm]}$) in a second step, and finally added parameters with structural priors (i.e. $Block_{ik}$, $(Block * Trt)_{i[kl]}$, and $Plot[Block * Trt]_{i[kl]}$) and corresponding hyperprior specifications, as required for the corresponding variance components (i.e. $\sqrt{\sigma^2_{Block\ i}}$, $\sqrt{\sigma^2_{Block*Trt\ i}}$, and $\sqrt{\sigma^2_{Plot\ i}}$, respectively).

3.3.5 The Dynamic Hamiltonian Monte Carlo (HMC) sampling algorithm

The HMC is a recently developed type of MCMC algorithm (Betancourt, 2017; Betancourt & Girolami, 2015) and as such, we used it in this study to obtain numerical samples from the posterior distribution of all unknown model parameters. The HMC performs strategic sampling of the typical set of the joint posterior density by using its gradient to efficiently guide exploration of the parameter space (Betancourt, 2017); this has been shown to enhance MCMC performance, particularly for high dimensional models (Betancourt & Girolami, 2015). By contrast, traditional MCMC samplers, such as Gibbs sampling and random-walk Metropolis Hastings can be inefficient in high dimensional spaces and spaces with complex interactions (Betancourt, 2017). The HMC sampler is built on an analogy to Hamiltonian systems within which one may envision a center of mass described by the probability density function of interest (i.e. joint posterior density), around which the sampler orbits in the parameter space. While the sampler orbits, it also proposes jumps between orbits around the center (Betancourt, 2017). Generally, HMC samplers require specifications of two hyperparameters, namely the step size and the number of steps, that control the jumps of the sampler to explore the parameter space (Hoffman & Gelman, 2014). In this study, we employed a dynamic HMC sampler, as implemented in Stan v. 2.25.0 (Stan Development Team, 2018), whereby these hyperparameters are automatically tuned.

3.3.6 Model implementation

All models were implemented in Stan with CmdStan, which is the command-line interface to the Stan statistical modeling language. For each model, four MCMC chains, each of 5,000 burn-in iterations and additional 5,000 saved iterations were run, resulting in a total of 20,000 saved posterior samples for each model. MCMC samples were post-processed in the R statistical software environment (R Core Team, 2020).

Convergence was monitored using trace plots and R-hat statistical tests (Gelman et al., 2013), whereby R-hat values were smaller than 1.01 for all parameters corresponding to the ODE and hierarchical linear model. Also, auto-correlation plots and effective sample size (ESS) for key lower-level parameters were monitored. Specifically, ESS for the variance component parameters from the hierarchical linear model (i.e. $\sqrt{\sigma^2_{Block\ i}}$, $\sqrt{\sigma^2_{Block*Trt_{i[kl]}}}$, $\sqrt{\sigma^2_{Plot\ i}}$, and $\sqrt{\sigma^2_{e\ i}}$) were greater than 7000 for both biomass and LAI. Similarly, ESS for variance components in the dynamic model (i.e. $\sqrt{\sigma^2_{Plot\ i}}$ and $\sqrt{\sigma^2_{e\ i}}$) and for the ODE model parameters ($Tbase, \alpha, K, TTL, senrate, RUE, TTM$) were greater than 5000. No divergences were encountered in the HMC. Figures were generated using the ggplot2 and gridExtra packages in R (Wickham, 2016; Auguie, 2017). Posterior summaries were produced using posterior medians and 95% highest posterior density intervals (HDIs), as implemented by the HDInterval package (Meredith & Kruschke, 2018). Tables were rendered using the pander package (Daróczi & Tsegelskyi, 2018). The R package tidyverse was used for data cleaning and organization (Wickham et al., 2019; Wickham, Hadley, 2017).

3.3.7 Model comparison

3.3.7.1 Goodness of fit

For the dynamic ODE model and the hierarchical linear model, we assessed goodness of fit to the complete dataset based on the posterior density of selected criteria, namely Root Mean Square Error (RMSE), Willmott agreement index (d; Willmott, 1981), and Nash-Sutcliffe Efficiency (NSE; Nash & Sutcliffe, 1970). For each MCMC iteration (s = 1,2...S), these criteria are computed as follows:

i) Root Mean Square Error (RMSE):

$$RMSE_s = \sqrt{\frac{1}{N}\sum_{n=1}^{N}(y_n - \hat{y}_n^s)^2} \tag{3.3.12}$$

where, N = Total number of data points, y_n is the n^{th} observation (n=1,2,... N), and $\hat{y}_n^s$ is the predicted value for the n^{th} observation obtained from equations (10) or (11) evaluated at parameter values obtained from the s^{th} MCMC iteration. Models with smaller values of RMSE are preferable.

ii) Willmott agreement index (d):

$$d_s = 1 - \frac{\sum_{n=1}^{N} (y_n - \hat{y}_n^s)^2}{\sum_{n=1}^{N} (|\hat{y}_n^s - \bar{y}| + |y_n - \bar{y}|)^2} \tag{3.3.13}$$

where, N, y_n, and $\hat{y}_n^s$ are as described above, and $\bar{y}$ is the average of the observed data points. This statistic ranges between 0 to 1 with values closer to 1 indicating better model fit.

iii) Nash-Sutcliffe Efficiency (NSE):

$$NSE_s = 1 - \frac{\sum_{n=1}^{N} (y_n - \hat{y}_n^s)^2}{\sum_{n=1}^{N} (y_n - \bar{y})^2} \tag{3.3.14}$$

where, N, y_n, $\hat{y}_n^s$, and $\bar{y}$ are as described above. The values of NSE can range from $-\infty$ to 1 and values closer to 1 indicate a better-fitting model.

3.3.7.2 Predictive ability

Leave-one-group out cross-validation was performed for all models following the methodology in Aki Vehtari et al. (2017), where each block-treatment combination was considered a cross-validation group, thus enabling a ten-fold cross-validation strategy. For each fold, a group was held out and the remaining nine groups were used as a training set to fit the model and make predictions on the held-out group. This process was repeated until each group was held out once. Predictive ability was assessed using

the expected log predictive density (elpd), computed as follows (Aki Vehtari et al., 2017):

$$elpd = \sum_{q=1}^{Q} \sum_{m=1}^{M_q} log(\frac{1}{S} \sum_{s=1}^{S} p(y_{m\ q}|\boldsymbol{\phi}^{-q,s})) \tag{3.3.15}$$

where,

q = 1,2,. . . ,10 identifies the fold, $y_{m\ q} = 1, 2, \ldots\ , M_q$ identifies the m^{th} observation within the q^{th} fold, s = 1,2,. . . ,S identifies the MCMC iteration, $\boldsymbol{\phi}^{-q,s}$ identifies all unknown parameters obtained from the s^{th} MCMC iteration fitting the training set corresponding to the q^{th} holdout fold, and $p(.)$ represents the data likelihood function.

Larger values of *elpd* are considered preferable. The difference in elpd between the two models, and corresponding standard error, were computed using the *compare* function within the *loo* package in R (Vehtari et al., 2020). Two sets of data likelihoods were extracted separately for LAI and biomass from the dynamic model to compute elpd in order to enable comparisons with the corresponding hierarchical linear models.

The statistical metrics described in section 3.3.7.1 for assessment of goodness of model fit to data, namely $RMSE$, d, and NSE, were recomputed under the 10-fold cross-validation to assess the predictive ability of the models.

3.3.7.3 Number of effective parameters

The number of effective parameters for both hierarchical linear and dynamic ODE models were estimated using equation 12 in Aki Vehtari et al. (2017) as follows:

$$p_i = \sum_{n=1}^{N} var_{post}(log\ p(y_n|\boldsymbol{\phi})) \tag{3.3.16}$$

where,

p_i = estimated effective number of parameters for i = 2 (LAI) and i = 3 (biomass).

$var_{post}\ log\ p(y_n|\boldsymbol{\phi})$ = Posterior variance of the log predictive density (i.e. log likelihood) for each data point y_n.

The total number of effective parameters for the dynamic ODE model was calculated as the sum of p values using separate log likelihoods for LAI and biomass. For the hierarchical linear model, p values were obtained for a model fitted to LAI (p_2) and also for a model fitted to biomass (p_3). These p values were then added together to enable comparison of model complexity with that of the ODE model.

3.4 Results

3.4.1 Dynamic ODE model

Table 3.3 shows posterior summaries for parameters of the dynamic ODE model. To assess sensitivity of posterior inference to prior specification, Figure 3.1 shows scaled smoothed densities for posterior distributions of the ODE model parameters side by side with the priors specified in Table 3.1. The departure of posterior distributions from the vague prior specifications used in this study, both in terms of mode and narrower breadth, illustrates Bayesian learning from data. For all ODE parameters, the posterior distribution showed a narrower spread around the mode compared to the corresponding prior, indicating that the data was informative for estimating the ODE parameters. The largest overlap between prior and posterior distributions was observed for $Tbase$ and, to a lesser extent TTM.

To further assess sensitivity to prior specification on ODE parameters, we considered posterior inference under prior specifications for increased vagueness (i.e. increase 10-fold in the square root of the prior variance of each parameter). Figure 3.2 shows posterior densities for ODE model parameters using priors specified in Table 3.1 and also priors of increased vagueness. For parameters α, K, RUE, $senrate$, TTL, posterior inference was robust to prior specification, as only subtle shifts in the posteriors were noticeable when using different priors. Indeed, the data were particularly informative for these parameters and tended to overwhelm prior information, regardless

of its specification (Figure 3.2). In turn, posterior inference on parameters $Tbase$ and TTM was found to be more sensitive to prior specification, as an increasingly vague prior specification yielded proportionately vague posteriors (Figure 3.2).This indicates that the data contained limited information to estimate these parameters. Therefore, a formal evidence-based justification for their prior specification (Table 3.1) was particularly important for these parameters.

Among ODE model parameters, correlations between posterior distributions were found to be of substantial magnitude between K and RUE (r = -0.73), $Tbase$ and TTL (r = -0.69), α and K (r = 0.59), α and RUE (r = -0.57), and $Tbase$ and α ($\hat{r}$ = 0.56) (Figure 3.3).

The differential effect of the irrigation treatment Trt_{il} on growth across the growing season and blocks had a posterior median of 0.67 with a 95% HDI of (0.53, 0.83) for LAI and a posterior median of 0.37 with an 95% HDI of (0.28, 0.46) for biomass. These treatment effects were interpreted as time-invariant multipliers in the ODE model fitted to state variables, whereby a LAI increase of somewhere between 53% and 83%, and a biomass increase of somewhere between 28% and 46% can be expected as a result of irrigation relative to rainfed conditions, with 95% probability. For instance, one might expect an average biomass of approximately 1370 $g\ m^{-2}$ (ranging from 1280 to 1460 with 95% probability) under irrigated conditions for a field that might otherwise have yielded approximately 1000 $g\ m^{-2}$ of biomass under rainfed conditions, everything else held constant.

3.4.2 Hierarchical linear model:

The posterior densities of the differential effects of the irrigation treatment at the time intervals represented by DAP_c, as expressed by the sum of the parameters for main effect of treatment (i.e. Trt_{il}) and treatment by time interaction (i.e. $(Trt*Time)_{i[lm]}$), are illustrated in Figure 3.4 and Figure 3.5 for LAI and biomass, respectively. Posterior

Table 3.3: Highest Density Interval (HDI) and posterior median for the ODE model parameters.

Parameter	Description	HDI	Median
$Tbase$	Base temperature	(-4.5, 2)	-1
α	Relative rate of LAI increase before the end of leaf expansion	(0.0066, 0.0076)	0.007
K	Light extinction coefficient	(0.33, 0.45)	0.39
TTL	Thermal time threshold at the end of leaf expansion	(1320, 1429)	1378
$senrate$	Rate of senescence	(0.0012, 0.0019)	0.0015
RUE	Radiation Use Efficiency	(1.7, 2)	1.81
TTM	Thermal time threshold at crop maturity	(2041, 2340)	2163

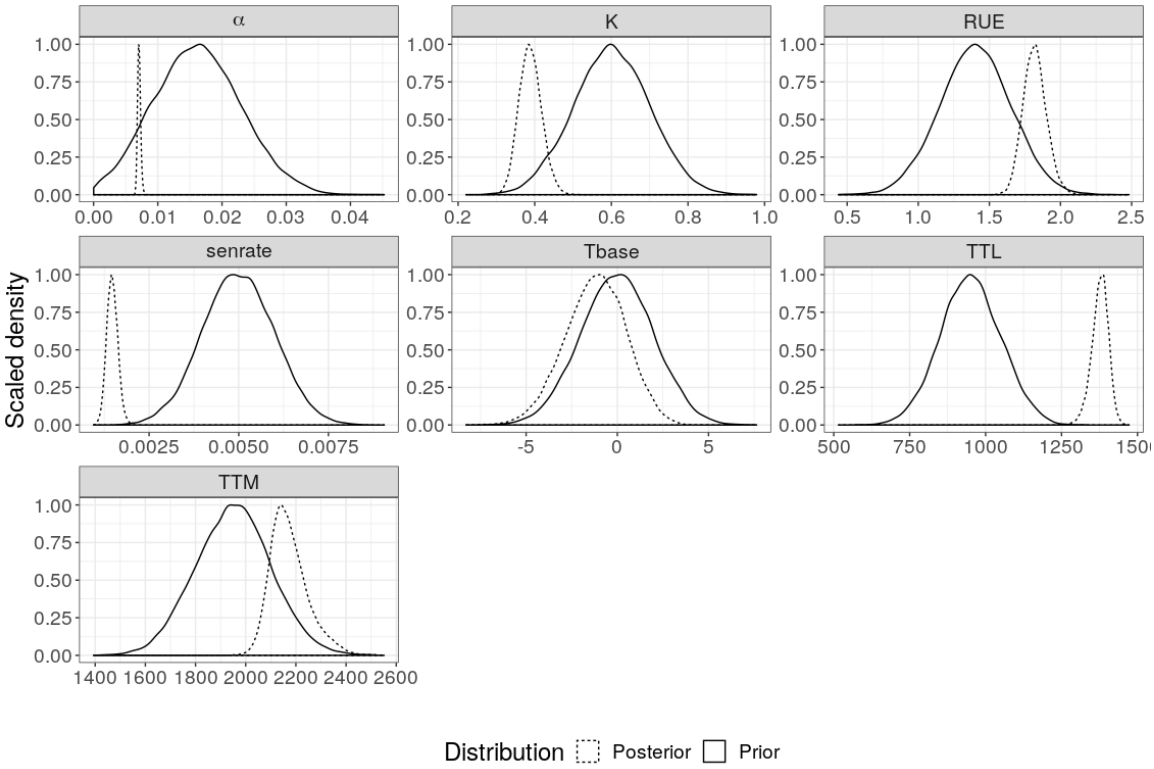

Figure 3.1: Scaled prior and posterior distributions of dynamic ODE model parameters, namely base temperature ($Tbase$), rate of leaf expansion during lag phase (α), light extinction coefficient (K), thermal time to the end of leaf expansion (TTL), rate of senescence ($senrate$), radiation use efficiency (RUE), and thermal time to maturity (TTM). Each distribution was scaled to a maximum density of 1 at its mode to facilitate visual comparisons

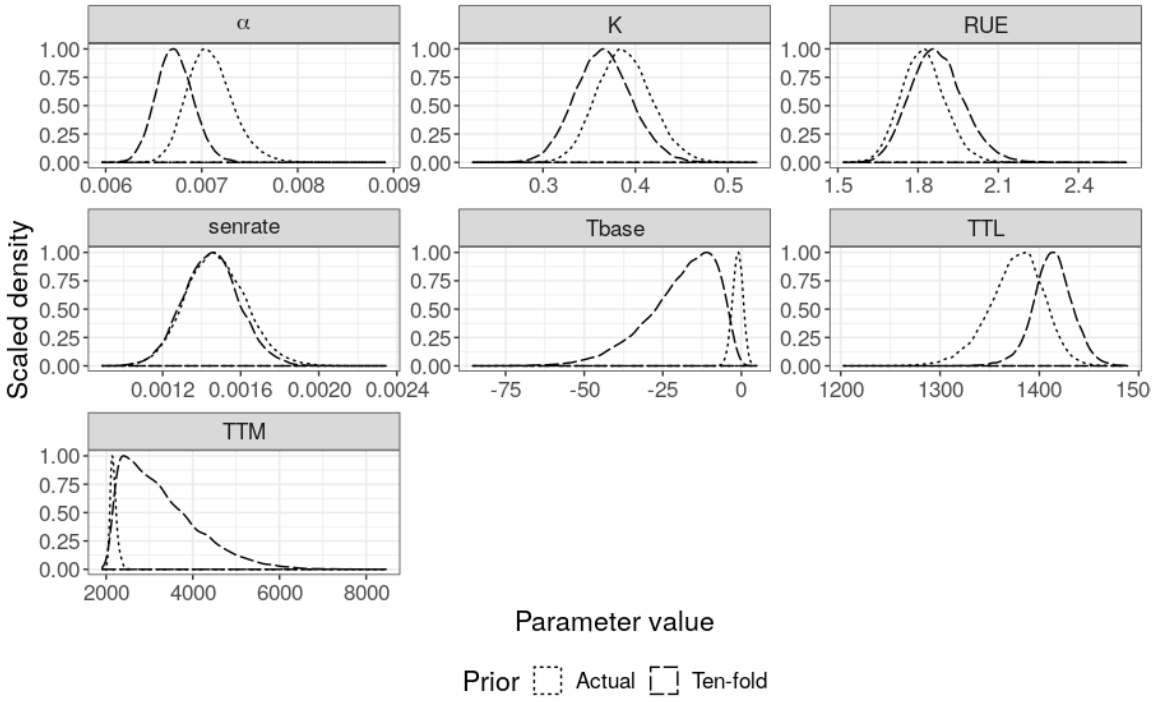

Figure 3.2: Scaled posterior distributions for ODE model parameters using actual prior specifications (as in Table 3.1) and priors of increased vagueness (i.e. square root of prior variance increased by tenfold). Parameters consist of base temperature ($Tbase$), rate of leaf expansion during lag phase (α), light extinction coefficient (K), thermal time to the end of leaf expansion (TTL), rate of senescence ($senrate$), radiation use efficiency (RUE), and thermal time to maturity (TTM). Each distribution was scaled to a maximum density of 1 at its mode to facilitate visual comparisons

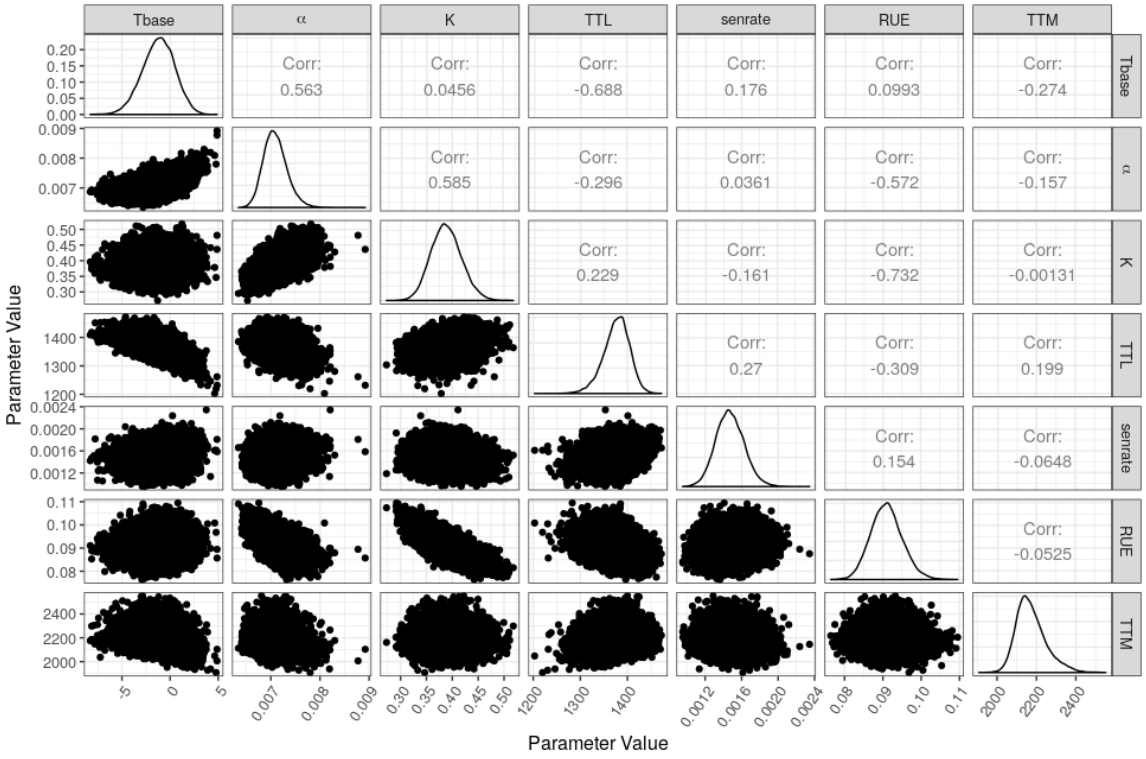

Figure 3.3: Posterior densities of ODE model parameters (main diagonal), pairwise scatterplots of posterior samples (lower triangle) and corresponding estimated Pearson correlation coefficients (upper triangle). ODE parameters presented here consist of base temperature ($Tbase$), rate of leaf expansion during lag phase (α), light extinction coefficient (K), thermal time to the end of leaf expansion (TTL), rate of senescence ($senrate$), radiation use efficiency (RUE), and thermal time to maturity (TTM)

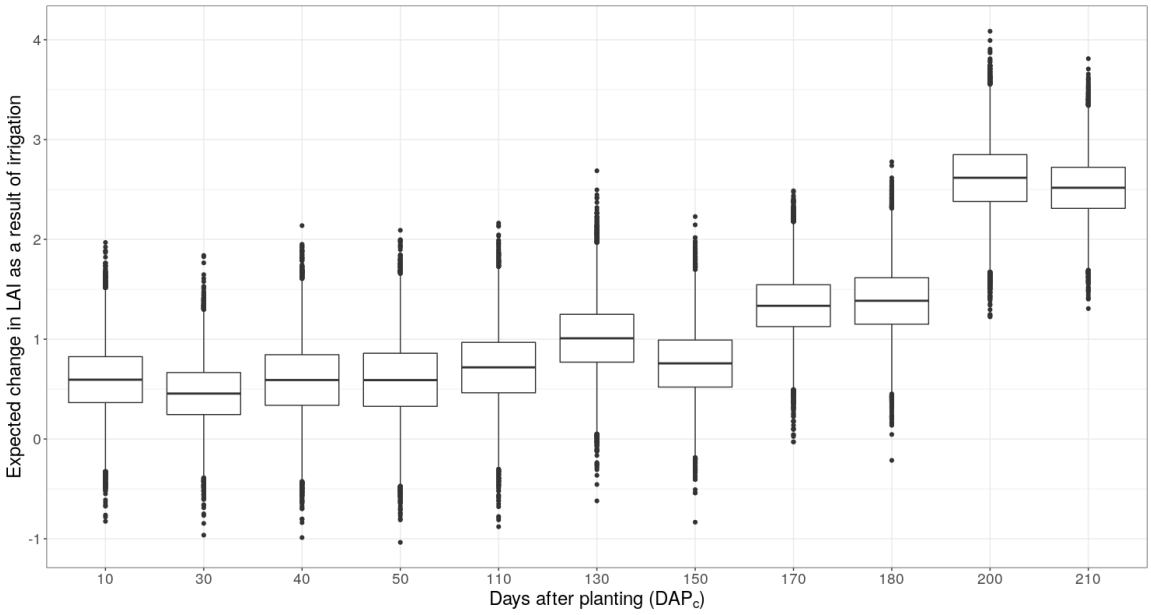

Figure 3.4: Posterior density of the differential irrigation effect relative to rainfed condition on LAI at selected time intervals throughout the growing season, as indicated by the linear combination of treatment and treatment-by-time interval combinations from the hierarchical linear (mixed) model

densities are presented as boxplots, whereby a box contains middle 50% of posterior density, delimited by 25^{th} and 75^{th} percentiles. Results show that as a result of applying irrigation, both LAI and biomass can be expected to increase and the effect would be more prominent towards the end of the growing season.

3.4.3 Model comparison

3.4.3.1 Goodness of fit

Figure 3.6 and Figure 3.7 show the posterior density of fit statistics Root Mean Squared Error ($RMSE$), Willmott's index of agreement (d), and Nash-Sutcliffe Model Efficiency (NSE) to assess goodness of fit of each model fitted to LAI and biomass, respectively, using the whole dataset.

The posterior medians of the goodness of fit statistics from the ODE model and

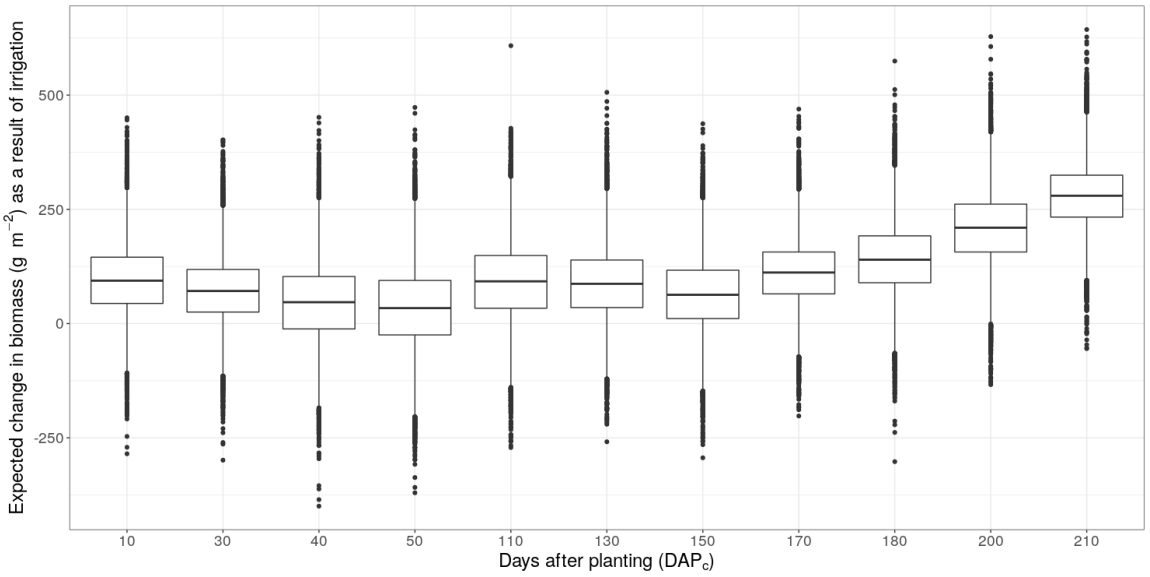

Figure 3.5: Posterior density of the differential irrigation effect relative to rainfed condition on biomass at selected time intervals throughout the growing season, as indicated by the linear combination of treatment and treatment-by-time interval combinations from the hierarchical linear (mixed) model

hierarchical linear model fitted to LAI were 1.16 and 1.04 for $RMSE$, 0.93 and 0.95 for d, and 0.78 and 0.82 for NSE. Likewise, the posterior medians from the ODE model and hierarchical linear model fitted to biomass were 210.73 and 187.11 for $RMSE$, 0.97 and 0.98 for d, and 0.89 and 0.91 for NSE.

Posterior inference for goodness of fit shows consistently lower RMSE, and higher d and NSE values for the linear mixed model relative to the ODE model with little overlap between the respective densities; this in turn supports better fit of the linear mixed model compared to the ODE model. It should be noted that the posterior densities are very high precision, therefore despite little overlap, the posterior modes of the goodness of fit statistics for either model are very close to each other in magnitude. However, the apparent improvement in the goodness of fit of mixed models relative to ODE models may be considered marginal from a practical standpoint given the small difference in magnitude of these statistics between the competing models.

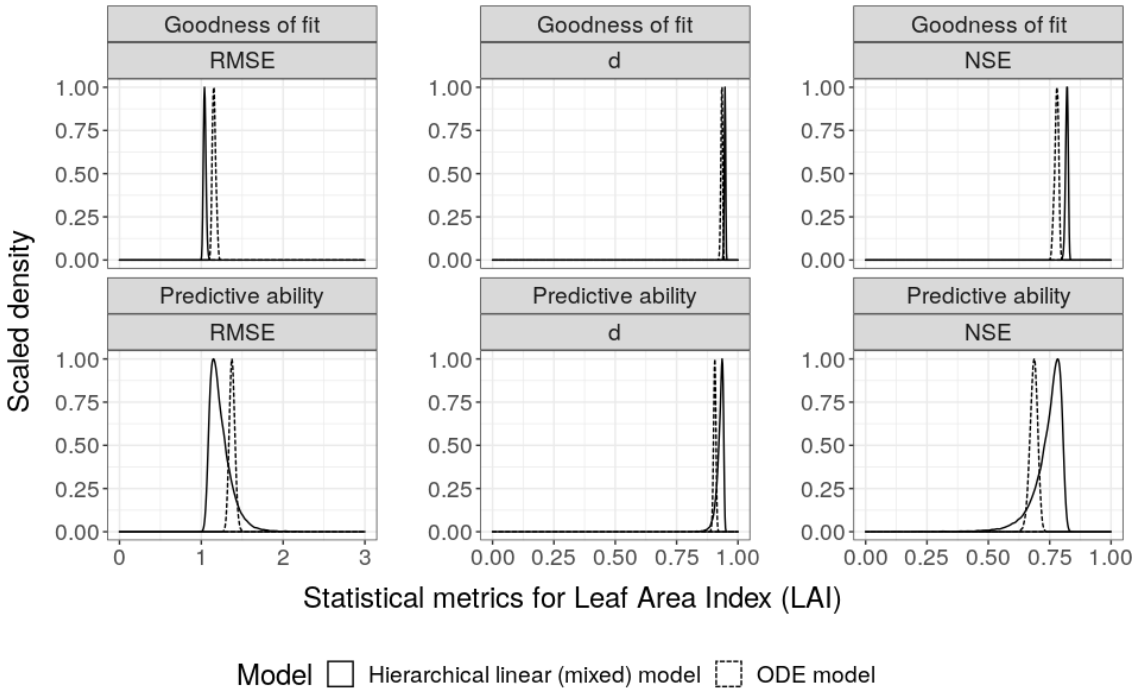

Figure 3.6: Scaled posterior densities of root mean squared error (RMSE), Wilmott agreement index (d), and Nash-Sutcliffe efficiency (NSE)used to assess goodness of fit based on the whole dataset and predictive ability based on a ten-fold cross-validation for the dynamic ODE model and the hierarchical linear model fitted to LAI

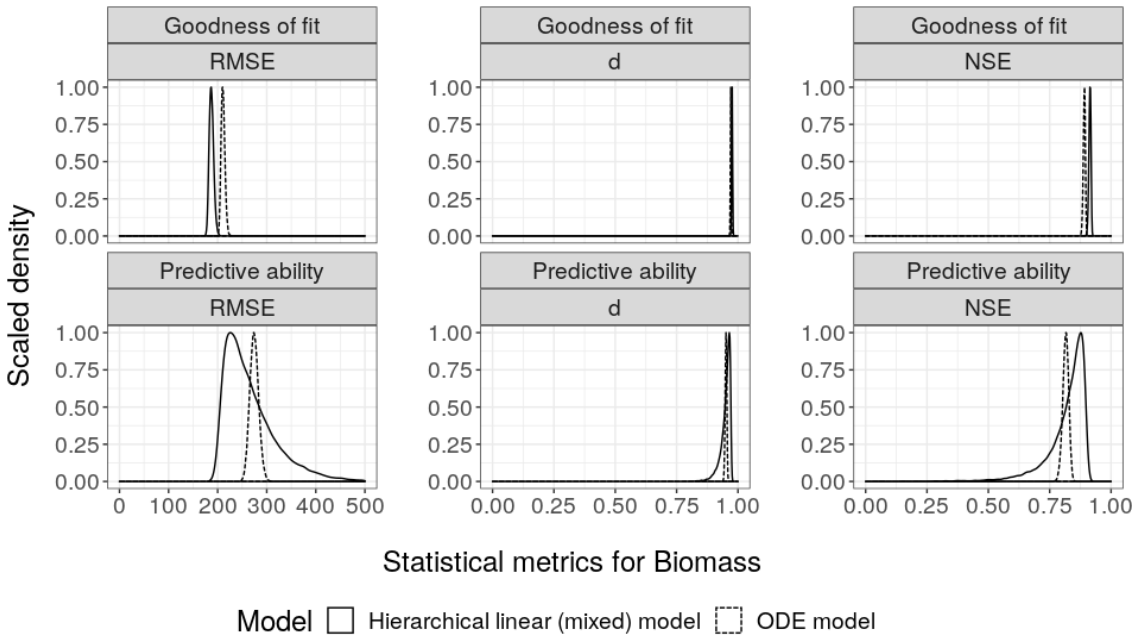

Figure 3.7: Scaled posterior densities of [write out statistics] used to assess goodness of fit (GoF) based on the whole dataset and predictive ability (Pred) based on a ten-fold cross-validation for the dynamic ODE model (ODE) and the hierarchical linear model (lm) fitted to biomass

3.4.3.2 Predictive ability

We used the 10-fold cross-validation-based difference in elpd between the dynamic ODE model and the hierarchical linear model to compare predictive ability between models. For LAI, the average elpd difference across cross-validation folds was estimated at 35.3 in favor of the hierarchical linear model model with an estimated standard error of 40.9. For biomass, the average elpd difference between models across cross-validation folds was 18.8 in favor of the hierarchical linear model with a standard error of 28.3. Notably, for both responses, the standard errors were larger in magnitude than the actual estimate of the elpd difference, thus suggesting that neither model was a clear winner for predictive ability on either response.

Figure 3.6 and Figure 3.7 show the posterior density of the statistics Root Mean Squared Error (RMSE), Willmott's index of agreement (d), and Nash-Sutcliffe Model Efficiency (NSE) computed under 10-fold leave-one-group-out cross-validation for each of the models fitted to LAI and biomass, respectively.

For LAI, the ODE model and hierarchical linear model yielded posterior medians for $RMSE_p$ of 1.38 and 1.21, d_p of 0.91 and 0.93, and NSE_p of 0.69 and 0.76, respectively. Similarly, for biomass, the ODE model and hierarchical linear model yielded posterior medians for $RMSE_p$ of 274.27 and 253.50, d_p of 0.95 and 0.95, and NSE_p of 0.82 and 0.84, respectively.

For biomass, the posterior densities of statistics for predictive ability were narrower, and thus more precise, under the ODE model compared to the hierarchical linear model. In fact, the broad range of posterior inference for predictive ability on biomass under the hierarchical linear (mixed) model indicates inconsistent predictive behavior of this model.

Furthermore, Figure 3.8 and Figure 3.9 show cross-validation- based predicted values of LAI and biomass, respectively, for each block-treatment combination over the growing season based on the dynamic ODE model and the hierarchical linear

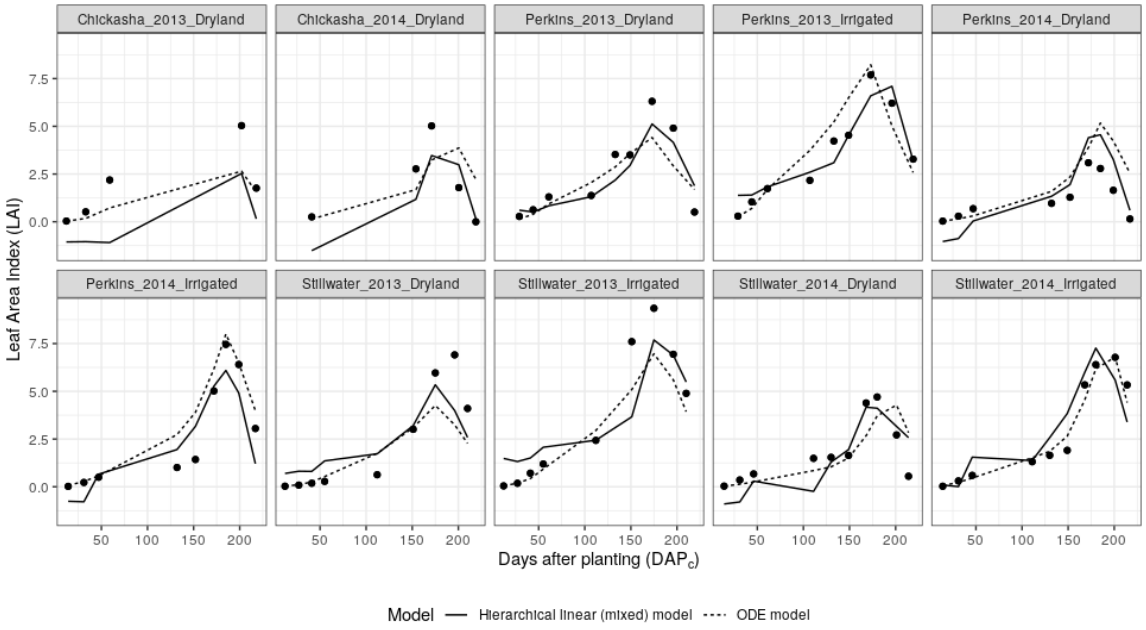

Figure 3.8: Observed LAI and corresponding predicted values for block-treatment combinations over the growing season, as obtained from fitting the dynamic ODE model and the hierarchical linear (mixed) model

model. The fitted lines follow a similar trend to that of observed data points, which indicates that the predictions from both models were acceptable.

3.4.3.3 Number of effective parameters

For the dynamic ODE model, the total number of effective parameters was estimated at 54. For the hierarchical linear model, the number of effective parameters was estimated at 26 for LAI and 32 for biomass, adding to a total of 58. As expected, the ODE model showed more parsimony, though the difference in total number of effective parameters between the models did not seem to be critical.

3.5 Discussion

In this study, we implemented a dynamic ODE model using a hierarchical Bayesian framework to analyze repeated measures data on LAI and biomass of wheat. The

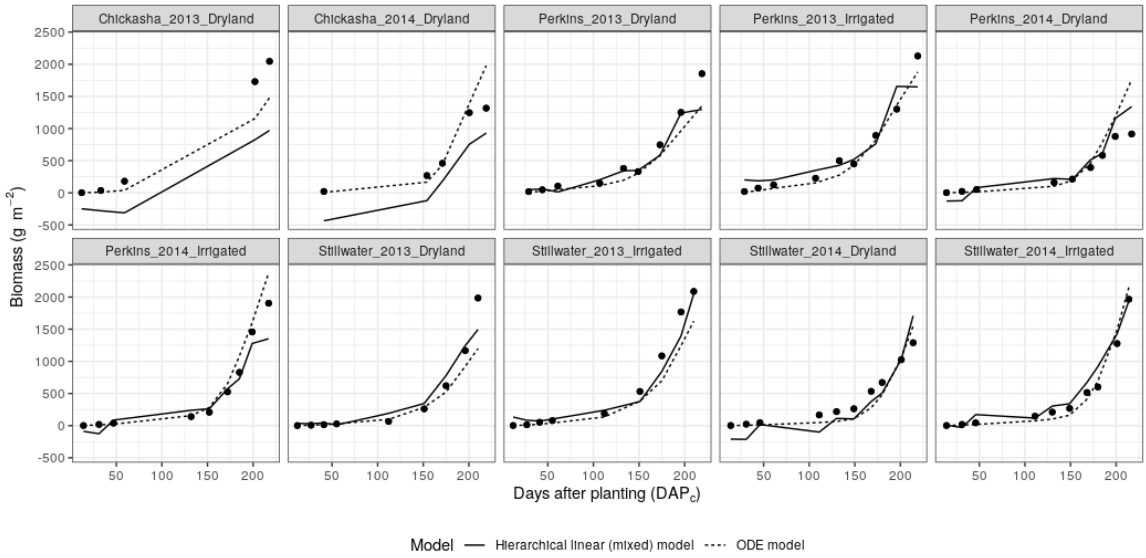

Figure 3.9: Observed biomass and corresponding predicted values for block-treatment combinations over the growing season, as obtained from fitting the dynamic ODE model and the hierarchical linear (mixed) model

Bayesian modeling framework enabled incorporation of uncertainty into estimation of ODE parameters and subsequent prediction. We also compared performance of the proposed ODE model with a traditional approach to data analysis for designed experiments, namely that of hierarchical linear mixed modeling. Admittedly, more sophisticated methods within linear mixed models are available, such as bivariate models or splines. However, the choice of a simple hierarchical linear modeling approach was intended to reflect commonly used methodology for the analysis of crop data from designed experiments.

For the ODE model, parameters $Tbase, \alpha, K, TTL, senrate, RUE, TTM$ carry direct biological meaning regarding the mechanism of wheat growth. For example, the *alpha* parameter can be considered a proxy for the trait of early vigor, whereas the parameter *senrate* would relate to the stay green trait. An advantage of utilizing the dynamic ODE model is that one can infer directly on the behavior of such biologically relevant parameters and provide a mechanistic interpretation of the process of interest.

In this study, posterior inference on α yielded a posterior median of 0.007 and 95% HDI of [0.0066, 0.0076]. Thus, we may quantify the rate of leaf expansion before the end of leaf expansion, to be approximately 0.7% of existing leaf area per degree day, with a 95% probability that this rate of change is between [0.66% and 0.77%] . To the best of our knowledge, there are no direct measurements of α reported for wheat to date.

Furthermore, in this study, we expressed the rate of senescence *senrate* relative to current leaf area and mediated by thermal time in the model. The 95% HDI of *senrate* was (0.0012, 0.0019) indicating that the decline in LAI per degree above the base temperature ranged from 0.12% to 0.19% with 95% probability, with a median of 0.15% starting after end of leaf elongation.

For the light extinction coefficient parameter K, the posterior median was 0.39 with 95% HDI of [0.33, 0.45]. Other studies have reported values ranging from 0.3 up to 0.8 for the light extinction coefficient (O'Connell et al., 2004; Calderini et al., 1997; Pradhan et al., 2018). Our study indicated a 99.9% posterior probability that K is indeed within this range though on the lower side of the values reported in the literature. Lower values of the light extinction coefficient indicate that more LAI is required to achieve a given level of light interception, and this can be expected to ultimately impact growth.

For RUE, the posterior median was 1.81 $g\ MJ^{-1}$ with an HDI of [1.7, 2]. Commonly, RUE values are reported per unit photosynthetically active radiation (RUE_{PAR}), which would roughly equal double RUE as calculated per unit total radiation, under the assumption that 50% of total solar radiation is PAR. Studies have reported RUE_{PAR} values from around 1.5 to 3 $g\ MJ^{-1}$ (Kiniry et al., 1989; O'Connell et al., 2004). The parameter RUE as estimated is RUE per unit total radiation, whereby the HDI would correspond to RUE_{PAR} of 3.4 to 4. Hence, the RUE value calculated by our model was higher than the literature reported values.

The medians for thermal time to end of leaf expansion (TTL) and thermal time to maturity (TTM) were estimated to be 1378 and 2163 with HDI of [1320,1429] and [2041, 2340] respectively, which are higher than the reported values in the literature. Specifically, estimates for TTL and TTM were reported to be 550 and 1352, respectively, by Bechini et al. (2006) whereby a fixed value of -1 $^{\circ}C$ was used for base temperature. Meanwhile, McMaster et al. (2019) reported estimates of 945 and 1970 for thetaTTL and thetaTTM, respectively, using a base temperature of 0 $^{\circ}C$. For the base temperature ($Tbase$), the posterior median was estimated to be -1 $^{\circ}C$ with an HDI of [-4.5, 2] by our model. The base temperature for wheat is usually assumed to be 0 $^{\circ}C$, but evidence suggests that $Tbase$ may be variable across genotypes and even across developmental stages (Porter & Gawith, 1999; Salazar-Gutierrez, Johnson, Chaves-Cordoba, & Hoogenboom, 2013; G. Slafer & Savin, 1991). In this study, the average minimum temperatures during early season across years and locations were well above -1 $^{\circ}C$ resulting in a continuous accumulation of thermal time leading to higher estimates for TTL and TTM values. The high values of TTL and TTM obtained in this study likely compensated for the fact that the vernalization process was not included in the model. If vernalization had been explicitly modeled, one would expect that the estimation of TTL and TTM would yield lower values because the vernalization process would be expected to reduce the development rate.

Specification of priors for parameters of the dynamic ODE models was informed with the help of literature, though priors were vague enough to allow for possible extreme values of the parameters. For most parameters, the posterior distribution was not only narrower in terms of spread, but also the posterior modes were heavily shifted as compared to the prior distribution. This indicates that the data contained information for estimation of most ODE parameters. Sensitivity analysis further indicated that posterior inference was heavily dominated by the prior for at most two parameters, namely $Tbase$ and TTM. The substantial amount of information

available for these parameters, especially $Tbase$, facilitate evidence-based justification of these priors (Porter & Gawith, 1999; Salazar-Gutierrez et al., 2013; G. Slafer & Savin, 1991).

Posterior correlations between parameters indicate how much information the data contains to allow disambiguation in the estimation of parameters. Usually, extreme posterior correlations among parameters are a reason for concern in instances where sampling efficiency of the MCMC is impaired. There were no such problems detected in this study.

The posterior correlation between $Tbase$ and TTL was negative and of large magnitude (i.e. $\hat{r}$ = -0.69), thus suggesting that higher base temperatures are associated with less cumulative thermal time to reach the end of leaf expansion, and vice-versa. It also suggests that when one parameter varies, it constrains the estimated values of the other. A common practice in crop modeling research is to fix the value of the parameter for base temperature and estimate the value of the parameter for thermal time to leaf expansion (McMaster et al., 2019; Bechini et al., 2006). This practice implicitly places a constraint on the estimate for the thermal time parameter. By contrast in this study, both $Tbase$ and TTL were simultaneously estimated allowing for fuller characterization of the uncertainty in both parameters meanwhile accounting for the mutual correlation.

The correlation observed between $Tbase$ and α ($\hat{r} = 0.56$) may be explained by the mathematical relationship expressed in the model in equation 3.3.4. Since higher $Tbase$ corresponds to lower thermal time accumulation per day, the leaf growth rate (i.e. α) would be expected to increase to achieve the same amount of leaf area for lower thermal time. Furthermore, the posterior correlation between α and K ($\hat{r} = 0.59$) may be explained as a consequence of these parameters mutually offsetting each other in equation 3.3.4. In turn, this suggests that these two parameters related to leaf area cannot be fully distinguished from the data available for this study given

the mathematical relationship imposed by the model. Taken together, posterior inference on the parameters α, K, RUE, and *senrate* helped us understand the canopy evolution over time. Specifically, low values of K were compensated with high values of RUE and low values of *senrate* to sustain growth until the end of the season (Fig. Figure 3.3). Similarly, posterior inference on parameters TTL and TTM provided estimates of thermal time. The high values of parameters related to thermal time and RUE and low value of the parameter related to senescence, namely *senrate*, indicate that the growing season was predicted to be longer than previous literature might suggest (McMaster et al., 2019; Bechini et al., 2006). This was also observed in the predicted LAI values over the growing season, where at the end of the growing season, predicted LAI was still substantially greater than zero. Inclusion of yield data in the estimation process might partially address this issue, given that yield is primarily determined based on growth at the end of the growing season and would therefore provide specific information about growth during this part of the season. Overall, the dynamic ODE model provided valuable information on biological parameters to understand the physiological mechanisms underlying crop phenotypes. This approach may also be useful to compare different wheat genotypes in their physiological responses.

From both models, we inferred that both LAI and biomass increased due to irrigation relative to the dryland control, and that the magnitude of this increase was time specific and was magnified over the growing season, which conforms to the literature (Thapa et al., 2019; Pradhan et al., 2018). The ODE model captured this increasing effect of treatment over time in the multiplicative nature of the Trt term, whereas the hierarchical linear model did so by explicitly specifying a treatment-by-time interaction term.

Goodness of fit comparisons showed that the hierarchical linear model had better fit to the data than the dynamic ODE model, although for any practical purposes the

magnitude of the difference in fit between models was small for both LAI and biomass.

From a prediction standpoint, posterior modes for the leave-one-group-out cross-validation statistics seemed to indicate preference of the hierarchical linear model over the ODE model. However, when considering the full posterior density of the statistics for predictive ability, the ODE model showed consistently greater predictive performance, thus rendering it preferable to the hierarchical linear model.

3.5.1 Model comparison

The results showed that the hierarchical linear model has a better goodness of fit than the dynamic ODE model, for both LAI and biomass, although the difference is small. The RMSE values for both hierarchical linear model and the dynamic model for LAI (1.05 and 1.16) are higher than the RMSE values (<1) reported in literature for LAI (Kanning, Kühling, Trautz, & Jarmer, 2018; Huang et al., 2015; Jin et al., 2015). However, these studies only reported LAI measurements from a single time point. The higher value of RMSE in our study could be the result of data on LAI from different time-points across the growing season which has a greater variability than data from a single time point. Likewise, the RMSE values for biomass for the hierarchical linear model and the dynamic model (192 and 210 $g\ m^{-2}$) are consistent with the RMSE values reported in the literature with different modeling techniques (Yue et al., 2017; Jin et al., 2016; Eitel, Magney, Vierling, Brown, & Huggins, 2014).

The results of leave-one-group-out cross-validation revealed that there is not enough evidence to claim a better model for prediction among the hierarchical linear model and dynamic model.

Furthermore, in regards to model complexity, the two models were found similar as indicated by the number of effective parameters.

3.6 Conclusion

In conclusion, the goodness of fit was acceptable for both models whereas the predictive ability was more consistent with the ODE model. The uncertainties in parameters were captured through the use of a Bayesian framework. The increasing effect of treatment over the growing season was captured by both models but through multiplicative terms in the ODE model and additive terms in the hierarchical model. The ODE model parameters were biologically meaningful and connected more readily to the overall goal of cohesive understanding of mechanisms underlying the system. The dynamic model also encompassed simultaneous fitting of both variables, LAI and biomass, as a part of the system, whereas the hierarchical linear modeling setting was limited to separate analyses for LAI and biomass. Dynamic ODE models fitted under a Bayesian framework, as presented in this article may be considered a valid alternative for statistical analyses of crop growth data when underlying physiological mechanisms are of interest.

CHAPTER IV

ANALYSIS OF WINTER WHEAT GROWTH IN OKLAHOMA USING A WATER BALANCE COMPONENT WITHIN AN ODE CROP GROWTH MODEL

4.1 Abstract

Crop models are widely used to simulate crop production. However, crop growth models are often complex, require diverse data on different aspects of crop growth, and thus face parameter non-identifiability issues. In this study, we propose a simple dynamic ordinary differential equation (ODE) model of soil water balance and crop growth for understanding wheat growth and yield patterns in Oklahoma. The water balance model we propose is a single layer lumped model which simulates soil water content and crop water stress at a daily time step throughout the growing season. We utilize a repeated measures dataset of observed winter wheat leaf area index (LAI) and biomass and end of season yield across multiple years, locations, and treatments to estimate parameters for the crop growth model. The objectives of this study were to: i) quantify improvements in predicted crop growth patterns by inclusion of a dynamic water balance, ii) understand how water availability affects winter wheat growth throughout the season, and iii) investigate how data quantity and diversity impact model performance. The crop growth model performed satisfactorily to predict LAI and yield as indicated by three statistics Root mean squared error (RMSE), Willmott's agreement index (d), and Nash-Sutcliffe efficiency (NSE). The prediction statistics for models with and without water balance, respectively, were: RMSE of

1.51 and 1.69, d of 0.89 and 0.85, and NSE of 0.62 and 0.52 for LAI, RMSE of 134.25 and 237.81, d of 0.88 and 0.32, and NSE of 0.25 and -1.36 for yield, and RMSE of 531.44 and 353.92, d of 0.88 and 0.93, and NSE of 0.43 and 0.75 for biomass. Water balance simulations improved yield predictions under water-limited conditions and improved overall model performance as indicated by lower root mean squared error and higher Willmott agreement index and Nash-Sutcliffe efficiency but need further improvement for accurate soil moisture simulations.

4.2 Introduction

The highly variable growing environment is the main driving factor for wheat yield differences across Oklahoma and the southern Great Plains (SGP) (Munaro et al., 2020; Lollato, Edwards, & Ochsner, 2017). A large portion of these environmental differences is due to variability in rainfall and soil water status. Most of the wheat grown in this area is rainfed and precipitation varies tremendously, both temporally and spatially. For example, in the past 20 years, the annual precipitation has ranged from 167 mm in northwest Oklahoma in 2011 to 1550 mm in southeast Oklahoma in 2015. Water limitation is one of the major problems for wheat grown in Oklahoma and the SGP (Maulana, Anderson, Butler, & Ma, 2019; Tahara, Carver, Johnson, & Smith, 1990). In this study, we utilize a water balance model in conjunction with an ODE crop growth model to account for plant available soil water in wheat cropping systems in Oklahoma. The goal of this study is to implement a simple dynamic growth model for wheat yield characterization while accounting for one of the major factors influencing yield, namely soil water.

Dynamic crop models are commonly used to simulate growth and yield of crops to understand the interactions between crops and environments (Brown, Huth, & Holzworth, 2018; Attia et al., 2016; Z. Li et al., 2015; Asseng, Zhu, Basso, Wilson, & Cammarano, 2014; Asseng, Van Keulen, & Stol, 2000). Successful usage of these

models requires accurate parameter estimation, calibration, and validation. Many existing crop models are complex, which complicates their usage because of parameter non-identifiability in many cases. In this study, we propose a simple crop model with few parameters along with a simple water balance model as an alternative way of accounting for water stress. If water is a dominant factor influencing crop growth, development, and yield, a crop model including a water balance factor should have a better prediction than one that does not account for water stress.

We propose a single layer lumped model which quantifies the effect of soil water deficits on plant growth, but is relatively simple in terms of model formulation and implementation. Other simple models such as AquaCrop (Steduto, Hsiao, Raes, & Fereres, 2009) and Simple Simulation Model (SSM) (Soltani, Maddah, & Sinclair, 2013) are fundamentally similar to our model in the derivation of available water content from the difference between a drained upper limit (field capacity) and a lower limit (permanent wilting point), but differ in including multiple soil layers and accounting for vertical soil water transfers between soil layers which makes these models more complex compared to our proposed model. Likewise, other complex crop models such as DSSAT-CERES (Jones et al., 2003a) and APSIM (Keating et al., 2003) also make use of a layered soil model which requires soil data for each layer. The complexity of these models increases the parameter identifiability issues.

Eventually, the long-term goal of this research is to utilize this type of model across multiple genotypes and years to explain genotype by environment interaction with extensive datasets such as wheat variety trials data. This study lays out a robust groundwork to achieve that. The specific objectives of this study were to: i) quantify the improvements in predicted crop growth patterns by inclusion of a dynamic water balance, ii) understand how water availability affects winter wheat growth throughout the season, and iii) investigate how data quantity and diversity impact model performance.

Table 4.1: Locations, years, and treatments included in the study

Location	Latitude	Longitude	Soil type	Harvest year	Treatment
Chickasha	35.05 N	97.94 W	Haplustoll	2013, 2014	Rainfed
Lahoma	36.39 N	98.09 W	Argiustoll	2013	Rainfed
Stillwater	36.12 N	97.06 W	Paleustoll	2013, 2014	Rainfed/Irrigated
Perkins	35.97 N	97.03 W	Argiustoll	2013, 2014	Rainfed/Irrigated

4.3 Methodology

4.3.1 Data description

Plant, soil, and irrigation data were obtained from a previous study by Lollato and Edwards (2015) in Oklahoma. The study was conducted in eleven different environments across multiple years, locations, and treatments (Table 4.1). An environment was thus defined as a location-harvest year-treatment combination. In each environment, 1000 m^2 area was sown and four plots were established within the area. Wheat variety Iba was planted in all plots.

4.3.1.1 Plant data

Leaf area index (LAI) and biomass data were collected throughout the growing season at an interval of 2-3 weeks, and end of season yield data were obtained from each plot in each environment. For LAI and biomass data collection, one meter of row (approximately 0.25 m^2) of above ground biomass was destructively sampled each sample date. An optical leaf area meter (Model LI-3100; LI-COR, Lincoln, NE) was used to obtain leaf area for LAI and samples were oven-dried at 60 °C to obtain dry biomass. Grain yield was obtained by harvesting three areas of approximately 20 m^2 per plot. Yield observations from these three areas were averaged to determine yield per plot.

4.3.1.2 Weather data

Average daily temperature, precipitation, solar radiation, wind speed at 2m, relative humidity, and atmospheric pressure were obtained from Oklahoma Mesonet stations near each location (McPherson et al., 2007; Brock et al., 1995). Missing data for all weather variables were filled by inverse distance weighting data from the nearest three Oklahoma Mesonet stations. Irrigation data were obtained from Lollato and Edwards (2015).

4.3.1.3 Soil data

Soil texture, available water holding capacity (AWHC), and plant available soil water (PAW) data were obtained from the previous study by Lollato and Edwards (2015). The PAW was monitored using a neutron probe (Model 503 DR; CPN, Concord, CA). The PAW data during the growing season were used for validation of the water balance model. The first observation of PAW (near the planting date) was used to initialize the water balance model.

4.3.2 The ODE crop growth model

4.3.2.1 Vernalization adjusted thermal time

The development of the crop is expressed the function of temperature over time as well as the vernalization status of the crop.

$$\frac{dTT_t}{dt} = f_{TT} \cdot f_{vrn} \tag{4.3.1}$$

where,

$\frac{dTT_t}{dt}$ is the rate of change of thermal time at time t.

$f_{TT\ t}$ is the thermal time factor, calculated as shown below.

$f_{vrn\ t}$ is factor corresponding to the vernalization requirement, calculated as shown below.

The thermal time factor represents the biochemical pathways that are purely controlled by temperature.

$$f_{TT\ t} = \left(\frac{1}{1 + e^{-5\left(\frac{Tavg_t}{10} - 1\right)}} \cdot 20 \right) \tag{4.3.2}$$

where,

$Tavg_t$ is the input variable representing observed daily average air temperature at time t for environment k.

The vernalization factor affects the crop development rate such that development is slower before the crop meets the vernalization requirement.

$$\begin{aligned} vrn_t = & \frac{1}{1 + e^{-100\left(\frac{2\ TT_t}{TTL} - 1\right)}} + \\ & \left(1 - \frac{1}{1 + e^{-100\left(\frac{2\ TT_t}{TTL} - 1\right)}}\right) \left(\frac{1}{1 + e^{\left(-2\frac{log(99)}{vrn}\right)\left(VRN_t - \frac{vrn}{2}\right)}} \right) \end{aligned} \tag{4.3.3}$$

where,

TT_t is observed thermal time at time t for environment k.

TTL is the parameter representing cumulative thermal time until the end of vegetative phase of growth, °C d.

vrn is the parameter representing vernalization requirement, vernalization days.

VRN_t is the state variable for vernalization at time t, calculated below.

$$\frac{dVRN_t}{dt} = 1 - \frac{1}{1 + e^{-5\left(\frac{Tavg_t}{8} - 1\right)}} \tag{4.3.4}$$

where,

$Tavg_t$ is as defined above.

4.3.2.2 Leaf Area Index

The change in LAI was calculated as the difference betwen leaf growth and senescence. The growth stage end of leaf expansion was used as a threshold for leaf growth to switch to senescence. The water stress factor was introduced to slow growth in presence of water stress.

$$\frac{dLAI_t}{dt} = \left(LAI_t \cdot \frac{dTT_t}{dt} \cdot \alpha \cdot f_{ws} \cdot e^{-K\ LAI_t} \cdot (1 - f_{gf})\right) - \left(LAI_t \cdot senrate \cdot \frac{dTT_t}{dt} \cdot f_{gf}\right) \tag{4.3.5}$$

where,

$\frac{dLAI_t}{dt}$ is the rate of change of LAI at time t.

LAI_t is leaf area index at time t.

α is the parameter representing relative rate of LAI increase when thermal time is less than TTL.

f_{ws} is the factor for water stress, calculated as shown below.

K is the parameter representing canopy light extinction coefficient.

f_{gf} is the factor to indicate a switch to grain filling, calculated as shown below.

$senrate$ is the parameter representing the rate of senescence per unit thermal time.

$\frac{dTT_t}{dt}$ is as described above.

The switch to grain filling was assumed to happen 200 degree days of thermal time after end of leaf expansion.

$$f_{gf} = \frac{1}{1 + e^{-\frac{log(99)}{200}(TT_t - (TTL + 200))}} \tag{4.3.6}$$

where,

TT_t and TTL are defined above.

The water stress factor was calculated such that crop starts experiencing water stress when PAW is 35% of AWHC.

$$f_{ws} = \frac{1}{1 + e^{-\frac{log(99)}{0.175}\left(\frac{PAW_t}{AWHC} - 0.175\right)}} \tag{4.3.7}$$

where,

PAW_t is available water content at time t.

$AWHC$ is the input variable representing available water holding capacity.

4.3.2.3 Biomass

Biomass was calculated primarily as a function of RUE, solar radiation (SRAD), and light interception. Water stress factor and thermal time constraints were also taken into account.

$$\frac{dBM}{dt} = RUE \cdot SRAD_t \cdot f_{ws} \cdot \frac{dTT_t}{dt} \cdot (1 - e^{-K\ LAI_t}) \tag{4.3.8}$$

where,

$\frac{dBM}{dt}$ is the rate of change of biomass at time t.

f_{ws}, $\frac{dTT}{dt}$ K, and LAI_t are defined above.

RUE is the parameter representing radiation use efficiency.

$SRAD_t$ is observed solar radiation at time t.

4.3.2.4 Yield

Yield was calculated as the amount of biomass accumulated after the beginning of grain filling.

$$\frac{dYLD_t}{dt} = \frac{dBM_t}{dt} \cdot f_{gf} \tag{4.3.9}$$

where,

$\frac{dYLD_t}{dt}$ is the rate of change of yield at time t.

$\frac{dBM_t}{dt}$ and f_{gf} are defined above.

4.3.2.5 Plant vailable water content

Plant available water content (PAW) was calculated as a function of rainfall, irrigation, available water holding capacity (AWHC), and crop evapotranspiration (ET_c).

$$\frac{dPAW_t}{dt} = \frac{rain_t + irrigation_t}{1 + e^{-\frac{log(99)}{0.25}\left(\frac{PAW_t}{AWHC} - 0.75\right)}} - ET_{c\ t} \cdot f_{sw} \tag{4.3.10}$$

where,

$\frac{dPAW_t}{dt}$ is the rate of change of plant available soil water content.

$rain_t$ is the input variable representing observed rainfall.

$irrigation_t$ is the input variable representing irrigation.

PAW_t, $AWHC$, and f_{sw} are as defined above.

$ET_{c\ t}$ is the crop evapotranspiration at time t, calculated as shown below.

$$ET_{c\ t} = ET_{0\ t} \cdot K_{c\ t} \tag{4.3.11}$$

where,

$ET_{0\ t}$ is reference evapotranspiration at time t, $mm\ day^{-1}$.

$K_{c\ t}$ is the crop coefficient at time t, calculated as shown below.

$$\begin{aligned} K_{c\ t} =& K_{c\ ini} + \left(1 - e^{-K\ LAI_t}\right)\left(K_{c\ mid} - K_{c\ ini} + \frac{K_{c\ ini} - K_{c\ end}}{e^{-100\left(\frac{TT_t}{TTL \cdot 200} - 1\right)} + 1}\right) - \\ & \frac{K_{c\ ini} - K_{c\ end}}{e^{-100\left(\frac{TT_t}{TTL \cdot 200} - 1\right)} + 1} \end{aligned} \tag{4.3.12}$$

The calculations of ET_0 and $K_{c\ ini}$, $K_{c\ mid}$, and $K_{c\ end}$ are shown in the supplementary materials, and follow the procedures in Allen, Pereira, Raes, and Smith (1998).

At each timestep, the value of the state variables were updated for each k^{th} block using Euler integration according to:

$$\mathbf{S}_{k\ t+1} = \mathbf{S}_{k\ t} + \frac{d\mathbf{S}_{k\ t}}{dt}\Delta t \tag{4.3.13}$$

where, $\mathbf{S}_{k\ t} = [VRN_{k\ t}, TT_{k\ t}, LAI_{k\ t}, BM_{k\ t}, YLD_{k\ t}, PAW_{k\ t}]$ are the observed state variables for block k at time t, $\mathbf{S}_{k\ t+1} = [VRN_{k\ t}, TT_{k\ t}, LAI_{k\ t}, BM_{k\ t}, YLD_{k\ t}, PAW_{k\ t}]$ at time $t+1$, and Δt is the fixed time step of one day.

The output of the ODE model is then represented by:

$$\beta_{0ikt} = f(\mathbf{I}_k, \boldsymbol{\phi}, \mathbf{S}_0)$$

where,f represents the numerical integration of the ODE system from time 0 to time t, $\mathbf{I}_k$ is a matrix of input variables, $\boldsymbol{\phi}$ is a vector of the ODE model parameters as described above, and $\mathbf{S}_0$ is the vector of state variables at time 0.

4.3.3 Integration of the ODE model into a Bayesian hierarchical framework

The ODE model was integrated into a Bayesian hierarchical framework as follows:

$$Y_{ijkt} = \beta_{0ikt} + Plot[Env]_{j[k]} + \epsilon \tag{4.3.14}$$

where,

Y_{ijkt} is observed value of the i^{th} response variable (i = 1 for LAI, i = 2 for biomass, and i = 3 for yield), corresponding to j^{th} plot in the k^{th} environment at time t. To recall, an environment is defined as a location-year-treatment combination.

β_{0ikt} is predicted value of the i^{th} response variable from the ODE model for environment k and time t.

$Plot[Env]_{j[k]}$ is differential effect of j^{th} plot within an environment on the i^{th} response variable, assumed $Plot[Env]_{j[k]} \sim NIID(0, \sigma^2_{Plot\ i})$.

ϵ is residual error, assumed $\epsilon \sim NIID(\sigma^2_{e\ i})$.

4.3.4 Model implementation

Two separate versions of the model were implemented, one with water balance and another without water balance to assess if the addition of water balance component contributed to better predictions by the model. The model with water balance included equations 4.3.10 and 4.3.11, whereas these equations were excluded in the model without water balance, and f_{ws} was fixed at 1 indicating no water stress.

The models were implemented within a Bayesian framework which allowed us to introduce stochasticity into the models and to utilize prior information available on the model parameters. In addition, with the Bayesian framework, the parameter estimations and model predictions are produced in the form of a posterior distribution rather than point estimates, which simultaneously provides an uncertainty estimate. Samples were drawn from the posterior distribution of interest using a dynamic Hamiltonian Monte Carlo (HMC) sampler as implemented within Stan version 2.25.0 (Stan Development Team, 2018). Dynamic HMC sampler is an Markov Chain Monte Carlo (MCMC) algorithm that is quick and efficient in sampling the parameter space (Betancourt, 2017). Four MCMC chains were run with 10,000 iterations including 50% burn-in, resulting in a total of 20,000 saved iterations. Two common convergence diagnostics, traceplots and R-hat values, were used to monitor chain convergence. The effective sample size (ESS) for the ODE model parameters and the hierarchical model hyperparameters were greater than 1,400. The computing was performed on the TIGER research cloud at the Oklahoma State University High Performance Computing Center using a KVM virtual machine backed by a hypervisor node with dual Intel "Skylake" 6130 CPUs and 768 GB RAM. The models were implemented in Stan with the command-line interface to the Stan modeling language, Cmdstan.

For cleaning and organizing the data, R package tidyverse was used (Wickham et al., 2019; Wickham, Hadley, 2017). The posterior samples were processed with the R statistical software environment (R Core Team, 2020). The figures were created

using the ggplot2 (Wickham, 2016) and gridExtra (Auguie, 2017) packages in R . The highest density intervals (HDIs) of the posterior distributions of the parameters were computed using the HDInterval package (Meredith & Kruschke, 2018). Figures and Tables were generated using the R packages knitr (Xie, 2020) and kableExtra (Zhu, 2019).

4.3.5 Prior specification

The prior distributions for the ODE model parameters except for *senrate* were estimated based on literature and were specified as truncated normals in the form of $TN(\mu, \sigma^2)$. All priors had a lower bound of zero and no upper bound.

$\alpha \sim TN(0.016, 0.007^2)$ (Rodriguez et al., 1998)

$K \sim TN(0.6, 0.1^2)$ (Bechini et al., 2006; Muurinen & Peltonen-Sainio, 2006; O'Connell et al., 2004; Calderini et al., 1997)

$TTL \sim TN(950, 100^2)$ (McMaster et al., 2019; Bechini et al., 2006)

$RUE \sim TN(1.4, 0.25^2)$ (Bechini et al., 2006; Muurinen & Peltonen-Sainio, 2006; O'Connell et al., 2004; Calderini et al., 1997)

$vrn \sim TN(42, 7^2)$ (G. Li et al., 2013; Crofts, 1989)

The prior for *senrate* was determined using a heuristic procedure. It was assumed that with a peak leaf area index at flowering of 5 and 30 °C daily average temperature, it would take approximately 35 days to reach full senescence. Values of *senrate* were tested heuristically to determine a range of values that resulted in plausible senescence durations. With a rate of senescence of 0.005, it took approximately 35 days to reach a leaf area index near zero from five, a *senrate* of 0.002 took approximately 60 days, and a *senrate* of 0.008 took approximately 20 days. Thus, the prior μ was specified as 0.005 with a sigma of 0.001, thereby providing support in the prior for a range of durations between 20 and 60 days within three standard deviations of prior μ.

Thereby, $senrate \sim TN(0.005, 0.001^2)$

The priors for the hyperparameters pertaining to the hierarchical component of the model were specified following the prior predictive procedure described in Schad et al. (2019). The prior information for σ^2_{Plot} was specified in a multiplicative form. The prior σ of 0.1 indicates a 10% variability across plots, thereby allowing a 30% variability within three standard deviations. Hence, the priors are:

$\sqrt{\sigma^2_{Plot\ LAI}} \sim TN(0, 0.1^2)$.

$\sqrt{\sigma^2_{Plot\ biomass}} \sim TN(0, 0.1^2)$.

$\sqrt{\sigma^2_{Plot\ yield}} \sim TN(0, 0.1^2)$.

$\sqrt{\sigma^2_{e\ LAI}} \sim TN(0, 1^2)$.

$\sqrt{\sigma^2_{e\ biomass}} \sim TN(0, 100^2)$.

$\sqrt{\sigma^2_{e\ yield}} \sim TN(0, 30^2)$.

4.3.6 Model predictive performance

A cross-validated dataset was generated with leave-one-group out cross-validation where each environment was considered a group, hence there were a total of eleven groups. For each iteration of the cross-validation, one group was held out and parameters were estimated based on the remaining ten groups. The parameter estimates were then used to predict for the data from the withheld group. The predictions were used to calculate three statistical metrics: Root Mean Square Error (RMSE), Willmott agreement index (d; Willmott, 1981), and Nash-Sutcliffe Efficiency (NSE; Nash & Sutcliffe, 1970). This process was repeated for all groups one at a time and for both versions of the model i.e. with and without the water balance component.

In addition, a validation check was performed using the same metrics between observed data and model estimated values for PAW. This process is termed a full validation in contrast to the cross-validation procedure described above given that no soil water data was used to estimate any model parameters.

The statistical metrics were calculated as follows:

i) Root Mean Square Error (RMSE):

$$RMSE_s = \sqrt{\frac{1}{N}\sum_{n=1}^{N}(y_n - \hat{y}_n^s)^2} \tag{4.3.15}$$

where, N = Total number of data points, y_n is the n^{th} observation (n=1,2,...N), and $\hat{y}_n^s$ is the predicted value for the n^{th} observation obtained from the s^{th} MCMC iteration. Models with smaller values of RMSE are preferable.

ii) Willmott agreement index (d):

$$d_s = 1 - \frac{\sum_{n=1}^{N}(y_n - \hat{y}_n^s)^2}{\sum_{n=1}^{N}(|\hat{y}_n^s - \bar{y}| + |y_n - \bar{y}|)^2} \tag{4.3.16}$$

where, N, y_n, and $\hat{y}_n^s$ are as described above, and $\bar{y}$ is the average of the observed data points. This statistic ranges between 0 to 1 with values closer to 1 indicating good model fit.

iii) Nash-Sutcliffe Efficiency (NSE):

$$NSE_s = 1 - \frac{\sum_{n=1}^{N}(y_n - \hat{y}_n^s)^2}{\sum_{n=1}^{N}(y_n - \bar{y})^2} \tag{4.3.17}$$

where, N, y_n, $\hat{y}_n^s$, and $\bar{y}$ are as described above. The values of NSE can range from $-\infty$ to 1 and values closer to 1 indicate a better-fitting model.

4.3.7 Parameter estimation with end of season data

Estimation of model parameters was also performed using only the end of season data for yield and biomass, heading date, and LAI value of zero to investigate the utility of the model when only end of season data are available. The model, however, encountered sampling problems due to parameter non-identifiability and was simplified

to reduce the number of parameters by fixing the parameter values of TTL and RUE at 950 and 1.4 (i.e. the prior μ value for the original parameter estimation). This step was performed to assess the impact of data quantity and diversity on model performance.

4.4 Results

4.4.1 ODE model parameters

Table 4.2 shows the posterior HDI and median for the ODE model parameters. The model yielded biologically plausible values for most parameters, except RUE, for which the estimated value was higher than the range of biologically plausible values.

The HDI for α ranged from 0.0087 to 0.0094 with a median of 0.009, which indicates that the expected LAI increase per day is 0.9% of existing LAI. Likewise, the canopy light extinction coefficient (K) was estimated to be 0.36 on average as indicated by the posterior median. The model estimated that it takes around 800 degree days to reach end of leaf expansion as indicated by the median for TTL, and the average vernalization requirement as indicated by the posterior median for vrn was 35 days. The parameter $senrate$ had a median of 0.0065, which indicates that it takes 30 days for the canopy to reach from maximum leaf area to near zero leaf area index at a daily average temperature of 30 °C.

Figure 4.1 shows the smoothed densities for posterior samples of the ODE model parameters for the models with and without water balance along with the densities of samples from the prior distributions. A heavy shift and/or narrowing down of the density curve from prior to posterior indicates that the data were informative in estimating the parameters. The parameters α, K, TTL, and vrn shifted lower than specified priors, whereas RUE and $senrate$ shifted higher for both models. Likewise, the densities of posterior distributions were considerably narrowed compared to that

Table 4.2: Posterior HDI and median for the ODE model parameters

Parameter	Description	HDI	Median
α	Relative rate of LAI increase before the end of leaf expansion	(0.0087, 0.0094)	0.009
K	Light interception coefficient	(0.32, 0.39)	0.36
TTL	Thermal time to the end of leaf expansion	(747, 855)	798
senrate	Rate of senescence	(0.0059, 0.0071)	0.0065
RUE	Radiation use efficiency	(2.4, 2.9)	2.7
vrn	Vernalization requirement	(22, 51)	35

of prior distributions for all parameters except *vrn*. The biggest differences in the posterior densities of the two models were observed in RUE and *vrn*. The parameter RUE was estimated to be higher for the model including water balance, whereas the vernalization requirement (*vrn*) was estimated to be higher with the model excluding water balance. The posterior distribution of the parameter *vrn* was also closer to the prior for the model without water balance.

Varying degrees of correlations were observed between the posterior samples of the ODE model parameters as shown in Figure 4.2, which indicate the degree of parameter non-identifiability in the model. Specifically, correlations were observed between TTL and *vrn* (r = -0.85), RUE and *senrate* (r = 0.77), and α and K (r = 0.46).

4.4.2 Model predicted LAI, biomass, and yield

In this section, we present model predictions for the response variables LAI, biomass, and yield. Leaf area index (LAI) and biomass were predicted over the growing season whereas yield was predicted at the end of the season. Figure 4.4 and Figure 4.5 show

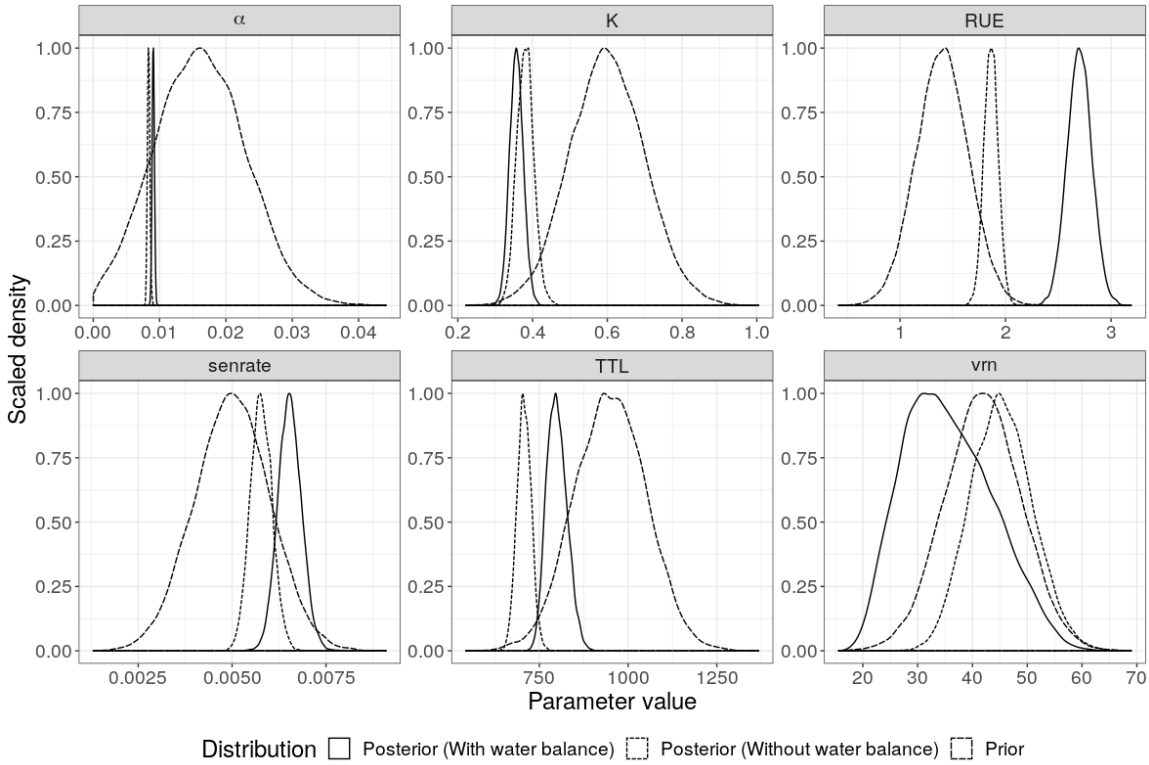

Figure 4.1: Density of prior and posterior distributions for the ODE model parameters for models with and without water balance, namely, relative rate of LAI increase before the end of leaf expansion (α), light extinction coefficient (K), Thermal time to end of leaf expansion (TTL), rate of senescence ($senrate$), Radiation use efficiency (RUE), and vernalization requirement (vrn).

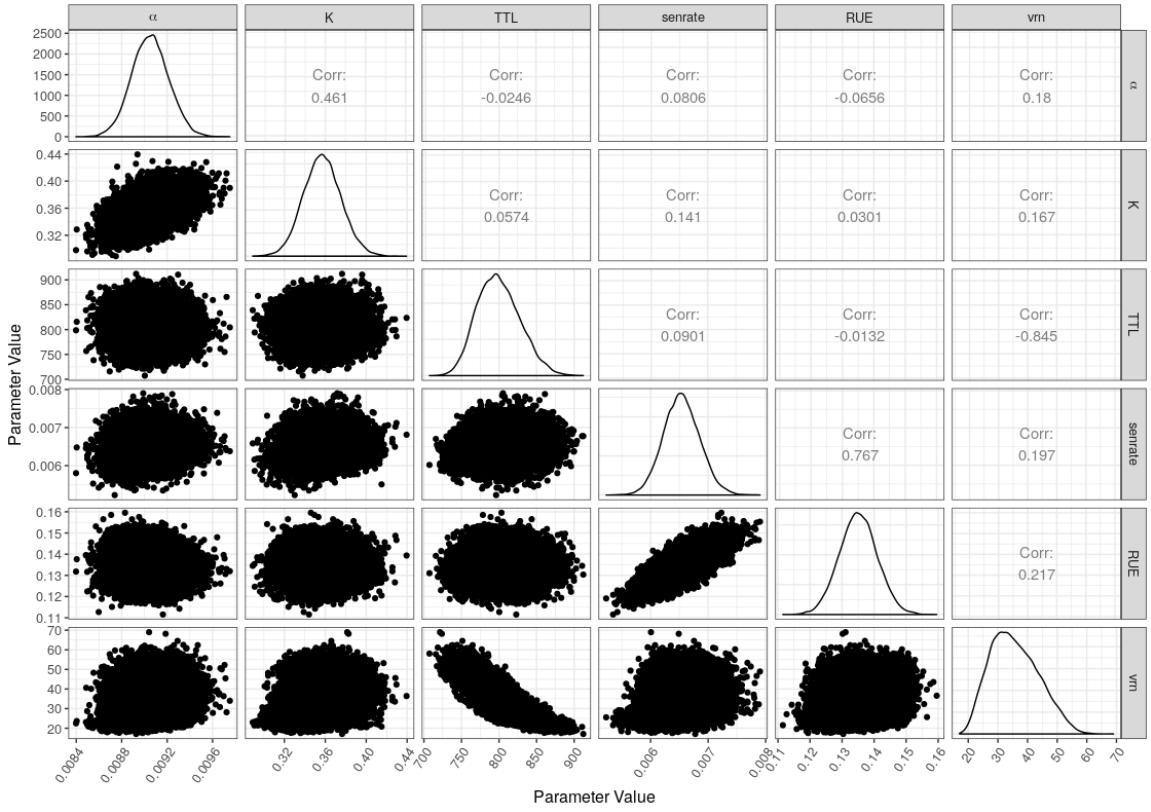

Figure 4.2: Joint posterior summary of the ODE model parameters, namely, relative rate of LAI increase before the end of leaf expansion (α), light extinction coefficient (K), Thermal time to end of leaf expansion (TTL), rate of senescence ($senrate$), Radiation use efficiency (RUE), and vernalization requirement (vrn).

the cross-validation predicted LAI and biomass values over the growing season from both models with and without water balance along with the observed data points for all eleven environments.

The model predictive performance was overall satisfactory. Specifically, adding the water balance component to the model better predicted yield as indicated by differences in the prediction statistics between the models with and without water balance component. Figure 4.3 shows the density plots of the prediction statistics where the model with water balance component has higher values for Nash-Sutcliffe efficiency (NSE) and Willmott agreement index (d) and lower values for RMSE for LAI and yield, indicating better prediction with the model with water balance. However, the results were opposite for biomass. The prediction statistics for models with and without water balance, respectively, were: $RMSE$ of 1.51 and 1.69, d of 0.89 and 0.85, and NSE of 0.62 and 0.52 for LAI, $RMSE$ of 134.25 and 237.81, d of 0.88 and 0.32, and NSE of 0.25 and -1.36 for yield, and $RMSE$ of 531.44 and 353.92, d of 0.88 and 0.93, and NSE of 0.43 and 0.75 for biomass.

The LAI predictions using the model with water balance are closer to the observed datapoints for most environments, and the difference between the two models is more prominent in rainfed conditions at all locations in 2013-14 growing season. At these environments, the LAI values predicted using the model with water balance were less than those predicted using the model without the water balance component.

Likewise, in the case of biomass prediction, the difference between the two models is more pronounced in rainfed conditions at all locations in 2013-14 growing season depicting a similar pattern to LAI. At these environments, especially Stillwater_2014_Dryland, the model with water balance severely underestimated biomass. This indicates that the water stress calculated by the model is more severe than the actual conditions. Compared to LAI, the difference between the models seems to be more prominent in biomass prediction. Furthermore, Table 4.3 shows averages for

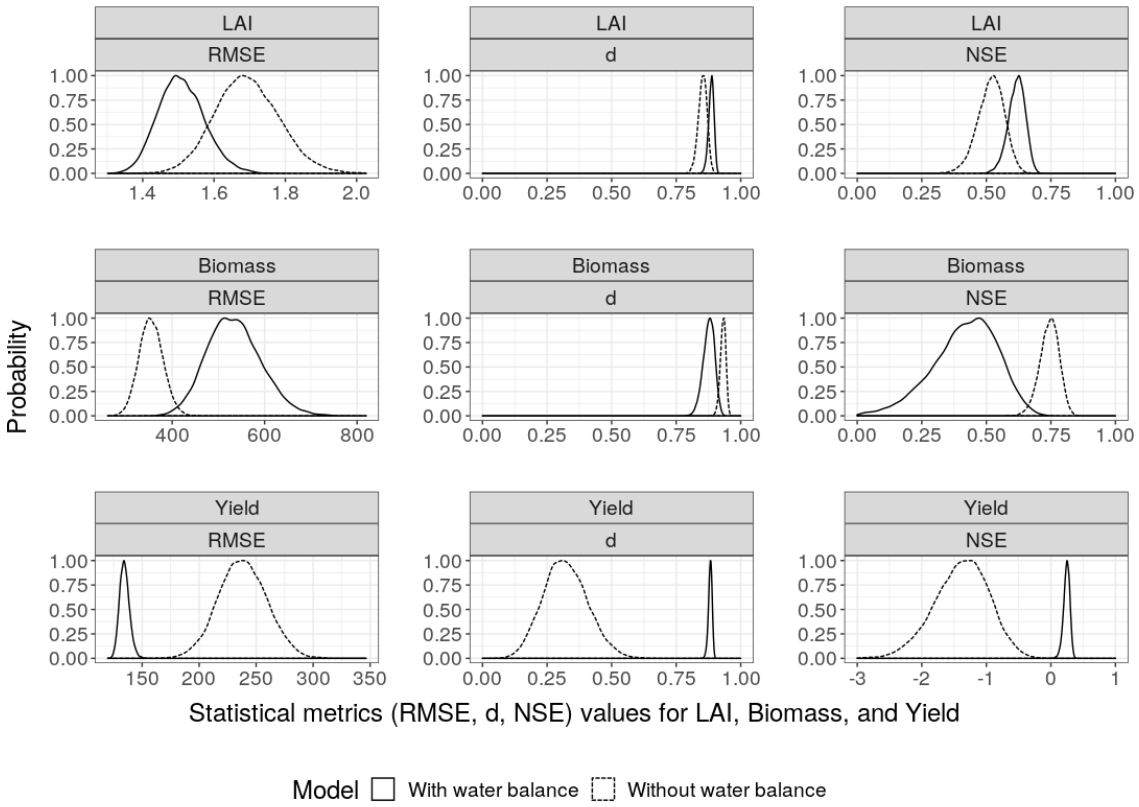

Figure 4.3: Predictive performance of models including and excluding the water balance component for leaf area index (LAI), biomass, and yield assessed with three statistical metrics: root mean squared error (RMSE), Willmott agreement index (d), and Nash-Sutcliffe efficiency (NSE).

Table 4.3: Observed means and cross-validation predicted medians for yield with models including and excluding water balance for all environments i.e. location-harvest year-treatment combinations

Environment	Observed yield (gm^{-2})	Model predicted yield (gm^{-2})	
		Model with water balance	Model without water balance
Chickasha_2013_Dryland	683	736	553
Chickasha_2014_Dryland	333	158	626
Lahoma_2013_Dryland	528	432	572
Perkins_2013_Dryland	553	590	528
Perkins_2013_Irrigated	643	661	504
Perkins_2014_Dryland	300	140	615
Perkins_2014_Irrigated	706	651	579
Stillwater_2013_Dryland	572	631	505
Stillwater_2013_Irrigated	552	662	500
Stillwater_2014_Dryland	333	58	609
Stillwater_2014_Irrigated	742	669	579

cross-validation predicted and observed yield for each environment. Like biomass, the difference between the two models is greatest in the 2013-14 season.

These patterns could be further explained with the help of water stress factor calculated by the model over time (Figure 4.6). Figure 4.6 shows that the water stress factors for the growing season 2013-14 is lower (i.e. more water stress) compared to the season of 2012-13.

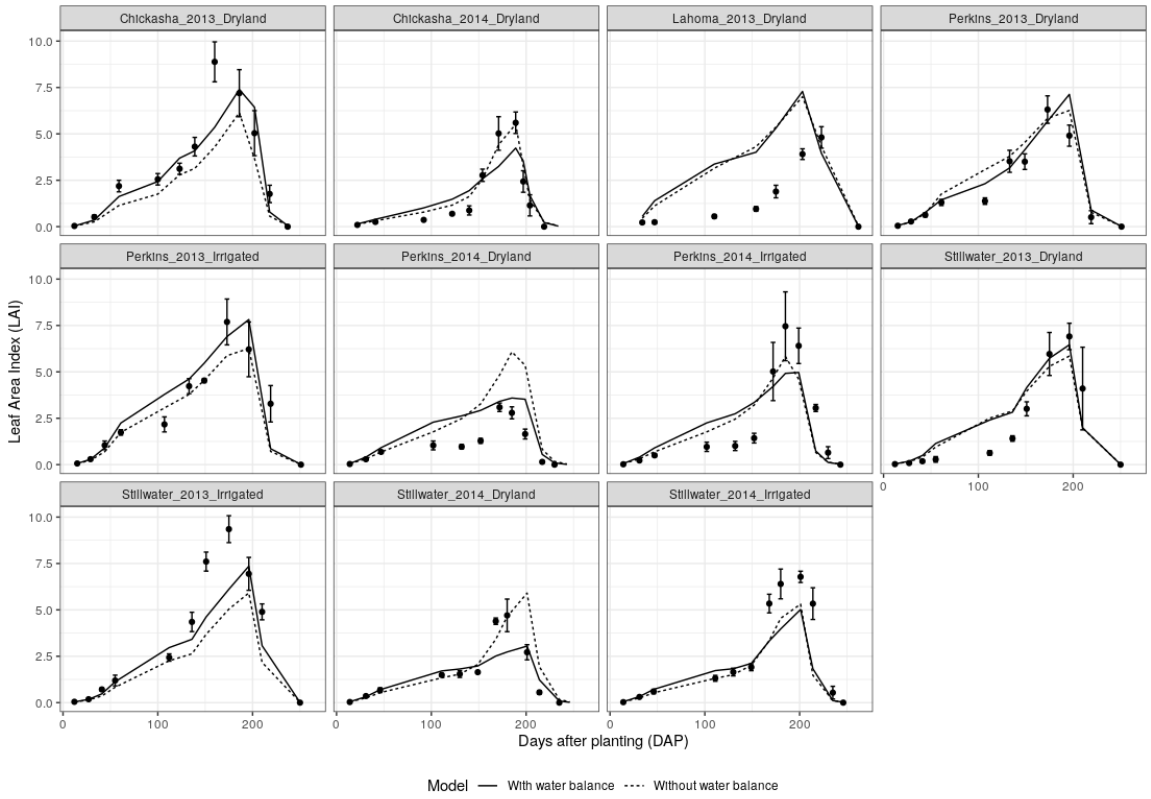

Figure 4.4: Cross-validation predictions of leaf area index (LAI) with models including and excluding the water balance component over the growing season at each time point along with the observed datapoints for dryland and irrigated winter wheat for all environments i.e. location-harvest year-treatment combinations

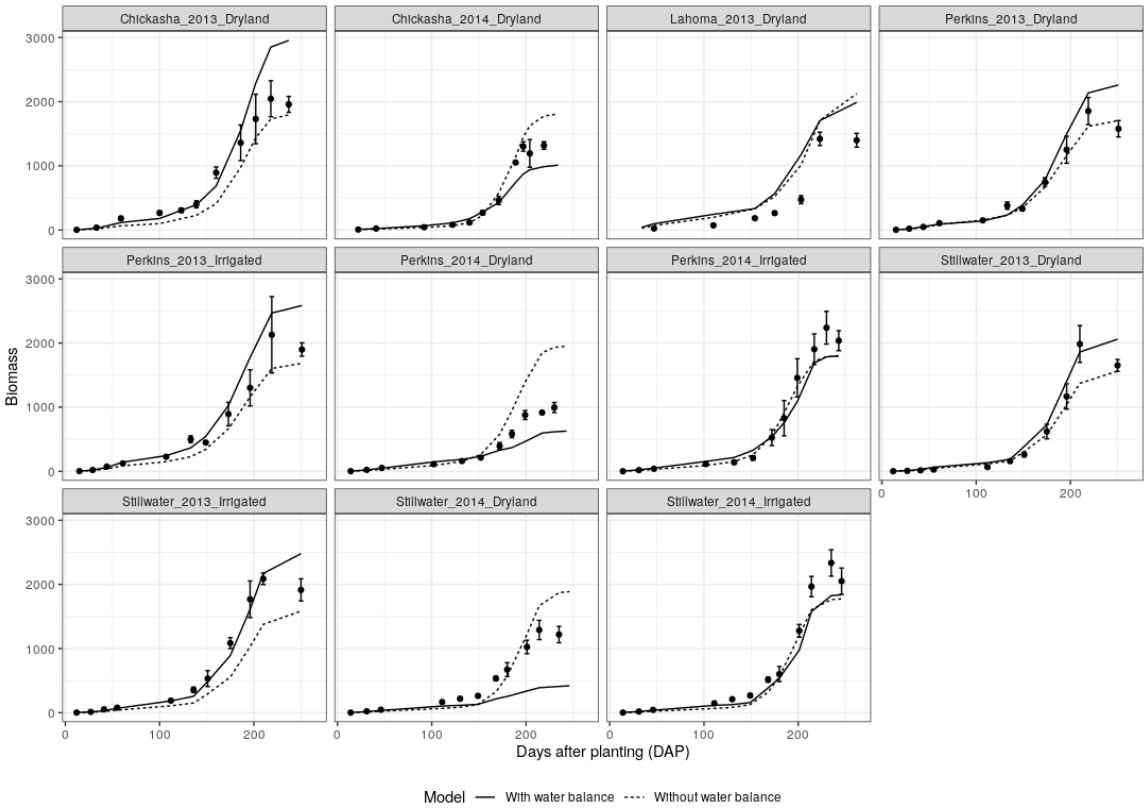

Figure 4.5: Cross-validation predictions of biomass with models including and excluding the water balance component over the growing season at each time point along with the observed datapoints for dryland and irrigated winter wheat for all environments i.e. location-harvest year-treatment combinations

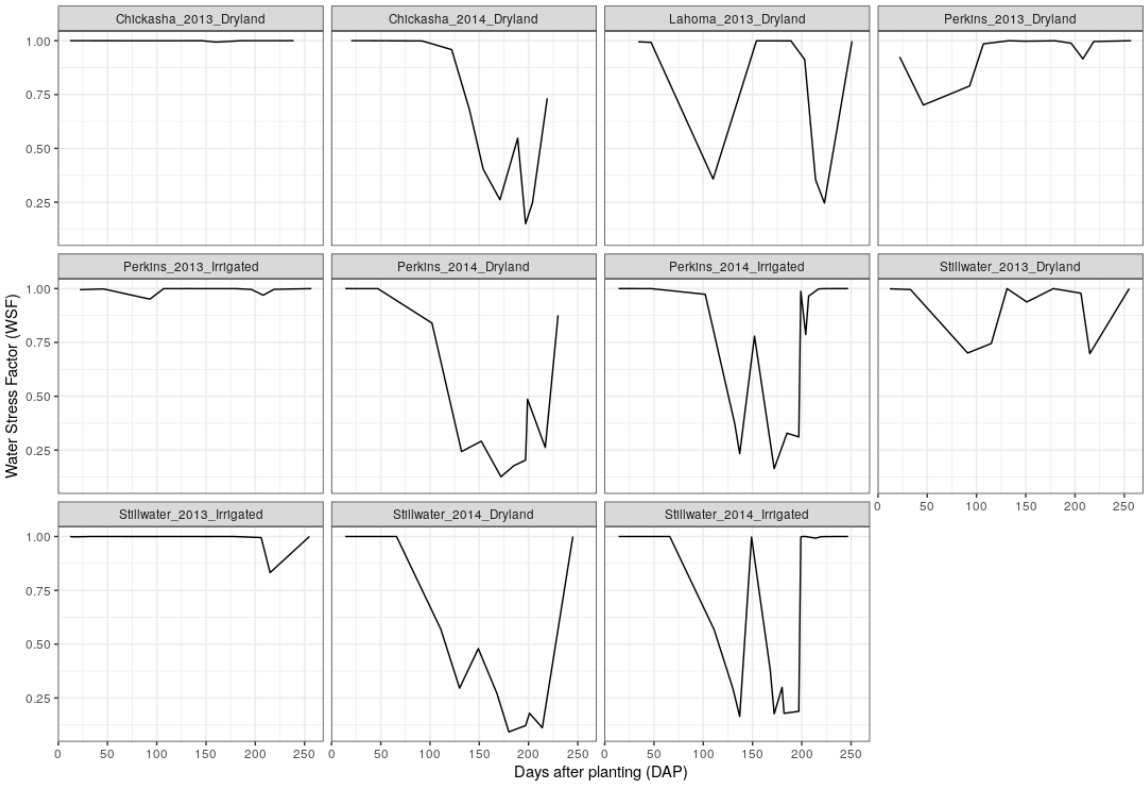

Figure 4.6: Water stress factor over the growing season estimated by the model including the water balance component for dryland and irrigated winter wheat in Oklahoma for all environments i.e. location-harvest year-treatment combinations

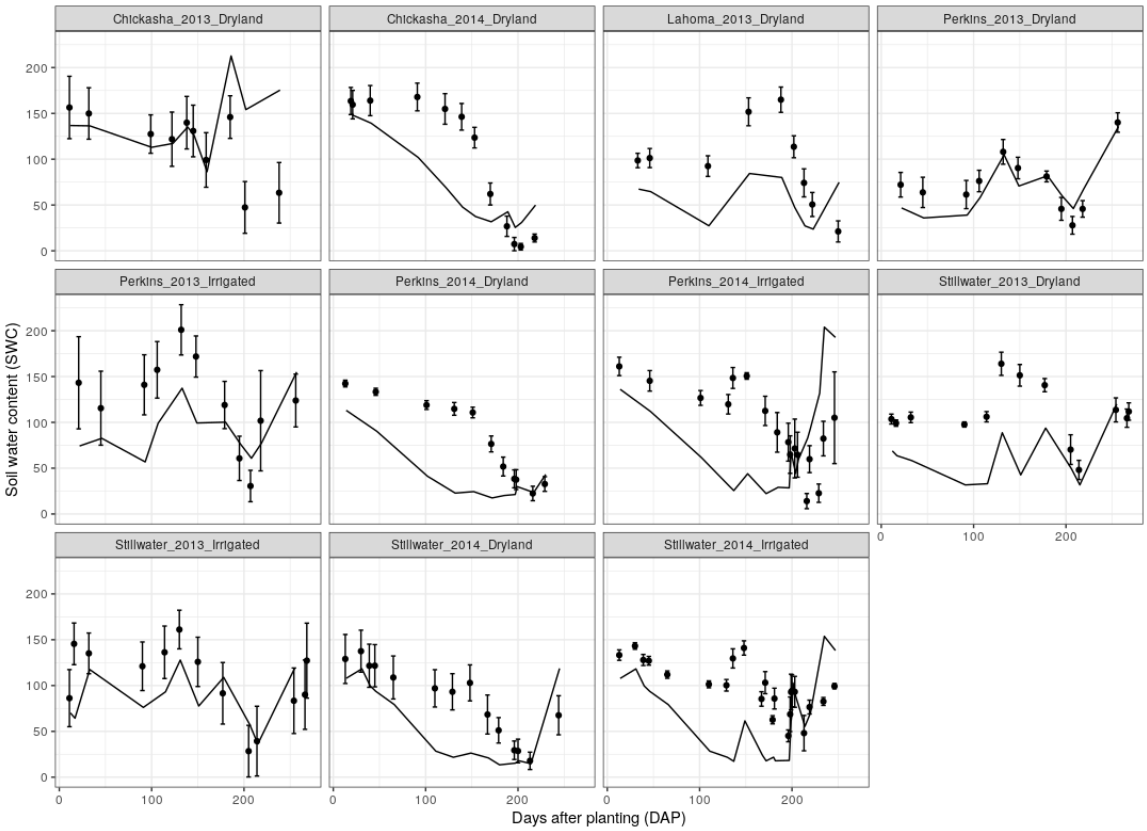

Figure 4.7: Soil water content (mm) estimated by the model including the water balance component over the growing season along with observed soil moisture data obtained using neutron probe for dryland and irrigated winter wheat in Oklahoma for all environments i.e. location-harvest year-treatment combinations

4.4.3 Soil water content

There was an overall bias in estimation where the estimated soil water content was less than the observed soil water content for most environments (Figure 4.7). The median values for statistics RMSE, d, and NSE for soil water content were 66 (mm), 0.4, and -1.6 respectively. A negative NSE value indicates that the observed data mean is a better estimate than the model predictions.

For futher investigation, the crop evapotranspiration values were calculated with the model at posterior median values of ODE model parameters. It was observed that the difference between potential cumulative crop ET and simulated actual crop ET

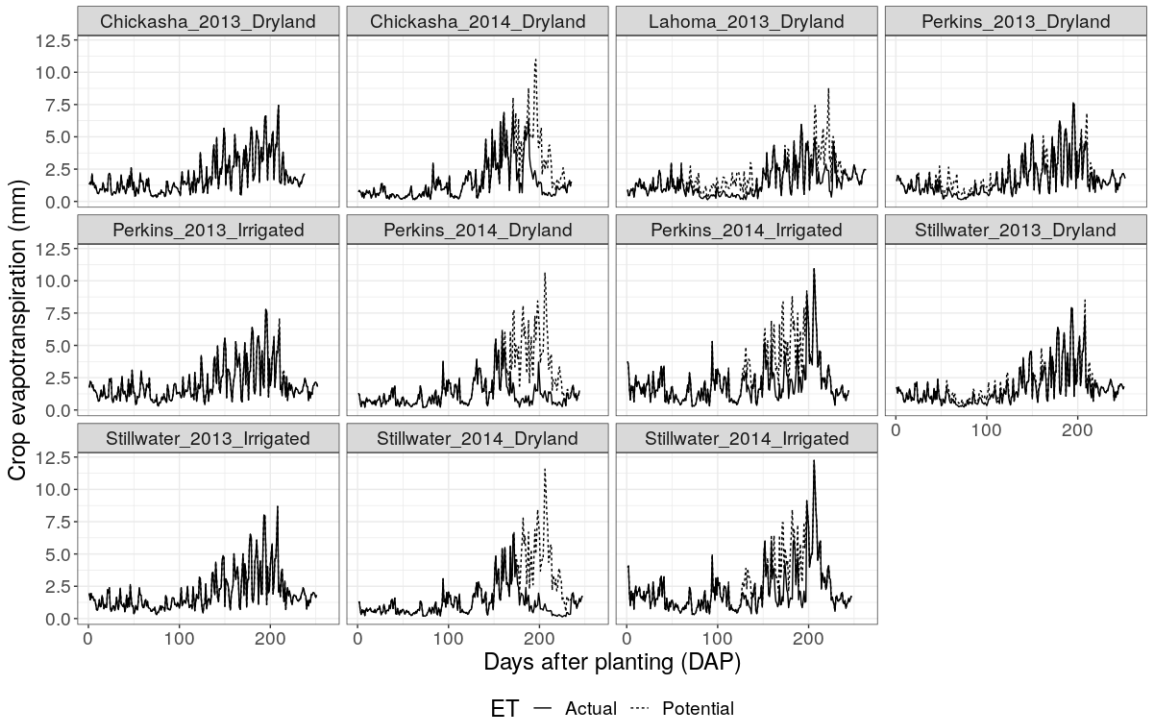

Figure 4.8: Potential and simulated actual crop evapotranspiration over the season, estimated at the posterior medians of the ODE model parameters for all environments i.e. location-harvest year-treatment combinations

(i.e. after factoring in the water stress) was higher in the dryland environments of 2013-14 compared to all environments in 2012-13 (Figure 4.8). Highest cumulative crop ET values were observed in irrigated treatments in both seasons (range of 478 to 509) followed by dryland treaments of 2012-13 (range of 390 to 464) and lowest ET values were associated with dryland treatments in 2013-14 (range of 269 to 327). This pattern is similar to the LAI and biomass results.

4.4.4 Parameters from the hierarchical component of the model

Table 4.4 shows the posterior HDI and median for the hierarchical component hyperparameters in the model. The variance parameters for residuals for the three response variables (LAI, biomass, and yield) shifted higher than the specified priors.

Table 4.4: Posterior HDI and median for the hyperparameters in the model

Parameter	HDI	Median
$\sqrt{\sigma^2_{e\ LAI}}$	(1, 1.15)	1.080
$\sqrt{\sigma^2_{e\ biomass}}$	(147, 169)	159.000
$\sqrt{\sigma^2_{e\ yield}}$	(93, 132)	110.000
$\sqrt{\sigma^2_{Plot\ LAI}}$	(0.16, 0.27)	0.210
$\sqrt{\sigma^2_{Plot\ biomass}}$	(0.34, 0.53)	0.430
$\sqrt{\sigma^2_{Plot\ yield}}$	(0.000002,0.08)	0.027

As mentioned previously, the plot effects were defined as a fraction of the ODE-model-simulated value for each variable. Thus, the median value of 0.21 for $\sqrt{\sigma^2_{Plot\ LAI}}$ indicates that the variability between plots within an environment was 21% of the LAI simulated at any given time point. The plot square root of variance is higher for biomass with a median of 0.43 and small for yield with a median of 0.027.

4.4.5 Parameter estimation with end of season data

The model did not efficiently sample from the posterior distribution. The number of effective samples ranged from 97 to 131 for the ODE model parameters and from 30 to 221 for the hyperparameters of the hierarchical component of the model. The chains didn't converge as indicated by the largest R-hat of 1.12 among all parameters. Hence, the results from this model are not further interpreted due to a very small number of samples and lack of convergence.

4.5 Discussion

In this study, we utilized an ODE crop growth model coupled with a simple water balance model to estimate certain wheat growth parameters in winter wheat. We

also compared the out of sample model predictions on three response variables (LAI, biomass, and yield) to assess model performance. In addition, we performed a validation analysis to examine how close the water balance estimates compared to the observed soil water content.

4.5.1 ODE model parameters

The posterior median for the light extinction coefficient parameter (K) was estimated to be 0.36, which is possible, but lower than most literature reported values that were used to formulate the priors. A study by Pradhan et al. (2018) in India obtained light extinction coefficient values between 0.47 to 0.65 under irrigated conditions, and also reported that the irrigation didn't have a significant effect on light extinction coefficient. Low light extinction coefficient indicates that it requires more leaf area to intercept the same amount of light compared to canopies with high light extinction coefficient.

Posterior estimates for the parameter representing RUE were compared for the model with water balance to the model without water balance. Both models resulted in RUE estimates that were higher than expected based on other studies, most of which were used for prior specification. The RUE values are commonly reported as RUE_{PAR} i.e. the RUE per unit photosynthetically active radiation, which would be approximately double the RUE value per unit total solar radiation. The study by Pradhan et al. (2018) reported RUE_{PAR} values between 1.97 to 2.73 (i.e. roughly 0.98 to 1.36 gMJ^{-1}), which is much lower compared to what was estimated by our model. Another study by Shearman et al. (2005) also reported a pre-anthesis RUE_{PAR} value of 2.47. Thus, the parameter for RUE was substantially overestimated by our model. In comparison between the two models, RUE was higher when estimated with the model with water balance, indicating that water stress might contribute to this change in posterior distribution of RUE from one model to the other. This

could be due to rapid decline in leaf area at the end of the growing season causing lower LAI and consequently lower light interception. The decline in leaf area was even more rapid in case of the model including water stress, for which higher values of RUE during estimation compensated. The higher values for RUE allowed biomass accumulation and yield formation even in the presence of reduced light interception and water stress during the grain-filling period. A possible improvement in the model to address this issue could be to accomodate the carbohydrate remobilization process, which would contribute to yield formation even under reduced photosynthetic capacity. Carbohydrate remobilization can play an important role in grain-filling especially under water-limited conditions (Yang, Zhang, Huang, Zhu, & Wang, 2000; Davidson & Chevalier, 1992).

The correlations between the ODE model parameters indicate a non-identifiability problem in the model to some extent. The correlation between these parameters can be interpreted in terms of model specification to understand how they offset each other. The positive correlation between $senrate$ and RUE indicates that lower light interception due to higher senescence rate can be compensated by higher RUE to sustain the growth rate. Likewise, the interplay between TTL and vrn indicate that there is not enough information in the data to adequately distinguish these two parameters. The dataset used in this study doesn't adequately represent diverse conditions in terms of planting time and temperatures which would be helpful in identifying variable vernalization requirements. A dataset from environments with variable planting time and more contrasting environmental conditions could potentially provide information to disambiguate these parameters. The correlation between α and K is a result of their offsetting influence on leaf area through equation 4.3.5, i.e. for a given unit increase in α, the effect of that change can be offset by a corresponding adjustment to the value of K. Thus, given the limitations of the data used for estimation, these two parameters cannot be fully distinguished.

4.5.2 Model predicted LAI, biomass, and yield

Results showed that water stress calculated by the model was likely overestimated as indicated by lower values of model predicted LAI than observed LAI in most environments. Likewise, the biomass in dryland environments in 2013-14 was predicted to be more severely affected by water stress compared to LAI. This is because the biomass is being affected by water stress twice, first through reduced light interception because of low LAI, and second due to the direct effect of water stress on biomass as shown in equation 4.3.8. Furthermore, the greatest differences in predicted yield between the models with and without water balance were observed in dryland environments in 2013-14. The difference in total water supplied between dryland and irrigated treatments at the same location in 2012-13 was smaller than in 2013-14 (results not shown). Thus, the difference between the models with and without water stress was more pronounced in environments where water stress was higher as indicated by the water stress factor.

Higher water stress calculated by the model in the growing season of 2013-14 could also have been indirectly influenced by temperature. The simulated early season LAI (especially between 50 to 100 DAP) in 2013-14 season and also Lahoma_2013_Dryland was greater than the observed LAI. Subsequent analysis showed that the average minimum temperature during that time period was close to 4 °C in Stillwater and Perkins in 2012-13 and and close to 0 °C in 2013-14 and in Lahoma in 2013. The base temperature in our model was set to 0 °C, which means the leaves continued to grow at all times in both seasons (albeit at a reduced rate). However, since the early season temperatures in 2012-13 were higher i.e., around 4 °C, the continuous leaf growth was expected. But in 2013-14, the leaf growth rate in the field was slower than the model simulation as shown by the LAI data during that time frame, which is possibly related to the lower temperatures. As a result, more leaf area than observed was simulated in 2013-14 leading to higher transpiration and exhaustion of soil water

content resulting in higher water stress and lower yield and biomass at the end of the season. This also points to the possibility that the base temperature for wheat used in this study may be greater than 0 °C. McMaster and Smika (1988) found that calendar days outperformed thermal time from emergence through jointing and G. Slafer and Savin (1991) found a base temp of 4 °C to 9.5 °C depending on growth stage.

To understand the low predictions of biomass values in dryland environments of 2013-14, we explored the two possibilities as mentioned above, first, reduced light interception through low LAI, and second through direct effect of water stress. To explore the first case, we supplied observed LAI values interpolated over the season to the model and examined resulting biomass. This did not show an increase in biomass, suggesting that lower biomass values could have been more related to the water stress. To explore the second case, we examined the cumulative crop ET values and crop coefficient (K_c) values. In general, the crop ET values were within plausible ranges (273 to 426 mm) across environments, yet lower when compared to the literature, where crop ET was mostly determined for irrigated environments (Howell et al., 2007; Howell, Steiner, Schneider, & Evett, 1995). A review by S. Zhang, Sadras, Chen, and Zhang (2013) reported that the crop ET for dryland wheat in China under conventional tillage ranged from 123 to 589 mm. The crop coefficient values, specifically for $K_{c\ ini}$ were high for the 2013-14 growing season. We ran the model with lower values for $K_{c\ ini}$, which resulted in lower ET values earlier in the season and higher biomass. Hence, the exploratory analyses of the results suggested that it was not leaf area, but the crop ET coefficient relationships that needs to be re-evaluated in future improvements of the model.

The fact that biomass and yield were more severely impacted by water stress than LAI also brings to attention that the link between variables could be advantageous or disadvantageous depending on model specification. The inclusion of water balance clearly improved model performance for LAI and yield. However, the fact that biomass

was not predicted as well by the model that contained water balance illustrates the challenges of working with a model structured to be biologically realistic. Due to the relationships between variables imposed by the structure of the ODE system, a bias due to model mis-specification for one variable (e.g. soil water) is more likely to result in a bias in other variables as well. If using a standard analytical approach based on linear modeling of soil water, LAI, biomass, and yield separately, a bias in one variable would not affect the other variables. Thus, care should be taken to ensure that the model is properly specified for all variables in the model.

4.5.3 Soil water content

The overall bias where estimated soil water is lower than observed results in the water stress factor calculated based on simulated soil water to be more severe than water stress was in reality.

One of the reasons for this could be the crop evapotranspiration (ET_c) values calculated as reference evapotranspiration (ET_0) multiplied by crop coefficient values (K_c) for initial, mid, and end growth phases. Upon assessment of ET_0 and K_c values, it was observed that the average ET_0 values didn't substantially vary between environments (range 2.69 to 3.01), however, the crop coefficient values, especially the crop coefficient for early growth stage ($K_{c\ ini}$) ranged from 0.24 to 0.96 across different environments with higher values associated with the growing season of 2013-14. These values are higher than the literature reported values where K_c values for wheat were determined for Texas environments (Howell et al., 2006; Ko, Piccinni, Marek, & Howell, 2009). Furthermore, the exploratory analysis of the results with lower $K_{c\ ini}$ values also resulted in a slower decline of soil water early in the season.

Thus, for further improvement of the model, the representation of crop coefficients should be improved. Using the dual crop coefficient approach, which separates ET into evaporation and transpiration as two separate components, might be an alternative

to more accurately estimate crop evapotranspiration. Another possible approach to address this issue could be to utilize a layered soil water model with two layers, which would still be simpler than the multi-layer models, where the evaporation is specified to only occur from the top layer. Estimation of parameters relating to crop evapotranspiration rather than calculating and supplying it to the model could be another alternative. Future work should emphasize improvements in this aspect of the model.

4.5.4 Parameters from the hierarchical component of the model

The unexplained variance was higher than expected as indicated by higher posterior medians compared to prior means for the hyperparameters. The estimate for the parameter representing plot variance in biomass ($\sqrt{\sigma^2_{Plot\ biomass}}$) was very high. However, the estimate for ($\sqrt{\sigma^2_{Plot\ yield}}$) was much smaller, which was estimated to be only 2.7% compared to 43% for biomass. This is most likely because the area from which yield was obtained was much larger (20 m^2) compared to the area biomass was sampled from (0.25 m^2). Data measured from a smaller sample area would be influenced by within-plot variability in addition to between-plot variability, whereas data measured from a larger area would be less influenced by the within-plot variability.

4.5.5 Model predictive performance

The addition of a water balance component to the model had the most positive effect on yield as indicated by the statistical metrics. This suggests that the water balance was important in later growth stages to model the terminal drought stress. The model with water balance was also better in predicting LAI; however, the addition of water balance seemed to have a negative effect on predictions for biomass. As described above, this is most likely a result of compound effect of water stress on biomass through LAI and the direct effect of water stress, which caused the estimates to be significantly

lower than what would be expected. This phenomenon was also reflected in the statistical metrics which showed that the model predicted biomass values are far from observed values. Figure 4.5 depicts that the end of season biomass was substantially higher than observed in Chickasha_2013_Dryland whereas Stillwater_2014_Dryland was much lower. Environments with extreme predictions like these contributed to the deviance of predictions from the observed means, therefore resulting in poor model performance as shown by low NSE and d values, and higher RMSE.

4.5.6 Parameter estimation with the end of season data

The results indicate that the model calibration approach needs to be refined in order to be used with only the end of season data. Estimating fewer parameters could be an option to reduce parameter non-identifiability. For instance, specific leaf area could be used to establish a bi-directional relationship between LAI and biomass, which would allow us to estimate LAI and biomass without estimating α. In addition, more stringent priors could be specified for well-studied parameters such as RUE to facilitate better sampling. Other sampling methods that can handle parameter correlations better also can be utilized as alternatives. The end of season data by itself also could be inadequate in estimating the parameters. Augmenting the end of season data with other information on growth stages (terminal spikelet, booting, heading, anthesis, maturity) and end of season PAW can also be valuable to get the phenology right. Such a modeling approach, if successful, would be highly useful to analyze big datasets such as variety trial data. These data usually do not have information on different variables througout the growing season, rather mostly contain end of season data with information on important developmental stages.

4.6 Conclusion

The water balance model was found to be improve the accuracy of simulated wheat LAI and yield, especially under water limited conditions. The ODE model parameters suggested that the model performed satisfactorily, however, many potential approaches for further improvements of the model were identified. The long-term goal is to develop a model which can synthesize information contained in extensive variety trial datasets for better understanding of the system and parameters, while also being able to analyze end of season data to make meaningful inferences. Thus, this project laid a foundation to incorporate a basic crop model with a water balance model to understand winter wheat growth and production.

4.7 Supplementary materials

4.7.1 Reference evapotranspiration (ET_0) and single crop coefficient (K_c) calculations

4.7.1.1 Calculations for crop coefficient (K_c):

Crop coefficient (K_c) was calculated for three development stages: initial, mid-season, and late-season. Length of crop development stages was determined based on Table 11 of Allen et al. (1998). However, the initial period was specified to be from planting date to 90 days after planting to accomodate typical growth rates in Oklahoma. The mid-season period was from 70 days prior to harvest to 30 days prior to harvest, and late-season was from 30 days prior to harvest until the harvest date. The K_c values were calculated for each development stages with the following formulae:

i)

$$K_{c\ ini} = \begin{cases} \frac{TEW-(TEW-REW)\ exp[\frac{-(t_w-t_1)E_{so}(1+\frac{REW}{TEW-REW})}{TEW}]}{t_w\ ET_o}, & t_w \geq t_1 \\ \frac{E_{so}}{ET_o} = 1.15, & t_w \leq t_1 \end{cases} \tag{4.7.1}$$

where,

TEW = Total evaporable water, calculated below.

REW = Readily evaporable water, calculated below.

ET_o = Mean reference evapotranspiration [$mm\ day^{-1}$] during the initial growing period.

E_{so} = Potential rate of evaporation [$mm\ day^{-1}$], calculated as: $1.15 * ET_o$

t_w = Mean interval between wetting events [days], calculated as: $t_w = \frac{L_{ini}}{n_w + 0.5}$, where, L_{ini} = length of initial growing period [days] = 30 taken from Table 12 of Allen et al. (1998), and n_w = Number of wetting events greater than $0.2 * ET_o$ during the initial period.

t_1 = Time when stage 1 drying is completed [days], calculated as: $t_1 = REW/E_{so}$

The values of corrected TEW and REW i.e. TEW_{cor} and REW_{cor} were used in the equation in place of TEW and REW to calculate $K_{c\ ini}$. TEW_{cor} and REW_{cor} were calculated following figures 29 and 30 in Allen et al. (1998), whereby,

For all soil textures having light infiltration depths ($< 10\ mm$):

$TEW_{cor} = 10mm\ REW_{cor} = min(max(2.5, 6/(ET_o)^{0.5}), 7)$

For coarse soil textures having large infiltration depths ($\geq 40\ mm$):

$TEW_{cor} = min(15, 7(ET_o)^{0.5})\ REW_{cor} = min(6, TEW_{cor} - 0.01)$

For medium and fine soil textures having large infiltration depths ($\geq 40\ mm$):

$TEW_{cor} = min(28, 13(ET_o)^{0.5})\ REW_{cor} = min(9, TEW_{cor} - 0.01)$

For infiltration depths between 10 mm and 40 mm:

$K_{c\ ini}$ = $K_{c\ ini}$ for light infiltration depths + $\frac{I-10}{40-10}$ [$K_{c\ ini}$ for large infiltration depths - $K_{c\ ini}$ for light infiltration depths]

Soil texture was determined using the values for clay percentage and silt percentage from Lollato and Edwards (2015). Sand percentage was calculated as 100-SLCL-SLSI and soils with greater than 70% sand and less than 15% clay were considered coarse, whereas the rest were considered medium and fine.

ii)

$$K_{c\ mid} = 1.15 + [0.04(u_2 - 2) - 0.004(RH_{min} - 45)](\frac{h}{3})^{0.3} \tag{4.7.2}$$

where,

1.15 is the value for $K_{c\ mid}$ taken from Table 12 of Allen et al. (1998).

u_2 = Mean value for daily wind speed at 2 m height during the mid-season growth stage $[ms^{-1}]$, for $1\ m\ s^{-1} \leq u_2 \leq 6\ m\ s^{-1}$

RH_{min} = Mean value for daily minimum relative humidity during the mid-season growth stage [%], for $20\% \leq RH_{min} \leq 80\%$

h = mean plant height during the mid-season stage [m], for $0.1\ m < h < 10\ m$

iii)

$$K_{c\ end} = 0.25 \tag{4.7.3}$$

where, 0.25 is the tabulated value for $K_{c\ end}$ for winter wheat. An adjustment with the following equation is only necessary if the tabulated $K_{c\ end}$ values exceed 0.45. The values didn't exceed 0.45 for any of the environments.

The K_c curve was then constructed as shown in Equation 4.3.12.

4.7.1.2 Calculations for reference evapotranspiration (ET_0) $[mm\ day^{-1}]$:

$$ET_0 = \frac{0.408\ \Delta(Rn - G) + \gamma\ \frac{900}{T+273}\ u_2\ (e_s - e_a)}{\Delta + \gamma\ (1 + 0.34\ u_2)} \tag{4.7.4}$$

where,

R_n = net radiation at the crop surface $[MJm^{-2}day^{-1}]$

G = Soil heat flux density $[MJm^{-2}day^{-1}]$

T = Mean daily air temperature at 2m height $[^{\circ}C]$

u_2 = Wind speed at 2m height $[ms^{-1}]$

e_s = Saturation vapor pressure [kPa]

e_a = Actual vapor pressure [kPa]

$e_s - e_a$ = Saturation vapor pressure deficit [kPa]

Δ = Slope vapor pressure curve $[kPa\ ^\circ C^{-1}]$

γ = Psychrometric constant $[kPa\ ^\circ C^{-1}]$

4.7.1.3 Net solar radiation (R_n) $[MJm^{-2}day^{-1}]$:

$$R_n = R_{ns} - R_{nl} \tag{4.7.5}$$

where,

R_{ns} = Net shortwave radiation $[MJm^{-2}day^{-1}]$

R_{nl} = Net longwave radiation $[MJm^{-2}day^{-1}]$

4.7.1.4 Net shortwave radiation (R_{ns}) $[MJm^{-2}day^{-1}]$:

$$R_{ns} = (1 - \alpha)R_s \tag{4.7.6}$$

where,

α = Albedo, which is 0.23 for the hypothetical grass reference crop [dimensionless]

R_s = Incoming solar radiation $[MJm^{-2}day^{-1}]$

4.7.1.5 Net longwave radiation (R_{nl}) $[MJm^{-2}day^{-1}]$:

$$R_{nl} = \sigma[\frac{T_{max,K}^4 + T_{min,K}^4}{2}](0.34 - 0.14\sqrt{e_a})(1.35\frac{R_s}{R_{so}} - 0.35) \tag{4.7.7}$$

where,

σ = Stefan-Boltzmann constant $[4.90310^{-9}\ MJ\ K^{-4}m^{-2}day^{-1}]$

$T_{max,K}$ = Maximum absolute temperature for the day $[K = \ ^\circ C + 273.16]$

$T_{min,K}$ = Minimum absolute temperature for the day $[K = \ ^\circ C + 273.16]$

e_a = Actual vapor pressure [kPa]

R_s = Incoming solar radiation $[MJm^{-2}day^{-1}]$

R_{so} = Clear-sky radiation $[MJm^{-2}day^{-1}]$

4.7.1.6 Clear-sky radiation (R_{so}) [$MJm^{-2}day^{-1}$]:

$$R_{so} = (0.75 + 2 \cdot 10^{-5}\ z)R_a \tag{4.7.8}$$

where,

z = Elevation above sea level [m]

R_a = Extraterrestrial radiation [$MJm^{-2}day^{-1}$]

4.7.1.7 Extraterrestrial radiation (R_a) [$MJm^{-2}day^{-1}$]:

$$R_a = \frac{24(60)}{\pi}\ G_{sc}\ d_r\ [\omega_s\ sin(\phi)\ sin(\delta) + cos(\phi)\cos(\delta)\ sin(\omega_s)] \tag{4.7.9}$$

where,

G_{sc} = solar constant [0.0820 $MJm^{-2}min^{-1}$]

d_r = Inverse relative distance Earth-Sun

ω_s = sunset hour angle

ϕ = latitude in radians

δ = solar declination

4.7.1.8 Inverse relative distance Earth-Sun (d_r):

$$d_r = 1 + 0.033\ cos(\frac{2\pi}{365}J) \tag{4.7.10}$$

where,

J = day of year

4.7.1.9 Solar declination (δ):

$$\delta = 0.409\ sin(\frac{2\pi}{365}J - 1.39) \tag{4.7.11}$$

where,

J = day of year

4.7.1.10 Sunset hour angle (ω_s):

$$\omega_s = arccos[-tan(\phi)tan(\delta)] \tag{4.7.12}$$

where,

ϕ = latitude in radian.

δ = solar declination

4.7.1.11 Saturation vapor pressure at temperature T ($e^o(T)$) [kPa]:

$$e^o(T) = 0.6108\ exp[\frac{17.27T}{T + 237.3}] \tag{4.7.13}$$

where,

T = Air temperature [$^\circ C$]

4.7.1.12 Mean saturation vapor pressure (e_s) [kPa]:

$$\begin{aligned} e_s =& \frac{e^o(Tmax) + e^o(Tmin)}{2} \\ =& \frac{0.6108\ exp[\frac{17.27\ T_{max}}{T_{max}+237.3}] + 0.6108\ exp[\frac{17.27\ T_{min}}{T_{min}+237.3}]}{2} \end{aligned} \tag{4.7.14}$$

where,

T_{max} = Maximum temperature [$^\circ C$]

T_{min} = Minimum temperature [$^\circ C$]

4.7.1.13 Actual vapor pressure (e_a) [kPa]:

$$e_a = e^o(T_{dew}) = 0.6108\ exp[\frac{17.27\ T_{dew}}{T_{dew} + 237.3}] \tag{4.7.15}$$

where,

T_{dew} = Dewpoint temperature [$^\circ C$]

4.7.1.14 Slope of saturation vapor pressure curve at air temperature T (Δ) [$kPa^{\circ}C$]:

$$\Delta = \frac{4098[0.6108\ exp(\frac{17.27T}{T+237.3})]}{(T+237.3)^2} \tag{4.7.16}$$

where,

T = Air temperature [$^{\circ}C$]

CHAPTER V

GENERAL CONCLUSIONS

This dissertation project investigated winter wheat growth and development in Oklahoma while introducing novel approaches to analyze data on crop growth. Winter wheat is the predominant crop in Oklahoma grown mostly under rainfed conditions. Thus, water availability is one of the important factors in understanding wheat growth dynamics. The broad areas this dissertation addressed were: i) Understanding wheat yield as a function of yield components and weather conditions, ii) Introducing a new methodology (a dynamic ordinary differential equations; ODE model) to analyze data collected over the season on wheat growth, and iii) Utilizing the dynamic ODE model in conjunction with a simple water balance model to understand how water availability affects crop growth and yield dynamics.

In Chapter 2, we explored wheat yield as a function of yield components to examine source-sink balance and assessed their association with weather conditions. The data were analyzed with a Bayesian hierarchical model to naturally reflect the hierarchical features of the system. The results showed that environment explained a large proportion of yield variability in Oklahoma. This study also found that the wheat yield in Oklahoma is co-limited by both source and sink.

In Chapter 3, we introduced a dynamic ODE model to analyze leaf area index (LAI) and biomass over the growing season. This model was implemented within a Bayesian framework to introduce stochasiticity to the deterministic ODE modeling approach. We also compared this new approach to data analysis with the conventional approach to analyzing these types of data. Results showed that the data were valuable in estimating

the ODE model parameters which enabled biologically meaningful interpretations that were not apparent from the linear modeling approach. The comparison showed that both approaches had mixed results indicating that neither approach conclusively outperformed the other in terms of model prediction. However, the ODE modeling approach enabled biologically meaningful interpretations of parameters that were not apparent from the linear modeling approach.

In Chapter 4, we added a water balance component to the dynamic ODE model to analyze the same dataset with additional data on yield. This study quantified the level of improvement in the model by including water balance while assessing the effects of water availability on crop growth throughout the season. We also explored the impact of data quantity and diversity on model predictions which showed that further research is required in this area to successfully model end of season data. Results indicated that the inclusion of a water balance component was important in making accurate inferences, especially on yield. The water balance model, although valuable for model performance, did not quite perform as expected, and needs to be improved for future analyses.

Thus, we presented an eco-physiological explanation for G $\times$ E interaction observed in Oklahoma wheat using a linear modeling approach. Upon recognizing that the environment is the dominant factor for yield variability, we explored the growth patterns on a single genotype, Iba, at different environments using a non-linear model to better represent the system. Finally, we augmented the non-linear model to encompass one of the important features of the Oklahoma wheat cropping system: water availability and delivered inferences on wheat growth and yield patterns. Further research calls for a better water balance model, inclusion of multiple genotypes, and a robust data-model combination to analyze end of season data. In summary, this dissertation project added to the understanding of wheat growth and yield dynamics in Oklahoma and introduced a novel modeling approach to facilitate biological interpretations of

statistical parameters.

REFERENCES

Alderman, P. D. & Stanfill, B. (2017). Quantifying model-structure-and parameter-driven uncertainties in spring wheat phenology prediction with bayesian analysis. *European Journal of Agronomy*, *88*, 1–9.

Allen, R. G., Pereira, L. S., Raes, D., & Smith, M. (1998). FAO irrigation and drainage paper No. 56. *Rome: Food and Agriculture Organization of the United Nations*, *56*(97), e156.

Alonso, M. P., Abbate, P. E., Mirabella, N. E., Merlos, F. A., Panelo, J. S., & Pontaroli, A. C. (2018). Analysis of sink/source relations in bread wheat recombinant inbred lines and commercial cultivars under a high yield potential environment. *European Journal of Agronomy*, *93*, 82–87.

Anar, M. J., Lin, Z., Hoogenboom, G., Shelia, V., Batchelor, W. D., Teboh, J. M., ... Khan, M. (2019). Modeling growth, development and yield of sugarbeet using dssat. *Agricultural Systems*, *169*, 58–70.

Asseng, S., Van Keulen, H., & Stol, W. (2000). Performance and Application of the APSIM Nwheat Model in the Netherlands. *European Journal of Agronomy*, *12*(1), 37–54.

Asseng, S., Zhu, Y., Basso, B., Wilson, T., & Cammarano, D. (2014). Simulation modeling: Applications in cropping systems.

Attia, A., Rajan, N., Xue, Q., Nair, S., Ibrahim, A., & Hays, D. (2016). Application of dssat-ceres-wheat model to simulate winter wheat response to irrigation management in the texas high plains. *Agricultural Water Management*, *165*, 50–60.

Auguie, B. (2017). *gridExtra: Miscellaneous functions for "Grid" graphics*. R package version 2.3. Retrieved from https://CRAN.R-project.org/package=gridExtra

Austin, R., Bingham, J., Blackwell, R., Evans, L., Ford, M., Morgan, C., & Taylor, M. (1980). Genetic improvements in winter wheat yields since 1900 and associated physiological changes. *The Journal of Agricultural Science*, *94*(3), 675–689.

Baker, J., Pinter Jr, P., Reginato, R., & Kanemasu, E. (1986). Effects of temperature on leaf appearance in spring and winter wheat cultivars 1. *Agronomy Journal*, *78*(4), 605–613.

Bechini, L., Bocchi, S., Maggiore, T., & Confalonieri, R. (2006). Parameterization of a crop growth and development simulation model at sub-model components level. an example for winter wheat (*Triticum aestivum* l.) *Environmental Modelling & Software*, *21*(7), 1042–1054.

Betancourt, M. (2017). A conceptual introduction to hamiltonian monte carlo. *arXiv preprint arXiv:1701.02434*.

Betancourt, M. & Girolami, M. (2015). Hamiltonian monte carlo for hierarchical models. *Current Trends in Bayesian Methodology with Applications*, *79*(30), 2–4.

Borrás, L., Slafer, G. A., & Otegui, M. E. (2004). Seed dry weight response to source–sink manipulations in wheat, maize and soybean: A quantitative reappraisal. *Field Crops Research*, *86*(2-3), 131–146.

Braun, H.-J., Atlin, G., & Payne, T. (2010). Multi-location testing as a tool to identify plant response to global climate change. *Climate Change and Crop Production*, *1*, 115–138.

Brock, F. V., Crawford, K. C., Elliott, R. L., Cuperus, G. W., Stadler, S. J., Johnson, H. L., & Eilts, M. D. (1995). The Oklahoma Mesonet: A technical overview. *Journal of Atmospheric and Oceanic Technology*, *12*(1), 5–19.

Brown, H., Huth, N., & Holzworth, D. (2018). Crop model improvement in APSIM: using wheat as a case study. *European Journal of Agronomy*, *100*, 141–150.

Calderini, D. F., Dreccer, M. F., & Slafer, G. A. (1997). Consequences of breeding on biomass, radiation interception and radiation-use efficiency in wheat. *Field Crops Research*, *52*(3), 271–281.

Calhoun, R., Carver, B., Hunger, B., Edwards, J., Watson, B., & Gillespie, C. (2019). 2017-18 Small grains variety performance tests, CR-2143 Rev. 0819. Stillwater: Oklahoma State University. Retrieved from http://pods.dasnr.okstate.edu/docushare/dsweb/Get/Document-11543/CR-2143web2019.pdf

Caviglia, O. & Sadras, V. (2001). Effect of nitrogen supply on crop conductance, water-and radiation-use efficiency of wheat. *Field Crops Research*, *69*(3), 259–266.

Chapman, S., Cooper, M., Hammer, G., & Butler, D. (2000). Genotype by environment interactions affecting grain sorghum. ii. frequencies of different seasonal patterns of drought stress are related to location effects on hybrid yields. *Australian Journal of Agricultural Research*, *51*(2), 209–222.

Chapman, S. C. [Scott C]. (2008). Use of crop models to understand genotype by environment interactions for drought in real-world and simulated plant breeding trials. *Euphytica*, *161*(1-2), 195–208.

Chitakasempornkul, K., Meneget, M. B., Rosa, G. J., Lopes, F. B., Jager, A., Gonçalves, M. A., ... Bello, N. M. (2019). Investigating causal biological relationships between reproductive performance traits in high-performing gilts and sows. *Journal of Animal Science*, *97*(6), 2385–2401.

Cotes, J. M., Crossa, J., Sanches, A., & Cornelius, P. L. (2006). A bayesian approach for assessing the stability of genotypes. *Crop Science*, *46*(6), 2654–2665.

Crofts, H. (1989). On defining a winter wheat. *Euphytica*, *44*(3), 225–234.

Cuevas, J., Crossa, J., Montesinos-López, O. A., Burgueño, J., Pérez-Rodríguez, P., & de los Campos, G. (2017). Bayesian genomic prediction with genotype × environment interaction kernel models. *G3: Genes, Genomes, Genetics*, *7*(1), 41–53.

Dai, J., Bean, B., Brown, B., Bruening, W., Edwards, J., Flowers, M., ... Wiersma, J. (2016). Harvest index and straw yield of five classes of wheat. *Biomass and Bioenergy*, *85*, 223–227.

Daróczi, G. & Tsegelskyi, R. (2018). *pander: An R 'Pandoc' writer*. R package version 0.6.3. Retrieved from https://CRAN.R-project.org/package=pander

Davidson, D. & Chevalier, P. (1992). Storage and remobilization of water-soluble carbohydrates in stems of spring wheat. *Crop Science*, *32*(1), 186–190.

Eitel, J. U., Magney, T. S., Vierling, L. A., Brown, T. T., & Huggins, D. R. (2014). Lidar based biomass and crop nitrogen estimates for rapid, non-destructive assessment of wheat nitrogen status. *Field Crops Research*, *159*, 21–32.

Fischer, R. [R.A.]. (1985). Number of kernels in wheat crops and the influence of solar radiation and temperature. *The Journal of Agricultural Science*, *105*(2), 447–461. Cited By :550. Retrieved from www.scopus.com

Fischer, R. [RA]. (2008). The importance of grain or kernel number in wheat: A reply to Sinclair and Jamieson. *Field Crops Research*, *105*(1-2), 15–21.

Foulkes, M. J., Slafer, G. A., Davies, W. J., Berry, P. M., Sylvester-Bradley, R., Martre, P., ... Reynolds, M. P. (2011). Raising yield potential of wheat. iii. optimizing partitioning to grain while maintaining lodging resistance. *Journal of Experimental Botany*, *62*(2), 469–486.

Gelman, A., Carlin, J. B., Stern, H. S., Dunson, D. B., Vehtari, A., & Rubin, D. B. (2013). *Bayesian data analysis*. CRC press.

Gelman, A., Goodrich, B., Gabry, J., & Vehtari, A. (2019). R-squared for Bayesian regression models. *The American Statistician*, *73*(3), 307–309.

Grieve, A. (1991). On the construction of shortest confidence intervals and Bayesian highest posterior density intervals. *Journal of Veterinary Pharmacology and Therapeutics*, *14*(4), 395–399.

He, Y., Wei, Y., DePauw, R., Qian, B., Lemke, R., Singh, A., ... Wang, H. (2013). Spring wheat yield in the semiarid Canadian prairies: Effects of precipitation timing and soil texture over recent 30 years. *Field Crops Research*, *149*, 329–337.

Hoffman, M. D. & Gelman, A. (2014). The no-u-turn sampler: Adaptively setting path lengths in hamiltonian monte carlo. *Journal of Machine Learning Research*, *15*(1), 1593–1623.

Hoops, S., Hontecillas, R., Abedi, V., Leber, A., Philipson, C., Carbo, A., & Bassaganya-Riera, J. (2016). Chapter 5 - ordinary differential equations (odes) based modeling. In J. Bassaganya-Riera (Ed.), *Computational immunology* (pp. 63–78). Academic Press. doi:https://doi.org/10.1016/B978-0-12-803697-6.00005-9

Howell, T., Evett, S., Tolk, J., Copeland, K., Dusek, D., & Colaizzi, P. (2006). Crop coefficients developed at Bushland, Texas for corn, wheat, sorghum, soybean, cotton, and alfalfa. In *World environmental and water resource congress 2006: Examining the confluence of environmental and water concerns* (pp. 1–9).

Howell, T., Steiner, J., Schneider, A., & Evett, S. (1995). Evapotranspiration of irrigated winter wheat—Southern High Plains. *Transactions of the ASAE*, *38*(3), 745–759.

Howell, T., Tolk, J., Evett, S., Copeland, K., Dusek, D., & Clemmens, A. (2007). Evapotranspiration of deficit irrigated sorghum and winter wheat. In *Uscid fourth international conference on irrigation and drainage. the role of irrigation and drainage in a sustainable future, sacramento, ca. 3–6 oct. 2007. us* (pp. 223–239). Committee on Irrigation and Drainage (USDID) Denver, CO.

Huang, J., Sedano, F., Huang, Y., Ma, H., Li, X., Liang, S., ... Wu, W. (2016). Assimilating a synthetic Kalman filter leaf area index series into the WOFOST model to improve regional winter wheat yield estimation. *Agricultural and Forest Meteorology*, *216*, 188–202.

Huang, J., Tian, L., Liang, S., Ma, H., Becker-Reshef, I., Huang, Y., ... Wu, W. (2015). Improving winter wheat yield estimation by assimilation of the leaf area index from landsat tm and modis data into the wofost model. *Agricultural and Forest Meteorology*, *204*, 106–121.

Hunger, R. M., Edwards, J. T., Bowden, R. L., Yan, L., Rayas-Duarte, P., Bai, G., ... Carver, B. F. (2014). 'billings' wheat combines early maturity, disease resistance, and desirable grain quality for the Southern Great Plains, USA. *Journal of Plant Registrations*, *8*(1), 22–31.

Instruments, P. (1995). SKCS 4100 Single Kernel Characterization System. *Instruction Manual*.

Jin, X., Kumar, L., Li, Z., Xu, X., Yang, G., & Wang, J. (2016). Estimation of winter wheat biomass and yield by combining the aquacrop model and field hyperspectral data. *Remote Sensing*, *8*(12), 972.

Jin, X., Yang, G., Xu, X., Yang, H., Feng, H., Li, Z., ... Zhao, C. (2015). Combined multi-temporal optical and radar parameters for estimating lai and biomass in winter wheat using hj and radarsar-2 data. *Remote Sensing*, *7*(10), 13251–13272.

Jones, J. W., Hoogenboom, G., Porter, C. H., Boote, K. J., Batchelor, W. D., Hunt, L., ... Ritchie, J. T. (2003a). The DSSAT Cropping System Model. *European Journal of Agronomy*, *18*(3-4), 235–265.

Jones, J. W., Hoogenboom, G., Porter, C. H., Boote, K. J., Batchelor, W. D., Hunt, L., ... Ritchie, J. T. (2003b). The dssat cropping system model. *European Journal of Agronomy*, *18*(3-4), 235–265.

Jordan, M. I. (1995). Why the logistic function? a tutorial discussion on probabilities and neural networks. Computational cognitive science technical report.

Kanning, M., Kühling, I., Trautz, D., & Jarmer, T. (2018). High-resolution UAV-based hyperspectral imagery for LAI and chlorophyll estimations from wheat for yield prediction. *Remote Sensing*, *10*(12), 2000.

Kaya, Y., Akcura, M., Ayranci, R., & Taner, S. (2006). Pattern analysis of multi-environment trials in bread wheat. *Commun. Biometry Crop Sci*, *1*(1), 63–71.

Keating, B. A., Carberry, P. S., Hammer, G. L., Probert, M. E., Robertson, M. J., Holzworth, D., ... CJ, S. (2003). An overview of APSIM, a model designed for farming systems simulation. *European Journal of Agronomy*, *18*(3-4), 267–288.

Kiniry, J., Jones, C., O'toole, J., Blanchet, R., Cabelguenne, M., & Spanel, D. (1989). Radiation-use efficiency in biomass accumulation prior to grain-filling for five grain-crop species. *Field Crops Research*, *20*(1), 51–64.

Ko, J., Piccinni, G., Marek, T., & Howell, T. (2009). Determination of growth-stage-specific crop coefficients (kc) of cotton and wheat. *Agricultural Water Management*, *96*(12), 1691–1697.

Kogan, F., Kussul, N., Adamenko, T., Skakun, S., Kravchenko, O., Kryvobok, O., ... Lavrenyuk, A. (2013). Winter wheat yield forecasting in Ukraine based on Earth observation, meteorological data and biophysical models. *International Journal of Applied Earth Observation and Geoinformation*, *23*, 192–203.

Kudryashov, N. A. (2015). Logistic function as solution of many nonlinear differential equations. *Applied Mathematical Modelling*, *39*(18), 5733–5742.

Li, G., Yu, M., Fang, T., Cao, S., Carver, B. F., & Yan, L. (2013). Vernalization requirement duration in winter wheat is controlled by T a VRN-A 1 at the protein level. *The Plant Journal*, *76*(5), 742–753.

Li, Z., Jin, X., Zhao, C., Wang, J., Xu, X., Yang, G., ... Shen, J. (2015). Estimating wheat yield and quality by coupling the DSSAT-CERES model and proximal remote sensing. *European Journal of Agronomy*, *71*, 53–62.

Lollato, R. P. & Edwards, J. T. (2015). Maximum attainable wheat yield and resource-use efficiency in the southern great plains. *Crop Science*, *55*(6), 2863–2876.

Lollato, R. P., Edwards, J. T., & Ochsner, T. E. (2017). Meteorological limits to winter wheat productivity in the us southern Great Plains. *Field Crops Research*, *203*, 212–226.

Marburger, D., Calhoun, R., Beedy, T., Carver, B., Hunger, B., Watson, B., & Gillespie, C. (2017). 2016-17 Small grains variety performance tests, CR-2143 Rev. 0917. Stillwater: Oklahoma State University. Retrieved from http://wheat.okstate.edu/variety-testing/grain-yield-previous-yrs/CR2143web2017.pdf

Marburger, D., Calhoun, R., Carver, B., Hunger, B., Watson, B., & Gillespie, C. (2018). 2017-18 Small grains variety performance tests, CR-2143 Rev. 0718. Stillwater: Oklahoma State University. Retrieved from http://wheat.okstate.edu/variety-testing/grain-yield-previous-yrs/cr-2143web2018-small-grains-vt

Marburger, D., Hunger, B., Carver, B., & Royer, T. (2018). Wheat variety comparison, PSS-2142. Stillwater: Oklahoma State University. Accessed: 2020-08-11. Retrieved from http://pods.dasnr.okstate.edu/docushare/dsweb/Get/Document-6107/PSS-2142web2018.pdf

Martin, C., Rousser, R., & Brabec, D. (1993). Development of a single-kernel wheat characterization system. *Transactions of the ASAE*, *36*(5), 1399–1404.

Maulana, F., Anderson, J. D., Butler, T. J., & Ma, X.-F. (2019). Improving dual-purpose winter wheat in the southern Great Plains of the United States. In *Recent advances in grain crops research* (pp. 1–16). IntechOpen.

McMaster, G. S., Edmunds, D. A., Marquez, R., Haley, S., Buchleiter, G., Byrne, P., ... Ascough II, J. (2019). Winter wheat phenology simulations improve when adding responses to water stress. *Agronomy Journal*, *111*(5), 2350–2360.

McMaster, G. S. & Smika, D. E. (1988). Estimation and evaluation of winter wheat phenology in the central Great Plains. *Agricultural and Forest Meteorology*, *43*(1), 1–18.

McMaster, G. S. & Wilhelm, W. (1997). Growing degree-days: One equation, two interpretations. *Agricultural and Forest Meteorology*, *87*(4), 291–300.

McPherson, R. A., Fiebrich, C. A., Crawford, K. C., Kilby, J. R., Grimsley, D. L., Martinez, J. E., ... Sutherland, A. J. (2007). Statewide monitoring of the mesoscale environment: A technical update on the Oklahoma Mesonet. *Journal of Atmospheric and Oceanic Technology*, *24*(3), 301–321.

Meredith, M. & Kruschke, J. (2018). *HDInterval: Highest (posterior) density intervals*. R package version 0.2.0. Retrieved from https://CRAN.R-project.org/package=HDInterval

Mohammadi, R., Abdulahi, A., Haghparast, R., & Armion, M. (2007). Interpreting genotype × environment interactions for durum wheat grain yields using nonparametric methods. *Euphytica*, *157*(1-2), 239–251.

Mohammadi, R. & Amri, A. (2008). Comparison of parametric and non-parametric methods for selecting stable and adapted durum wheat genotypes in variable environments. *Euphytica*, *159*(3), 419–432.

Mohammadi, R., Roustaii, M., Haghparast, R., Roohi, E., Solimani, K., Ahmadi, M. M., ... Amri, A. (2010). Genotype × environment interactions for grain yield in rainfed winter wheat multi-environment trials in Iran. *Agronomy Journal*, *102*(5), 1500–1510.

Monsi, M. & Saeki, T. (2005). On the factor light in plant communities and its importance for matter production. *Annals of Botany*, *95*(3), 549.

Montesinos-López, O. A., Montesinos-López, A., Hernández, M. V., Ortiz-Monasterio, I., Pérez-Rodríguez, P., Burgueño, J., & Crossa, J. (2019). Multivariate bayesian analysis of on-farm trials with multiple-trait and multiple-environment data. *Agronomy Journal*, *111*(6), 2658–2669.

Munaro, L., Hefley, T., DeWolf, E., Haley, S., Fritz, A., Zhang, G., ... Lollato, R. (2020). Exploring long-term variety performance trials to improve environment-specific genotype × management recommendations: A case-study for winter wheat. *Field Crops Research*, *255*, 107848.

Muurinen, S. & Peltonen-Sainio, P. (2006). Radiation-use efficiency of modern and old spring cereal cultivars and its response to nitrogen in northern growing conditions. *Field Crops Research*, *96*(2-3), 363–373.

Nain, A., Dadhwal, V., & Singh, T. (2004). Use of CERES-Wheat model for wheat yield forecast in central Indo-Gangetic Plains of India. *The Journal of Agricultural Science*, *142*(1), 59.

Nash, J. E. & Sutcliffe, J. V. (1970). River flow forecasting through conceptual models part I—A discussion of principles. *Journal of Hydrology*, *10*(3), 282–290.

O'Connell, M., O'leary, G., Whitfield, D., & Connor, D. (2004). Interception of photosynthetically active radiation and radiation-use efficiency of wheat, field pea and mustard in a semi-arid environment. *Field Crops Research*, *85*(2-3), 111–124.

Osborne, B. & Anderssen, R. (2003). Single-kernel characterization principles and applications. *Cereal Chemistry*, *80*(5), 613–622.

OSU Small Grains Extension. (2020). Variety Characteristics. Stillwater: Oklahoma State University. Retrieved from http://wheat.okstate.edu/variety-characteristics-1/variety-characteristics

Paine, C. T., Marthews, T. R., Vogt, D. R., Purves, D., Rees, M., Hector, A., & Turnbull, L. A. (2012). How to fit nonlinear plant growth models and calculate growth rates: An update for ecologists. *Methods in Ecology and Evolution*, *3*(2), 245–256.

Patrignani, A., Lollato, R. P., Ochsner, T. E., Godsey, C. B., & Edwards, J. T. (2014). Yield gap and production gap of rainfed winter wheat in the southern great plains. *Agronomy Journal*, *106*(4), 1329–1339.

Peña-Bautista, R. J., Hernandez-Espinosa, N., Jones, J. M., Guzmán, C., & Braun, H. J. (2017). CIMMYT series on carbohydrates, wheat, grains, and health: Wheat-based foods: Their global and regional importance in the food supply, nutrition, and health. *Cereal Foods World*, *62*(5), 231–249.

Piepho, H., Büchse, A., & Richter, C. (2004). A mixed modelling approach for randomized experiments with repeated measures. *Journal of Agronomy and Crop Science*, *190*(4), 230–247.

Porter, J. R. & Gawith, M. (1999). Temperatures and the growth and development of wheat: A review. *European Journal of Agronomy*, *10*(1), 23–36.

Pradhan, S., Sehgal, V. K., Bandyopadhyay, K., Panigrahi, P., Parihar, C., & Jat, S. (2018). Radiation interception, extinction coefficient and use efficiency of wheat crop at various irrigation and nitrogen levels in a semi-arid location. *Indian Journal of Plant Physiology*, *23*(3), 416–425.

R Core Team. (2020). *R: A language and environment for statistical computing*. R Foundation for Statistical Computing. Vienna, Austria. Retrieved from https://www.R-project.org/

Ray, D. K., Gerber, J. S., MacDonald, G. K., & West, P. C. (2015). Climate variation explains a third of global crop yield variability. *Nature Communications*, *6*(1), 1–9.

Reynolds, M. P. [Matthew P.], Pask, A. J. D., Hoppitt, W. J. E., Sonder, K., Sukumaran, S., Molero, G., ... Joshi, A. K. (2017). Strategic crossing of biomass and harvest index—source and sink—achieves genetic gains in wheat. *Euphytica*, *213*(11), 257.

Reynolds, M., Pellegrineschi, A., & Skovmand, B. (2005). Sink-limitation to yield and biomass: A summary of some investigations in spring wheat. *Annals of Applied Biology*, *146*(1), 39–49.

Reynolds, M., Trethowan, R., Crossa, J., Vargas, M., & Sayre, K. (2002). Physiological factors associated with genotype by environment interaction in wheat. *Field Crops Research*, *75*(2-3), 139–160.

Rezig, M., M'hamed, H. C., & Naceur, M. B. (2015). Durum wheat (*Triticum durum* desf): Relation between photosynthetically active radiation intercepted and water consumption under different nitrogen rates. *Journal of Agricultural Science*, *7*(8), 225.

Rodriguez, D., Keltjens, W., & Goudriaan, J. (1998). Plant leaf area expansion and assimilate production in wheat (*Triticum aestivum* l.) growing under low phosphorus conditions. *Plant and Soil*, *200*(2), 227–240.

Roozeboom, K. L., Schapaugh, W. T., Tuinstra, M. R., Vanderlip, R. L., & Milliken, G. A. (2008). Testing wheat in variable environments: Genotype, environment, interaction effects, and grouping test locations. *Crop Science*, *48*(1), 317–330.

Sadras, V. O. [Victor O]. (2007). Evolutionary aspects of the trade-off between seed size and number in crops. *Field Crops Research*, *100*(2-3), 125–138.

Sadras, V. O. [Victor O] & Slafer, G. A. [Gustavo A]. (2012). Environmental modulation of yield components in cereals: Heritabilities reveal a hierarchy of phenotypic plasticities. *Field Crops Research*, *127*, 215–224.

Sadras, V., Whitfield, D., & Connor, D. (1991). Transpiration efficiency in crops of semi-dwarf and standard-height sunflower. *Irrigation Science*, *12*(2), 87–91.

Salazar-Gutierrez, M., Johnson, J., Chaves-Cordoba, B., & Hoogenboom, G. (2013). Relationship of base temperature to development of winter wheat. *International Journal of Plant Production*, *7*(4), 741–762.

Savin, R. [Roxana] & Slafer, G. A. [Gustavo A]. (1991). Shading effects on the yield of an argentinian wheat cultivar. *Journal of Agricultural Science, 1991, vol. 116, núm. 1, p. 1-7.*

Schad, D. J., Betancourt, M., & Vasishth, S. (2019). Toward a principled Bayesian workflow in cognitive science. *arXiv preprint arXiv:1904.12765.*

Serrago, R. A., Alzueta, I., Savin, R., & Slafer, G. A. (2013). Understanding grain yield responses to source–sink ratios during grain filling in wheat and barley under contrasting environments. *Field Crops Research*, *150*, 42–51.

Serrago, R. A. & Miralles, D. J. (2014). Source limitations due to leaf rust (caused by *Puccinia triticina*) during grain filling in wheat. *Crop and Pasture Science*, *65*(2), 185–193.

Shearman, V., Sylvester-Bradley, R., Scott, R., & Foulkes, M. (2005). Physiological processes associated with wheat yield progress in the UK. *Crop Science*, *45*(1), 175–185.

Slafer, G. & Savin, R. (1991). Developmental base temperature in different phenological phases of wheat (*Triticum aestivum*). *Journal of Experimental Botany*, *42*(8), 1077–1082.

Slafer, G. A. [Gustavo A] & Savin, R. [Roxana]. (1994). Postanthesis green area duration in a semidwarf and a standard-height wheat cultivar as affected by sink strength. *Australian Journal of Agricultural Research*, *45*(7), 1337–1346.

Slafer, G. A. [Gustavo A], Savin, R., & Sadras, V. O. (2014). Coarse and fine regulation of wheat yield components in response to genotype and environment. *Field Crops Research*, *157*, 71–83.

Soltani, A., Maddah, V., & Sinclair, T. (2013). SSM-wheat: A simulation model for wheat development, growth and yield. *International Journal of Plant Production*, *7*(4), 711–740.

Stan Development Team. (2018). Stan modeling language users guide and reference manual, version 2.18.0. Retrieved from http://mc-stan.org

Stan Development Team. (2019). RStan: The r interface to Stan. R package version 2.19.2. Retrieved from http://mc-stan.org/

Steduto, P., Hsiao, T. C., Raes, D., & Fereres, E. (2009). AquaCrop—The FAO crop model to simulate yield response to water: I. Concepts and underlying principles. *Agronomy Journal*, *101*(3), 426–437.

Sukumaran, S., Crossa, J., Jarquin, D., & Reynolds, M. (2017). Pedigree-based prediction models with genotype × environment interaction in multienvironment trials of CIMMYT wheat. *Crop Science*, *57*(4), 1865–1880.

Tahara, M., Carver, B. F., Johnson, R. C., & Smith, E. L. (1990). Relationship between relative water content during reproductive development and winter wheat grain yield. *Euphytica*, *49*(3), 255–262.

Thapa, S., Xue, Q., Jessup, K. E., Rudd, J. C., Liu, S., Marek, T. H., ... Baker, S. (2019). Yield determination in winter wheat under different water regimes. *Field Crops Research*, *233*, 80–87.

Tian, L. & Quiring, S. M. (2019). Spatial and temporal patterns of drought in Oklahoma (1901–2014). *International Journal of Climatology*, *39*(7), 3365–3378.

Ugarte, C., Calderini, D. F., & Slafer, G. A. (2007). Grain weight and grain number responsiveness to pre-anthesis temperature in wheat, barley and triticale. *Field Crops Research*, *100*(2-3), 240–248.

USDA, N. (2019). Oklahoma agricultural statistics. https://www.nass.usda.gov/Statistics_by_State/Oklahoma/Publications/Annual_Statistical_Bulletin/ok-bulletin-2019.pdf. Accessed: 2020-08-24.

Valente, B. D. & de Magalhães Rosa, G. J. (2013). Mixed effects structural equation models and phenotypic causal networks. In *Genome-wide association studies and genomic prediction* (pp. 449–464). Springer.

Vehtari, A., Gabry, J., Magnusson, M., Yao, Y., Bürkner, P., Paananen, T., & Gelman, A. (2020). Efficient leave-one-out cross-validation and WAIC for bayesian models. r package version 2.3.1.

Vehtari, A. [Aki], Gelman, A., & Gabry, J. (2017). Practical Bayesian model evaluation using leave-one-out cross-validation and WAIC. *Statistics and Computing*, *27*(5), 1413–1432.

Vitale, J., Adam, B., & Vitale, P. (2020). Economics of wheat breeding strategies: Focusing on oklahoma hard red winter wheat. *Agronomy*, *10*(2), 238.

Wardlaw, I. & Moncur, L. (1995). The response of wheat to high temperature following anthesis. i. the rate and duration of kernel filling. *Functional Plant Biology*, *22*(3), 391–397.

White, J. W., Kimball, B. A., Wall, G. W., & Ottman, M. J. (2012). Cardinal temperatures for wheat leaf appearance as assessed from varied sowing dates and infrared warming. *Field Crops Research*, *137*, 213–220.

Wickham, Hadley. (2017). Tidyverse: Easily install and load the 'tidyverse'. R package version 1.2.1. Retrieved from https://CRAN.R-project.org/package=tidyverse

Wickham, H. (2016). *ggplot2: Elegant graphics for data analysis*. Springer-Verlag New York. Retrieved from https://ggplot2.tidyverse.org

Wickham, H., Averick, M., Bryan, J., Chang, W., McGowan, L. D., François, R., ... Yutani, H. (2019). Welcome to the tidyverse. *Journal of Open Source Software*, *4*(43), 1686. doi:10.21105/joss.01686

Williams, R., O'Brien, L., Eagles, H. A., Solah, V. A., & Jayasena, V. (2008). The influences of genotype, environment, and genotype × environment interaction on wheat quality. *Australian Journal of Agricultural Research*, *59*(2), 95–111.

Willmott, C. J. (1981). On the validation of models. *Physical Geography*, *2*(2), 184–194.

Xie, Y. (2020). *Knitr: A general-purpose package for dynamic report generation in r*. R package version 1.29. Retrieved from https://yihui.org/knitr/

Yan, W. & Hunt, L. (2001). Interpretation of genotype × environment interaction for winter wheat yield in ontario. *Crop Science*, *41*(1), 19–25.

Yang, J., Zhang, J., Huang, Z., Zhu, Q., & Wang, L. (2000). Remobilization of carbon reserves is improved by controlled soil-drying during grain filling of wheat. *Crop Science*, *40*(6), 1645–1655.

Yue, J., Yang, G., Li, C., Li, Z., Wang, Y., Feng, H., & Xu, B. (2017). Estimation of winter wheat above-ground biomass using unmanned aerial vehicle-based snapshot hyperspectral sensor and crop height improved models. *Remote Sensing*, *9*(7), 708.

Zhang, H., Turner, N. C., & Poole, M. L. (2010). Source–sink balance and manipulating sink–source relations of wheat indicate that the yield potential of wheat is sink-limited in high-rainfall zones. *Crop and Pasture Science*, *61*(10), 852–861.

Zhang, S., Sadras, V., Chen, X., & Zhang, F. (2013). Water use efficiency of dryland wheat in the loess plateau in response to soil and crop management. *Field Crops Research*, *151*, 9–18.

Zhu, H. (2019). *kableExtra: Construct complex table with 'kable' and pipe syntax*. R package version 1.1.0. Retrieved from https://CRAN.R-project.org/package=kableExtra

VITA

Pratishtha Poudel

Candidate for the Degree of

Doctor of Philosophy

Dissertation: A STUDY OF WINTER WHEAT GROWTH AND DEVELOPMENT IN OKLAHOMA USING A HIERARCHICAL BAYESIAN APPROACH

Major Field: Crop Science

Biographical:

Education:

Completed the requirements for the Doctor of Philosophy in Crop Science at Oklahoma State University, Stillwater, Oklahoma in July, 2021.

Completed the requirements for the Master of Science in Plant and Soil Sciences at Oklahoma State University, Stillwater, Oklahoma in 2016.

Completed the requirements for the Bachelor of Science in Agriculture at Tribhuvan University, Kathmandu, Nepal in 2013.

Professional Memberships:

Crop Science Society of America, American Society of Agronomy, Soil Science Society of America